SEISMIC INVESTIGATION OF CRUSTAL STRUCTURE AND UPPER MANTLE VELOCITY IN THE STATE OF NEW MEXICO AND VICINITY

A Dissertation
Presented to the Faculty
of the New Mexico Institute of
Mining and Technology

In Partial Fulfillment
of the Requirements for the
Degree of Doctor of Philosophy
in Geoscience

152 pp.

by
Tousson Mohamed Roushdy Toppozada

January 1974

This dissertation is accepted on behalf of the faculty of the Institute by the following committee:

Adviser

January 17, 1974

Date

ABSTRACT

A seismic study was made of the earth's crust and uppermost mantle in New Mexico and vicinity, using various earthquake and explosive sources.

Interpretation of the seismic profile extending 548 km southward from the Gasbuggy nuclear test of 10 December 1967 resulted in a crustal model for central New Mexico. The crust is 39.9 km thick below the basement. It consists of an upper crust 18.6 km thick having P velocity 6.15 km/sec, and a lower crust 21.3 km thick having P velocity 6.5 km/sec. The apparent upper mantle velocity is 8.12 km/sec. This model applies at the cross-over distance, 50 km west of Albuquerque. Additional information from earthquakes and explosions suggests that the upper crustal velocity drops to 5.8 km/sec in the Rio Grande rift, and that the true upper mantle velocity is 7.9 km/sec. The drop in upper crustal velocity in the Rio Grande rift can be detected on the Gasbuggy profile.

Upper mantle velocities were measured across intervals of two or more stations. Contour lines of equal velocity show that the velocity decreases to the

west, from more than 8.3 km/sec in Oklahoma and northern Texas to less than 7.7 km/sec in north-central Utah. The southern Colorado Plateau Province has upper mantle velocity up to 8.0 km/sec, and is surrounded to the north, west, and south, by lower velocities in the Basin and Range Province. An exceptional area in the Basin and Range Province of southeastern Arizona has P_n velocity greater than 8.0 km/sec. This high velocity area is separated from the high velocities to the east and north by a zone having a velocity less than 7.9 km/sec. This zone, in southern New Mexico, is centered on the western flank of the Rio Grande rift.

Regional dip and depth of the Mohorovicic discontinuity were estimated from the values of reversed upper mantle velocity. This information was added to existing control points, and the crustal thickness was contoured. The crust is more than 50 km thick in Colorado, northeastern New Mexico, northern Texas, and Oklahoma. The southern Colorado Plateau Province has a crustal thickness greater than 40 km, and is surrounded to the north, west, and south by the Basin and Range Province having crustal thickness less than 30 km. A finger of thin crust extends northeastward into the Basin and Range Province of New Mexico, to the west of the Rio Grande rift.

ACKNOWLEDGMENTS

I am grateful to Dr. Allan R. Sanford, my advisor and committee chairman, for his guidance and advice throughout this study. I am also grateful to Dr. Antonius J. Budding, Dr. Ralph M. McGehee, and Dr. Charles E. Chapin for serving on the advisory committee.

My wife typed the numerous drafts of this dissertation, and key-punched the digital data of the Gasbuggy profile. She also helped in checking the lists of seismograms requested against the seismograms received. For her assistance, as well as for her patience and encouragement, I am grateful.

I wish to thank Mr. Robert A. Bieberman for his assistance in obtaining the velocities of seismic waves in the rocks overlying basement, and in estimating the depth to basement along the Gasbuggy profile. This information came from the logs of deep wells on file at the New Mexico State Bureau of Mines and Mineral Resources.

Professor Charles B. Moore allowed me access to

a demonstration model of a Hewlett-Packard digitizer. This greatly simplified digitizing the seismograms for the Gasbuggy profile.

Dr. Marshall A. Reiter permitted me to use the geologic maps in Figures 1.2 and 1.3, which had been compiled from various sources.

I wish to thank Mr. John J. Kosovich, of the Trinidad State Junior College in Colorado, for sending me original seismograms from the station TJC.

Mr. David H. Warren, of the National Center for Earthquake Research, Menlo Park, California, kindly provided me with copies of seismograms for the 2 U.S.G.S. stations on the Gasbuggy south profile.

The Air Force Technical Applications Center, Alexandria, Virginia, authorized Geotech-Teledyne to provide me with seismograms for the stations DRC, KNU, LCN, TFO, UBO and WMO. My thanks to both organizations.

Finally, the Research Committee of the American Association of Petroleum Geologists awarded me a Grant-In-Aid, which paid for seismograms, travel, and manuscript preparation.

TABLE OF CONTENTS

LIST OF FIGURES

LIST OF TABLES

1. INTRODUCTION

The general purpose of the research described in this dissertation was to obtain information on the earth's crust and uppermost mantle in the state of New Mexico and surrounding areas. Seismic data from various earthquake and explosive sources, recorded at permanent and temporary seismograph stations, were studied. The research included (1) construction of a model of the earth's crust in central New Mexico, giving the thicknesses and seismic velocities of the crustal layers, and the velocity in the uppermost mantle; (2) study of the variation of velocity in the upper mantle in New Mexico and vicinity; and (3) mapping the variation in thickness of the crust with the aid of reversed values of upper mantle velocity.

Geologic Setting

The state of New Mexico covers parts of four physiographic provinces as shown in Figure 1.1. These are the Rocky Mountains, the High Plains, the Basin and Range, and the Colorado Plateau (Fenneman, 1946).

The Rio Grande rift, which is a structural as well as a physiographic feature, is outlined in the same figure. The rift structure consists of a series of en

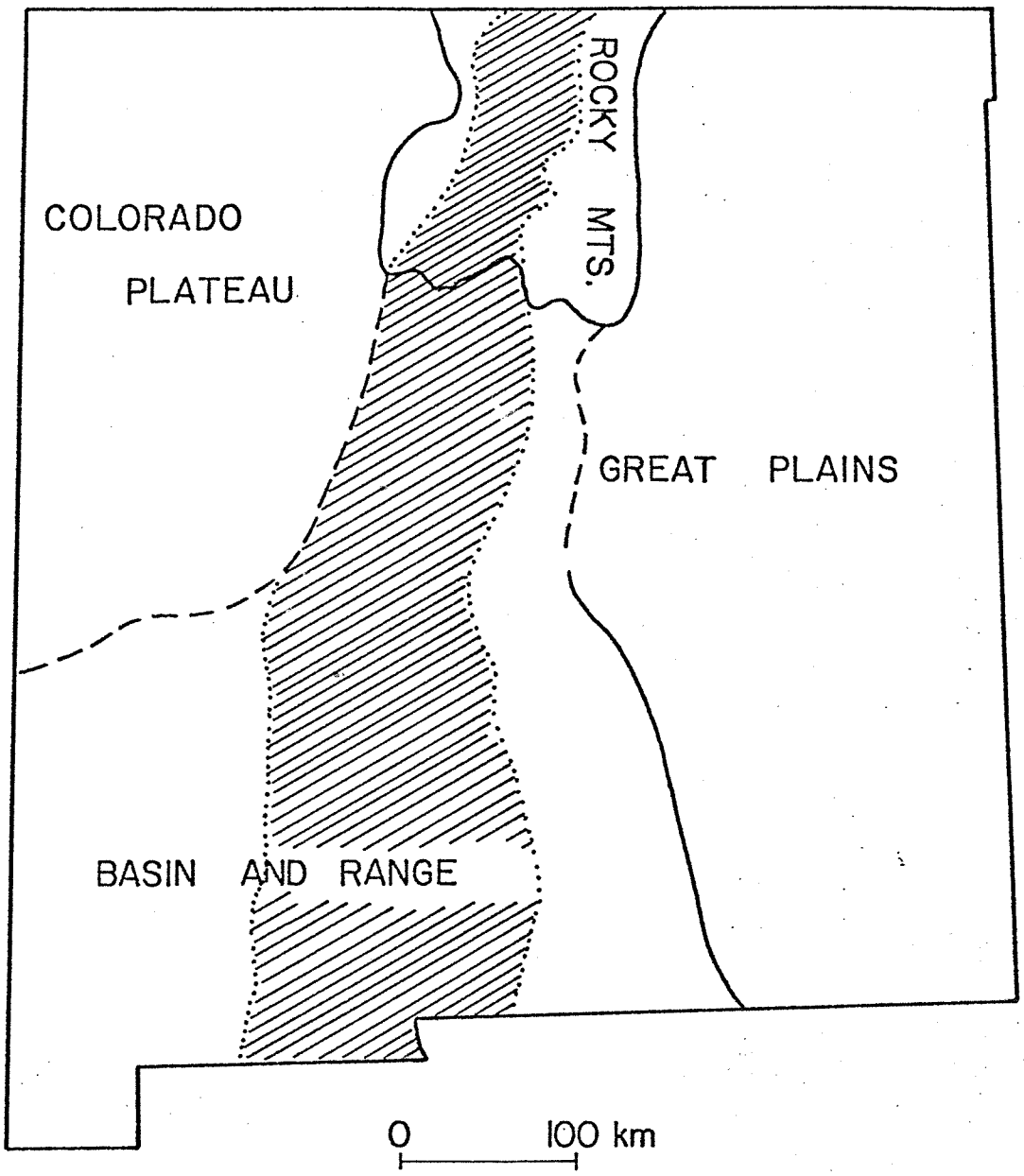

Figure 1.1. Physiographic provinces in New Mexico, after Fenneman (1946); Rio Grande rift is shaded, after Chapin (1971).

echelon structural depressions having raised margins (Kelley, 1952) extending from northern Mexico to central Colorado (Chapin, 1971). It is up to 150 km wide, at the southern end, and has up to 2.5 km of topographic relief, and up to 10.5 km of structural relief (Chapin, 1971).

A map of Late Cenozoic volcanic and sedimentary outcrops, showing the major faults within and bordering these rocks, appears in Figure 1.2. The v pattern indicates volcanic rocks, and the wavy pattern sedimentary rocks. This map shows that the preponderance of both young faulting and young volcanism falls within and west of the Rio Grande rift. Hot springs also occur mainly within the rift and to the west (Summers, 1965). Heat flow measurements conform to this pattern, showing low values to the east and high values in the rift and to the west (Hartman and Reiter, 1972; Smithson and Decker, 1972; Edwards *et al.*, 1973; Decker and Smithson, 1973; Reiter *et al.*, 1973).

Configuration of the Precambrian surface, below sea level, is shown in Figure 1.3. Precambrian outcrops appear to flank the rift at many places. The Precambrian surface generally becomes deeper away from the rift borders, producing deep sedimentary basins, such as the San Juan basin in the northwest and the Delaware basin in

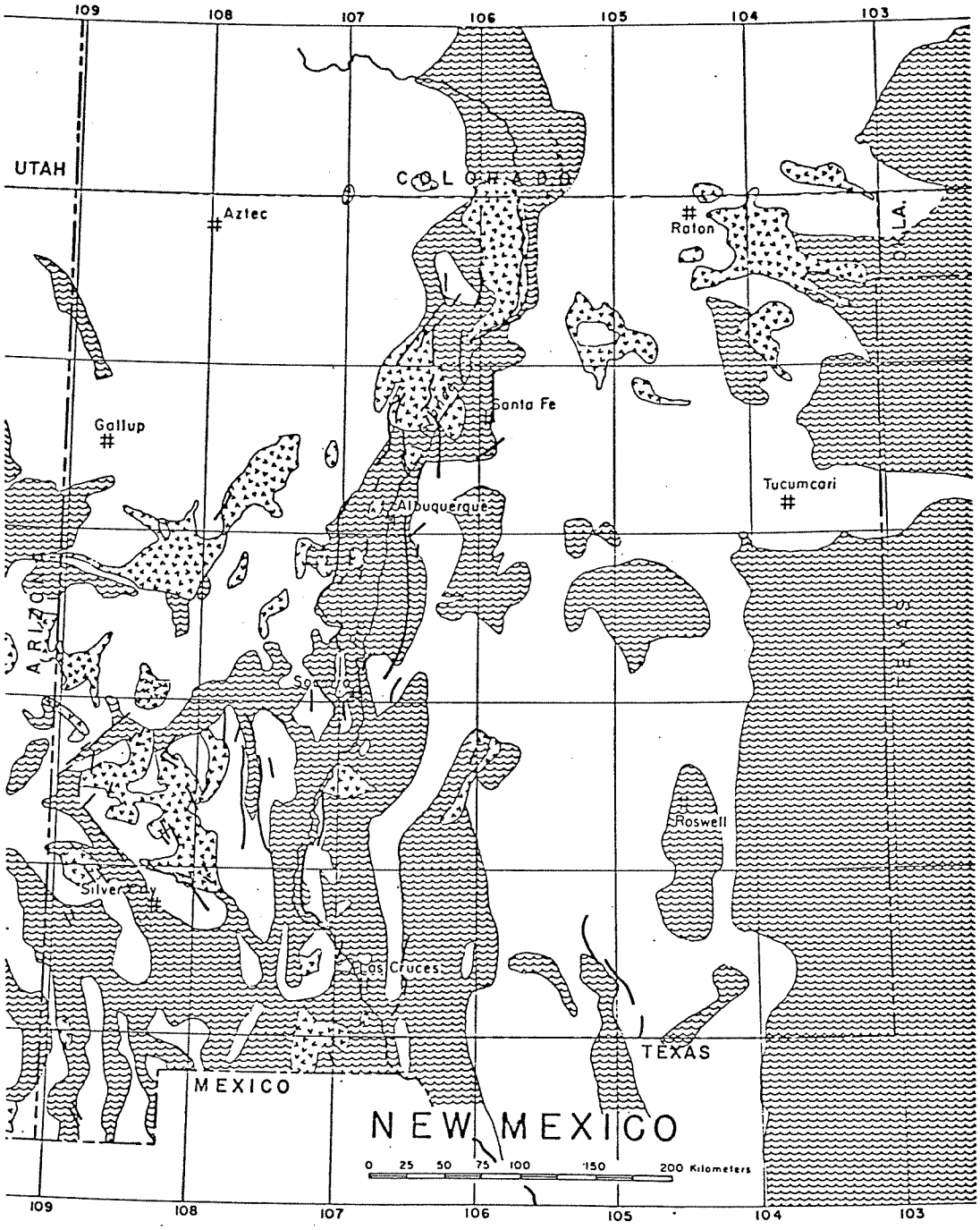

Figure 1.2. Outcrops of Late Cenozoic volcanic (v pattern) and sedimentary (wavy pattern) rocks, showing faults within and bordering these rocks. Simplified from Amer. Assoc. Petr. Geol., 1967; New Mexico Geol Soc., 1961; Dane and Bachman, 1965.

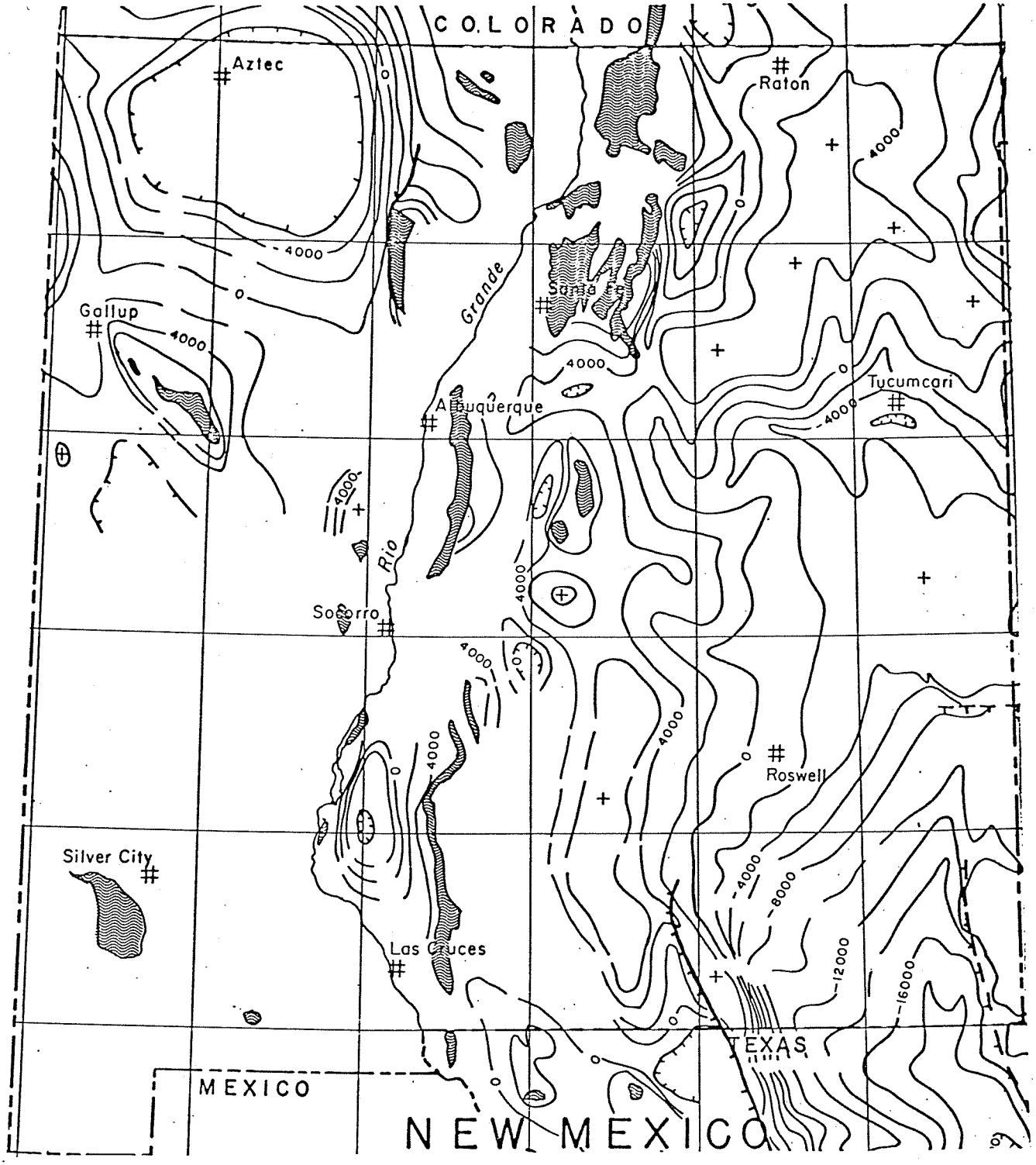

Figure 1.3. Depth of Precambrian surface below sea level; contour interval 2000'. Outcrops and major faults are shown. After Foster and Stipp (1961).

the southeast.

Conventions Adopted

The compressional seismic wave phases utilized in this study are defined following Pakiser (1963) and Hill (1971), as follows :

P_g first arrivals critically refracted or nearly critically refracted from the upper crystalline (granitic) horizon having a P-wave velocity of 6.0 $\pm$0.2 km/sec. When geologic corrections are applied to remove the sedimentary cover, P_g becomes a direct arrival. Earthquakes normally occur beneath the sedimentary cover, and P_g is the direct arrival for earthquakes.

P^* first arrivals critically refracted from a horizon of moderate depth (basaltic) having a P-wave velocity of 6.75 $\pm$0.25 km/sec. This horizon is generally called the Conrad discontinuity (Richter, 1958; Steinhart and Meyer, 1961).

P_n first arrivals critically refracted from the base of the crust or Mohorovicic discontinuity (Moho), having a P-wave velocity 7.9 $\pm$0.4 km/sec.

The velocities of these waves have been designated

as follows :

V_g for P_g
V^* for P^*
V_n for P_n

The average velocity of compressional waves in the rocks overlying the basement was designated V_0.

Method of Study and Presentation

Following this introductory section, a section is devoted to the review of previous investigations of crustal structure and upper mantle velocity in the area of study.

The third section is the largest in the dissertation, and deals with deriving a crustal model from a detailed interpretation of a long seismic refraction profile in central New Mexico.

The fourth section describes measurements of the P velocity in the uppermost mantle. The newly obtained values are then added to the values known from previous investigations, and a study is made of the regional variation in P_n velocity.

In the fifth section, the reversed values of P_n velocity are used to determine the dip of the Moho

surface. The dips are converted to differences in depth, and then into values of crustal thickness by extrapolating from points where the thickness is known. This information is added to that known from previous investigations, to map the regional variation in crustal thickness.

Finally, the concluding section summarizes the most important results obtained in the dissertation.

2. PREVIOUS WORK

This section is a historical review of crustal studies in New Mexico and surroundings. Derived crustal sections are listed, and maps of crustal thickness and upper mantle velocity are discussed.

Crustal Sections

Figure 2.1 is a map showing summary columnar sections of the earth's crust. All known sections within New Mexico and a strip 200 km wide surrounding the state appear in this figure. Beyond this strip, only the most significant sections are shown.

In Figure 2.1, the crust was divided into upper and lower layers to simplify representation. The lower crust was arbitrarily taken to have a P wave velocity of 6.5 km/sec or greater, and is shaded in Figure 2.1. The sections are numbered chronologically, and are located with their tops at the respective shot points. All the sections were derived from seismic refraction profiles, except section Number 8. This section was based on spectra of ground motion recorded on long period seismographs. The ranges of thickness for the upper and lower crust given by this method are plotted.

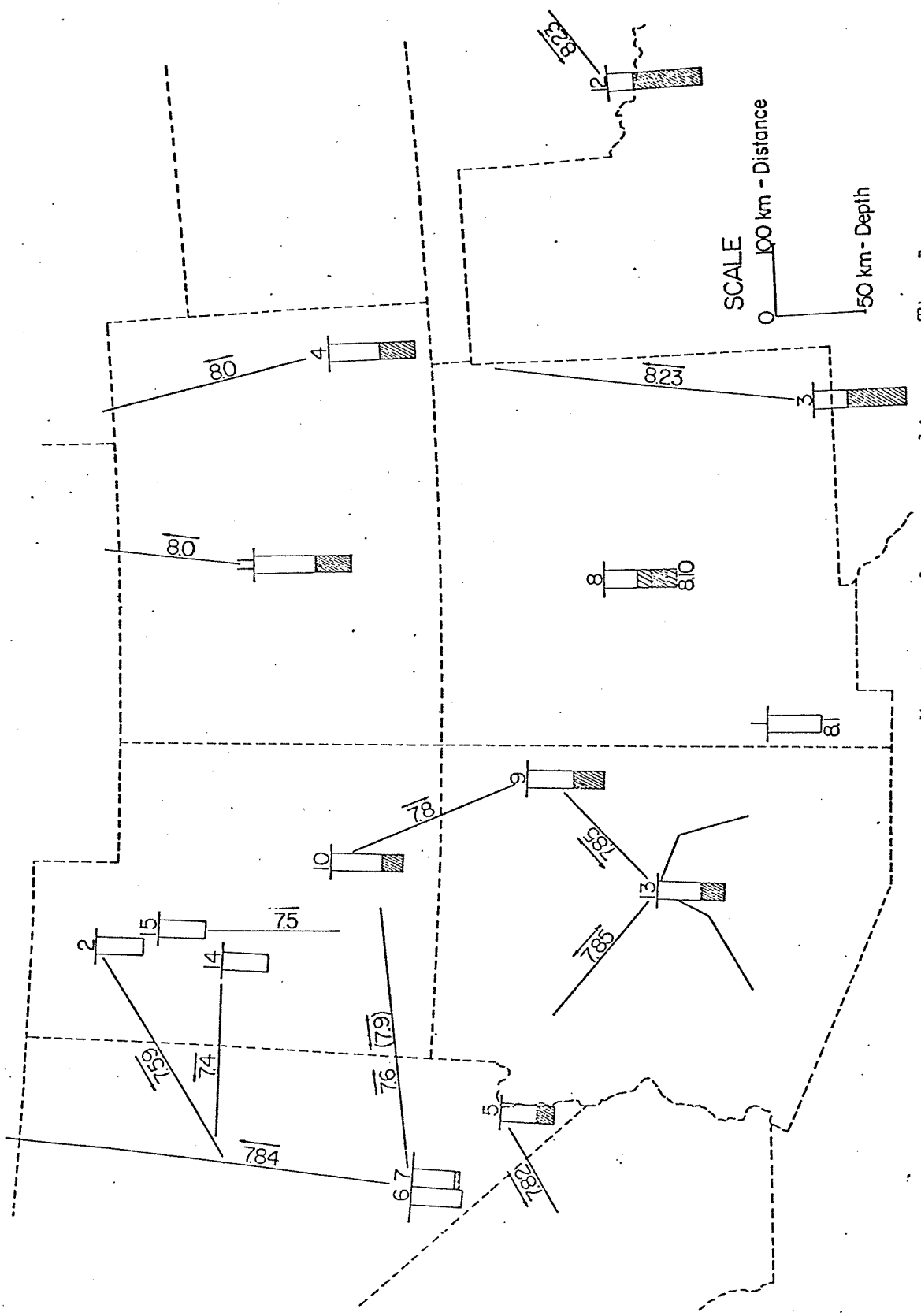

Figure 2.1. Crustal sections in New Mexico and surroundings. The lower crust is shaded, and P_n velocity is given.

The direction of the profiles issuing from the various shot points is indicated in the figure. The numbers on the profiles are the values of the P_n velocity and the arrows indicate the direction of coverage. The reference for section 1 does not give a specific trend for the seismic profile, and section 8 had no profile. Consequently, for sections 1 and 8, the P_n velocity is given at the base of the crust in Figure 2.1.

Several observations can be made from Figure 2.1 :

(1) The crust is thick in western Oklahoma, eastern New Mexico, and in Colorado. In general, the crust becomes thinner going to the west and southwest. The crust is thin in southwestern New Mexico, southern Nevada, and northwestern Utah.

(2) The lower crust becomes thinner as the total crustal thickness is reduced, and eventually it disappears where the crust is thinnest.

(3) Upper mantle velocity is highest in eastern New Mexico and western Oklahoma, and lowest in northern Utah.

Table 2.1 gives the reference for each crustal section in Figure 2.1. The sections are given in detail in Table 2.2, which provides the thicknesses and

Table 2.1. References for Crustal Sections

1. Tatel, and Tuve, 1955.
2. Berg, Cook, Narans, and Dolan, 1960.
3. Stewart, and Pakiser, 1962.
4. Jackson, Stewart, and Pakiser, 1963.
5. Roller, and Healy, 1963.
6. Pakiser, and Hill, 1963.
7. Ryall, and Stuart, 1963.
8. Phinney, 1964.
9. Roller, 1965.
10. Roller, 1965.
11. Jackson, and Pakiser, 1965.
12. Tryggvason, and Qualls, 1967.
13. Warren, 1969.
14. Mueller, and Landisman, 1971.
15. Keller, Smith, and Braile, 1973.

Table 2.2. Detail of Crustal Sections, Numbered According to Figure 2.1.

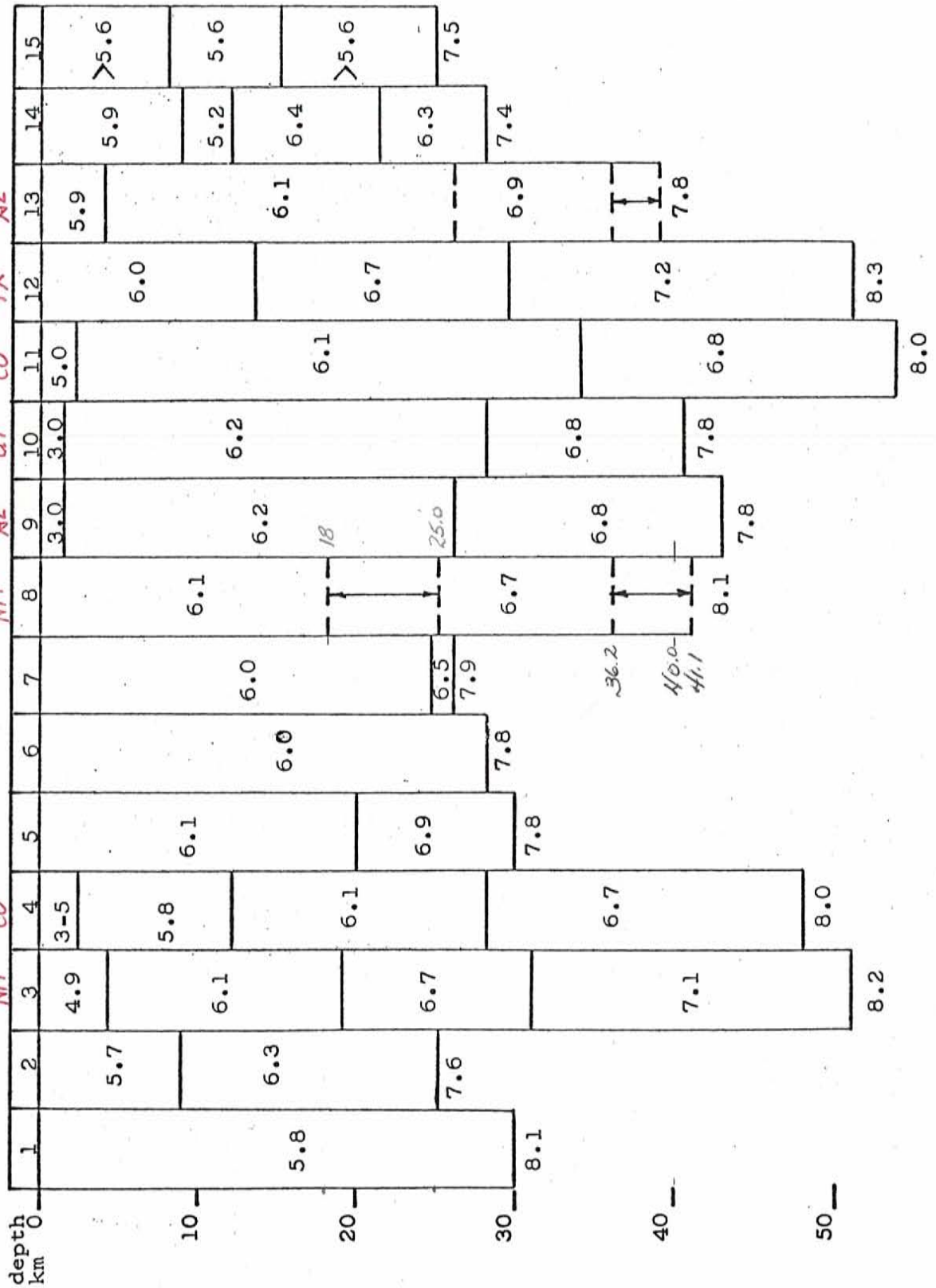

P wave velocites for the various layers in each section. Sections 14 and 15 both have low velocity layers within the crust. The detection of such layers cannot come from refraction data alone, but requires supplementary reflection information.

Regional Maps of Crustal Thickness and P_n Velocity

Generalized contour maps of crustal thickness and of P_n velocity have been compiled by various investigators. These maps are based largely on data of the same type as those listed in the previous subsection.

Crustal Thickness

Figure 2.2 is a map published by Stuart, Roller, Jackson and Mangan in 1964. The control points appearing on this map illustrate the scarcity of data upon which such maps are based. For New Mexico this map shows a southwestward thinning of the crust, from more than 50 km in the northeast to less than 30 km in the southwest. Pakiser and Zeitz (1965) also published a map of crustal thickness for the United States, which does not indicate the control points used. Their map resembles that of Stuart *et al.* (1964) for northeastern New Mexico, but indicates that the crust is about 10 km thicker than that shown in Figure 2.2 in southern and southwestern New Mexico.

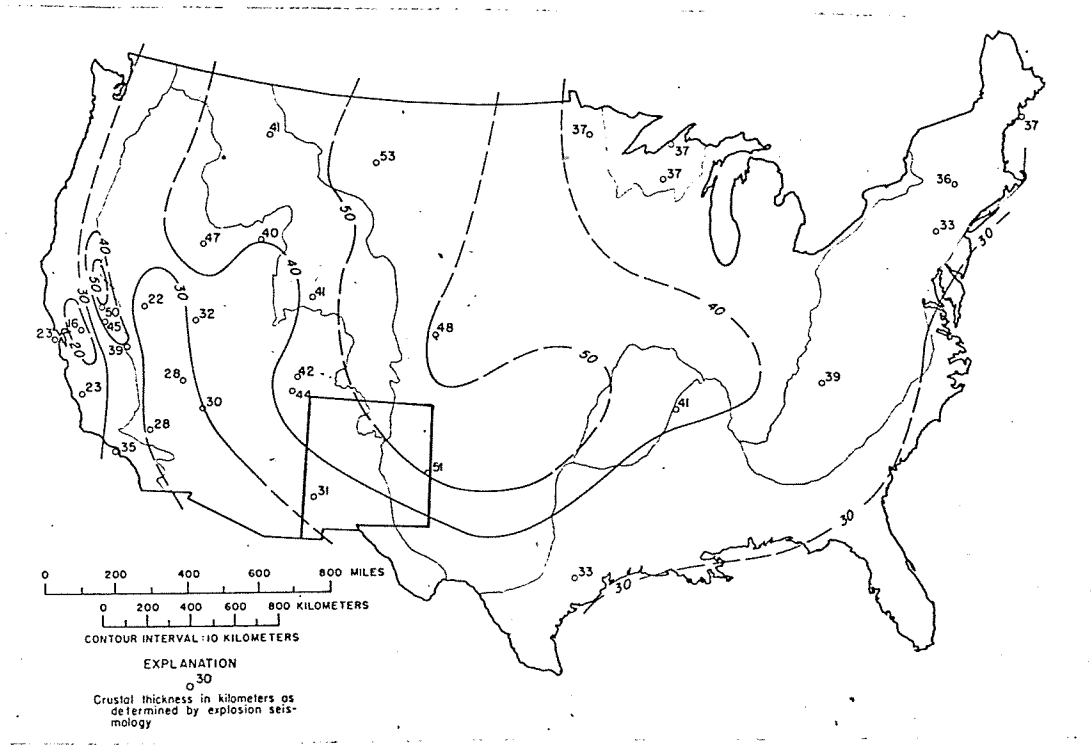

Figure 2.2. Crustal thickness in the United States, after Stuart et al. (1964).

P_n Velocity

In 1962, Herrin and Taggart published a map showing the variation of P_n velocity across the United States, reproduced here as Figure 2.3. This map was based on the interval velocity data shown in Figure 2.4, as well as data from small explosions (Berg et al., 1960; Diment et al., 1961; Ryall, 1962; and Steinhart and Meyer, 1961). Figure 2.4 illustrates the general sparsity of data, and the lack of reversed velocities in the vicinity of New Mexico. Herrin updated the P_n velocity map in 1966. The updated map was published by James and Steinhart in 1966, and by Herrin in 1969. It is reproduced here as Figure 2.5, and for the area surrounding New Mexico, it resembles a subdued version of the original map, Figure 2.3.

Stuart, Roller, Jackson and Mangan (1964) published a map of P_n velocity, reproduced here as Figure 2.6. This map agrees with Figure 2.5 in the northeastern half of New Mexico. But in the southwestern corner of the state there is strong disagreement. Figure 2.5 indicates a velocity of 8.0 km/sec, whereas Figure 2.6 indicates a velocity less than 7.8 km/sec for southwestern New Mexico.

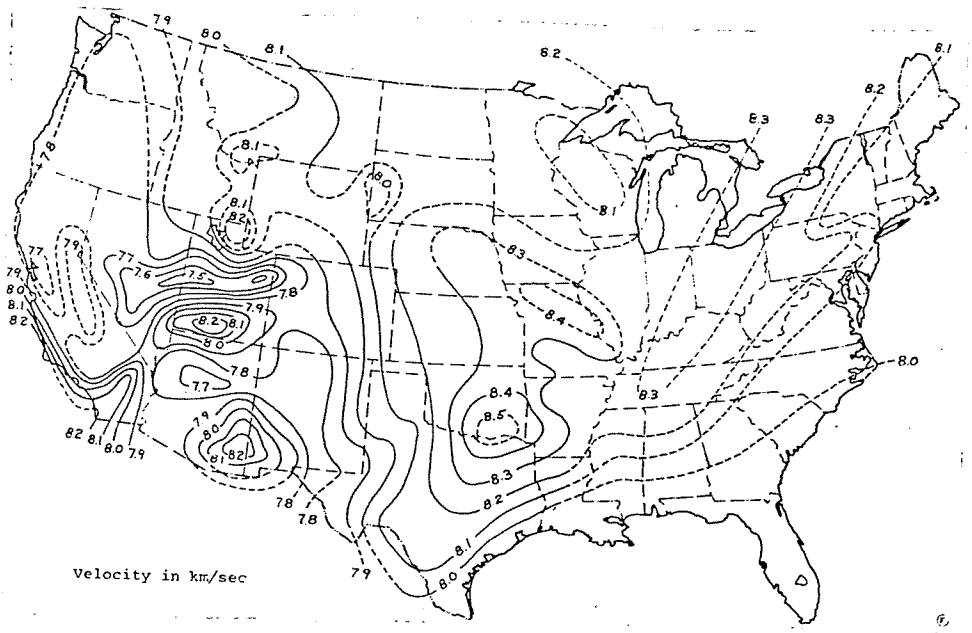

Figure 2.3. P_n velocities in the United States, after Herrin and Taggart (1962).

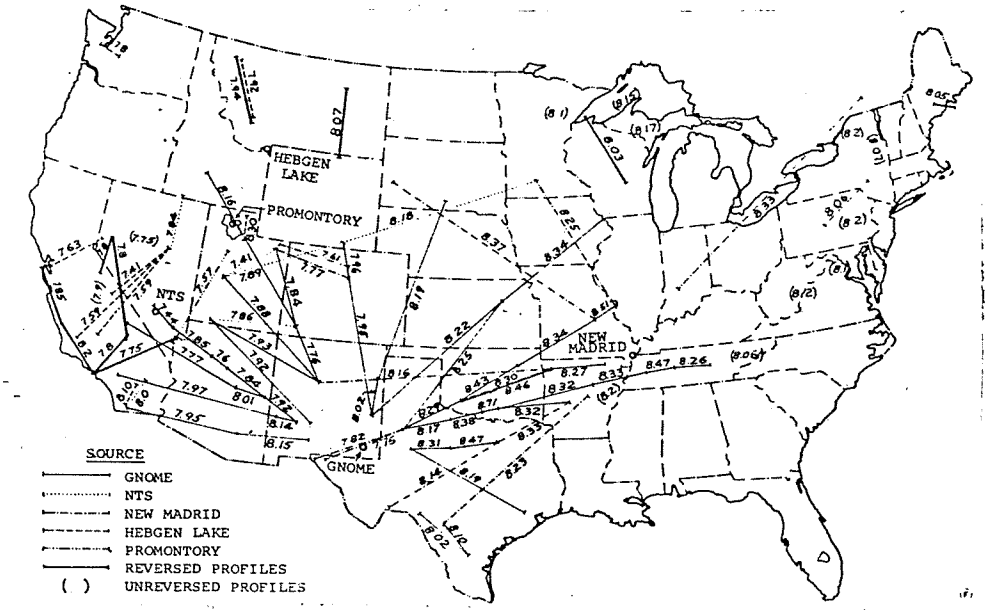

Figure 2.4. P_n interval velocity data for the United States, after Herrin and Taggart (1962).

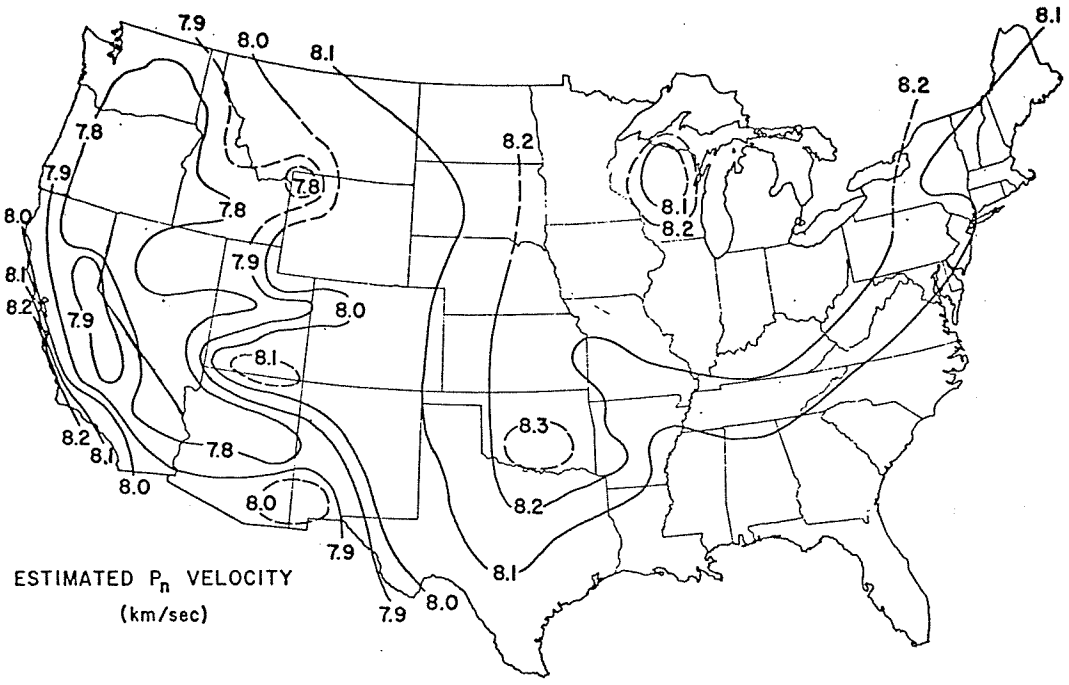

Figure 2.5. P_n velocities in the United States, after Herrin (1969).

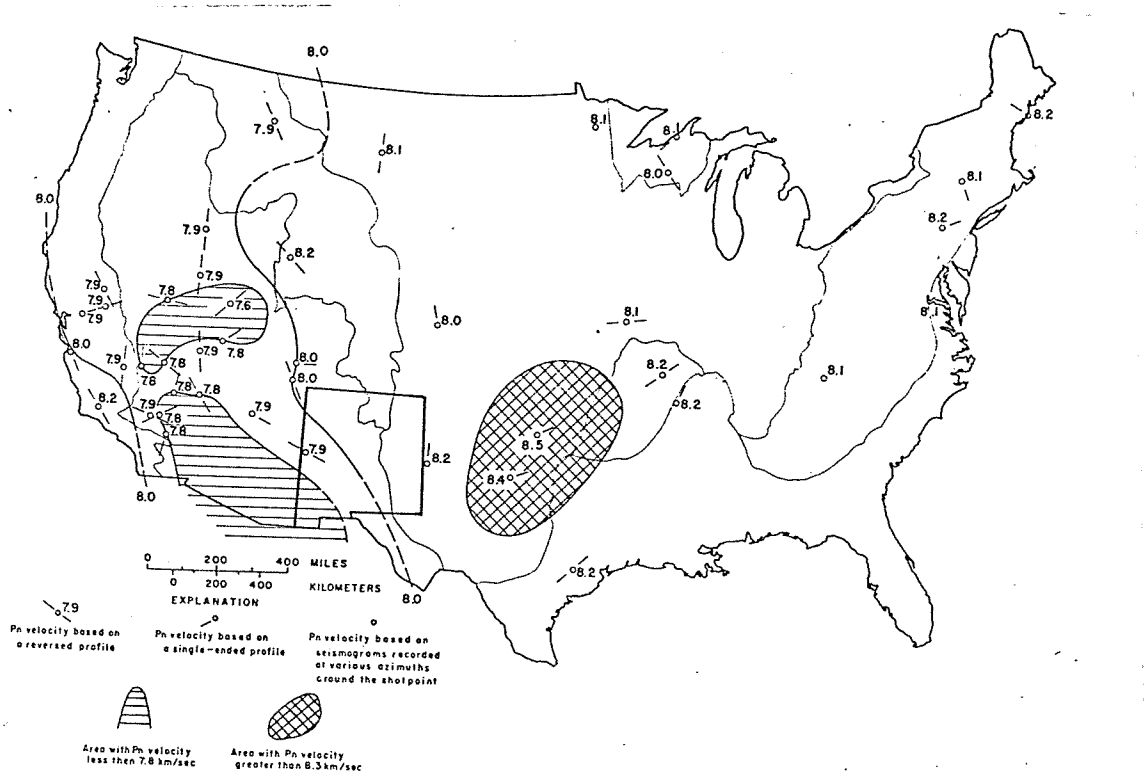

Figure 2.6. P_n velocities in the United States, after Stuart et al. (1964).

Summary

The regional maps discussed above are clearly based on scanty data, especially in New Mexico. Consequently, the differences between them are probably caused by differences in interpretation and interpolation. The present study will add a crustal section in northwestern New Mexico, and 30 values of apparent V_n' from measurements of interval velocity. Values of P_n velocity along reversed paths will be used to determine the configuration of the base of the crust. This new control data provides added constraints on the interpretation of crustal structure and upper mantle velocity in and near the state of New Mexico.

3. GASBUGGY SOUTH PROFILE

On the 10th of December 1967 a nuclear test, Gasbuggy, occurred in northwestern New Mexico, to stimulate the production of oil and gas. Information on this event, e.g. location, origin time, etc., appears in Table 3.1. Five seismic profiles were set up radiating from the site, to the north, west, southwest, south and east, as shown in Figure 3.1. Of these, the southern profile was the best instrumented, and consisted of 16 stations extending out to 548 km from the shot. This profile was interpreted, and a model was derived for the earth's crust in central New Mexico.

Geology and Physiography

The shot was located in the San Juan sedimentary basin of northwestern New Mexico, to the west of the southern Rocky Mountains.

The physiographic boundary between the southern Colorado Plateau and the Basin and Range, according to Fenneman (1946), is indicated by a dashed line in Figure 3.1. The southern profile traverses this boundary some 200 km from the shot, and enters the Rio Grande rift where it remains till its termination

Table 3.1. Gasbuggy Explosion Parameters

Date	10 December 1967
Time	19:30:00.1 U.T.
Latitude	36°40'40.4"N
Longitude	107°12'30.3"W
Elevation of surface ground zero	2194 meters
*Depth to top of Paleozoic	4023 meters
Depth of emplacement	1292 meters
Thickness of Post Paleozoic rocks below shot	2731 meters
Environment of emplacement	Shale
Yield	26 kilotons
Body wave magnitude (m_b)	5.2

*Based on extrapolation from known depth 10 km away, using regional dip

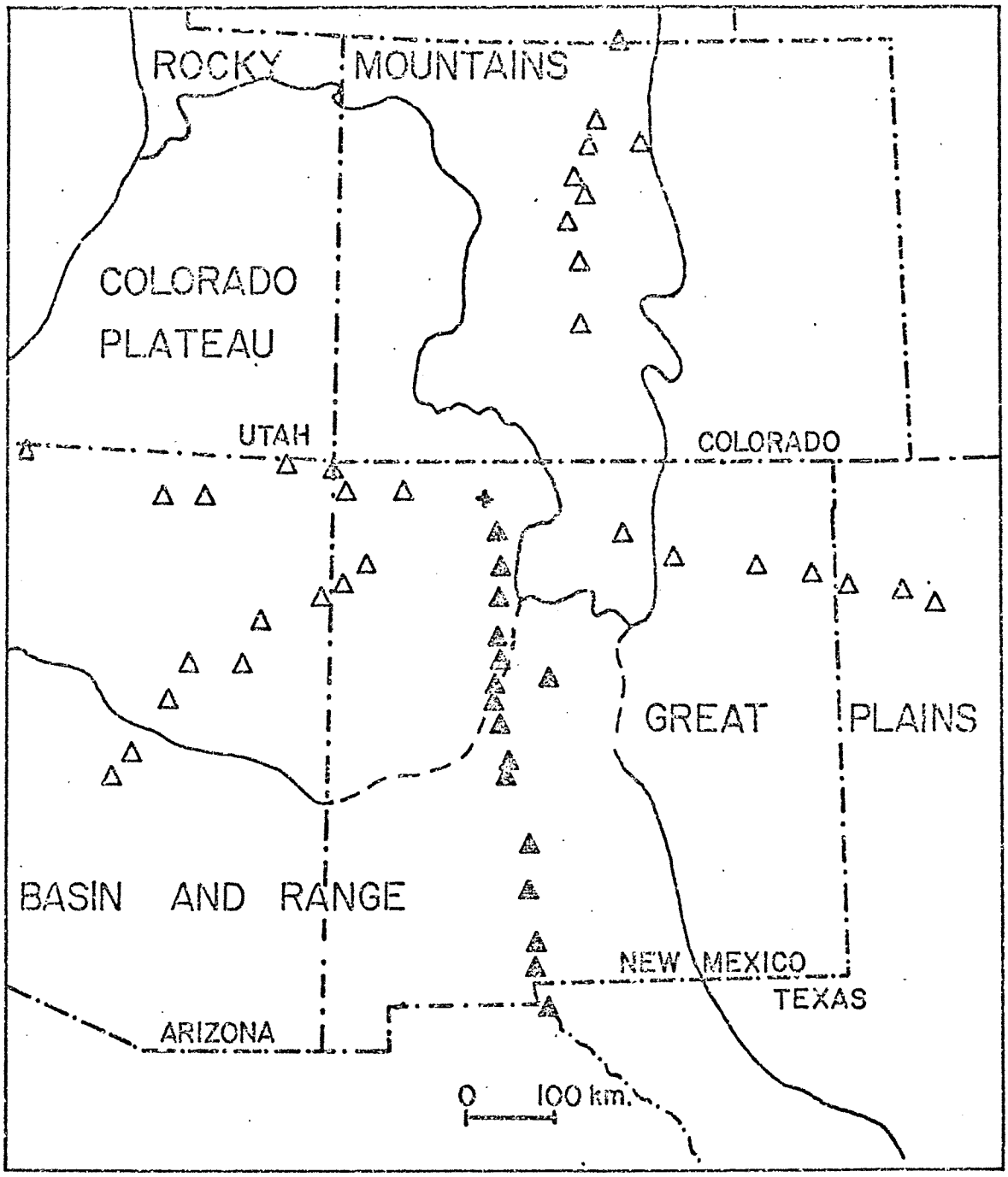

Figure 3.1. Location of the Gasbuggy test site (marked +). Triangles are seismographs within 550 km of the site. Solid triangles indicate southern profile. Physiographic divisions after Fenneman, 1946.

at El Paso.

Figure 3.2 shows the location of stations along the southern profile, and a simplified outline of the Rio Grande rift (Chapin, 1971). Inside the rift, the seismograph stations were placed on intrarift horsts, to avoid delays and distortion of the seismic signal (E.S.S.A.-C.G.S., 1968) from thick sedimentary deposits.

Previous Work

Warren and Jackson (1968) studied travel times and amplitudes of first arrivals on the U.S.G.S. profiles, to the north, west, southwest and east, and for 3 stations on the south profile. They made no detailed interpretation of crustal structure, but simply presented their arrival times as plots consisting of linear segments. Their travel time plots had a maximum of 8 data points each, and were not corrected for geologic effects. Intercept times and slopes from these plots were used here to produce the layering presented in Table 3.2 for the various profiles. The salient features of this model are a single layer crust having P velocity 6.4 km/sec, overlying a mantle having P velocity 7.9 km/sec, with a jump to 8.4 km/sec some 25 km below the Moho. Beneath the shot point, the Moho dips about 4^{o} to the north. Their amplitude measurements showed

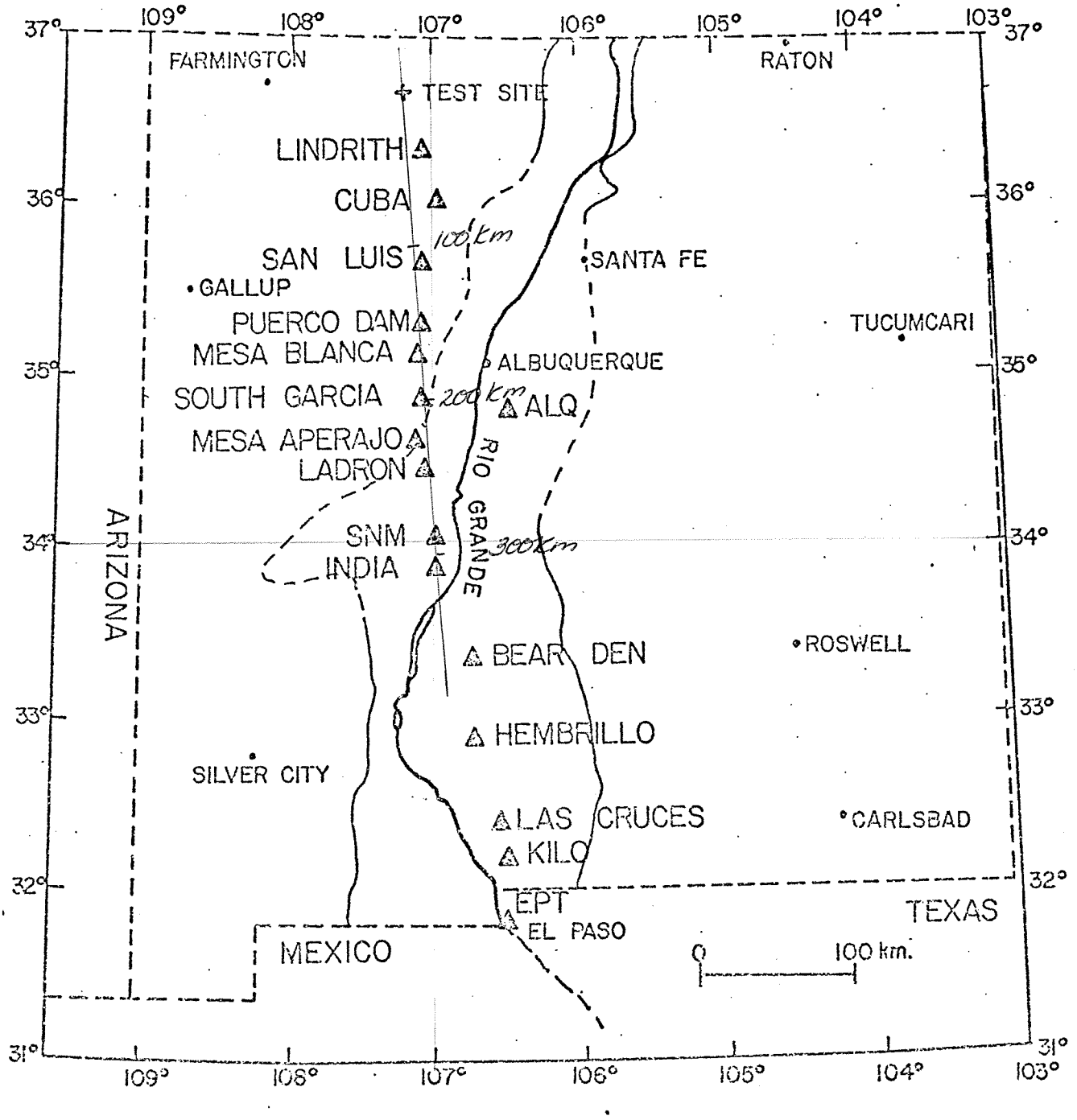

Figure 3.2. Gasbuggy south profile showing seismograph stations. Outline of the Rio Grande rift is simplified from Chapin, 1971.

Table 3.2. Crustal Structure Derived from Warren and Jackson's (1968) Travel Time Curves for the 5 Gasbuggy Profiles.

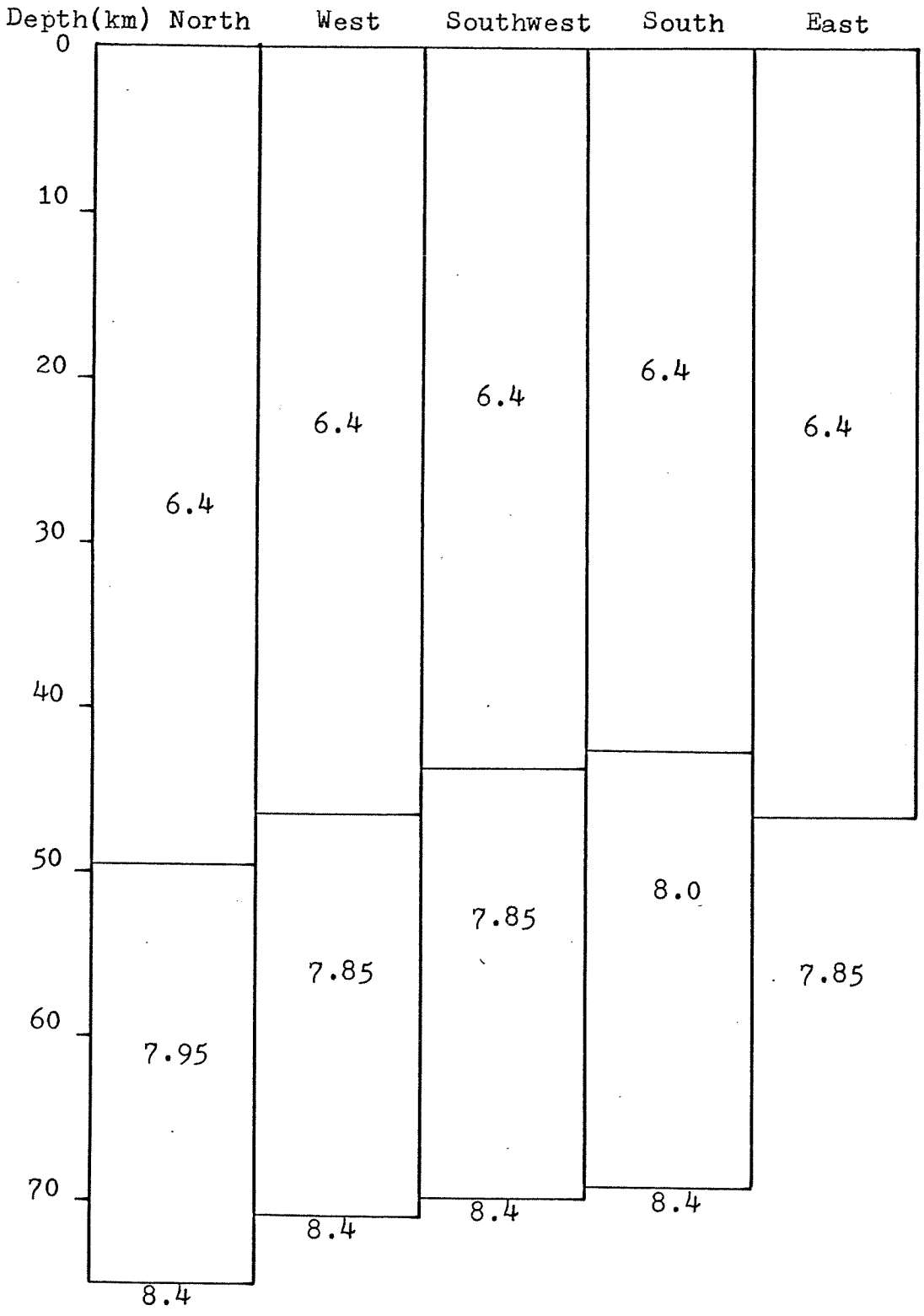

considerable scatter, and yielded no conclusions.

Lee and Borcherdt (1968) studied the P_n spectral variations at 300 km and 500 km on all 5 profiles. They found much higher spectral energies to the southwest and north, than to the east and south. This indicates that the crust and uppermost mantle are more rigid, and transmit elastic energy more efficiently to the southwest and north, than to the east and south.

Reagor, Gordan and Jordan (1968) made a general seismic analysis of the explosion out to teleseismic distances. Their data from all azimuths suggest a two-layer crust, with an upper layer 7.1 km thick having P velocity 5.34 km/sec and a lower layer 26.2 km thick having P velocity 6.29 km/sec, overlying a mantle with P velocity 7.9 km/sec. This model differs considerably from Warren and Jackson's (1968). Their amplitude contours indicate more efficient transmission of P_n to the east and west than to the north and south. Their velocity residuals show a high P_n velocity along the south profile. This could result from a progressively thinner crust in this direction, producing smaller delays for the P_n wave. On comparing the teleseismic results of Gasbuggy to those of the earlier Gnome explosion in southeastern New Mexico, they found that whereas Gnome showed lower amplitudes and velocities to the west than

to the east, Gasbuggy showed equal amplitudes and a smaller velocity difference in the east-west direction.

Data Used

Analog Seismograms

Table 3.3 lists information on the stations along the profile. Analog seismograms for all stations listed were available. The United States Department of Commerce, Environmental Science Services Administration, Coast and Geodetic Survey (E.S.S.A.-C.G.S., 1968) published seismograms for 13 stations on the profile. Tracings of the two U.S.G.S. seismograms were obtained from the National Center for Earthquake Research, Menlo Park, California. The sixteenth seismogram was from a Long Range Seismic Measurements (L.R.S.M.) station, and was obtained from Geotech-Teledyne with the approval of the Air Force Technical Applications Center (A.F.T.A.C.), Alexandria, Virginia.

Table 3.3 shows that the time bases of the available reproductions ranged from 1.00 mm/sec to 25.27 mm/sec. First arrivals were generally good, and could be timed with confidence to 0.1 sec using the times standards on the seismograms. Seismograms for the two U.S.G.S. stations at India and Kilo were low gain

Table 3.3. Information on Seismograph Stations along the South Profile

Station	Operator	Latitude[+] (North)	Longitude[+] (West)	Distance[*] (km)	Elevation (meters)	Paper Rate[**] (Millimeters/sec)
Lindrith	CGS	36.304	107.044	44.09	2210	12.55
Cuba	CGS	36.021	106.958	76.34	2103	12.65
San Luis	CGS	35.680	107.050	111.71	1905	4.04 , 24.20
Puerco Dam	CGS	35.320	107.039	151.5	1761	4.54 , 19.40
Mesa Blanca	CGS	35.161	107.039	169.06	1804	4.83 , 20.60
South Garcia	CGS	34.877	107.084	200.19	1626	4.86 , 20.77
Albuquerque	CGS	34.942	106.458	204.25	1844	1.00
Mesa Aparejo	CGS	34.676	107.106	222.36	1798	4.03 , 17.20
Ladron	CGS	34.461	107.033	246.53	1737	6.35
Socorro	CGS	34.073	106.945	290.03	1554	1.48
Socorro	NMIMT	34.070	106.943	290.37	1511	25.27
India[++]	USGS	33.973	106.954	301.60	1605	24.07
Bear Den	CGS	33.368	106.656	370.65	1631	6.28
Hembrillo	CGS	32.885	106.681	423.51	1653	6.38

Table 3.3 (continued)

Station	Operator	Latitude[+] (North)	Longitude[+] (West)	Distance[*] (km)	Elevation (meters)	Paper Rate[**] (Millimeters/sec)
Las Cruces	AFTAC	32.402	106.599	477.56	1591	2.82 , 11.80
Kilo[++]	USGS	32.307	106.596	499.65	1417	24.07
El Paso	U.of Tex.	31.772	106.505	547.92	1219	1.00 , 6.26

[+] From E.S.S.A.-C.G.S. (1968).

[++]India and Kilo were seismometer spreads, coordinates listed are for the seismometer used in timing.

[*] Calculated using the geodetic formulas of Ball (1972).

[**]First number is rate on available seismograms, second number is rate after photographic enlargement, if any.

tracings, consequently their first arrival times were taken from Warren and Jackson (1968).

Digitizing

Vertical component seismograms were digitized in order to control amplitudes and time bases, and to construct a record section for the purpose of interpretation. To facilitate digitizing, records with low recording speeds were photographically enlarged. This was not possible for the Albuquerque (ALQ) seismogram because of the very large amplitudes on the record. Of the two systems operating at SNM, the N.M.I.M.T. seismogram was digitized because it had a higher recording speed.

Digitizing was performed with a Hewlett-Packard Model 9864A digitizer using a sampling rate that varied from 4 to 20 samples per cycle according to the complexity of the signal. The digital data was read from a paper tape printout and punched on cards for input to a computer and subsequent plotting at prescribed time bases and amplitudes.

Geologic Corrections

Selection of Datum

According to the E.S.S.A.-C.G.S. (1968, p.3)

field report,

> "... it was possible to place stations from Garcia southward on Paleozoic formations having rather uniform physical properties. The one exception is the Ladron site which is located on intrusive rocks of Tertiary Age at the foot of Ladron Mountain."

Consequently it was decided to correct the travel times to what they would be if the shot and all stations were on Paleozoic "basement" rocks. The implied assumption that velocities in the Paleozoic section (mostly sandstone and limestone) are not drastically different from those in Precambrian rocks, is reasonable.

Figure 3.3 is a schematic crustal model for making the corrections to datum. Effectively these geologic corrections remove the V_0 layer and place the shot and all detectors on basement, which is the upper surface of the V_g layer. Basement elevation has no effect on the P_g arrival which travels parallel to this surface, but it does affect the P_n arrival whose ray path is shown in the figure. However, the maximum basement relief from South Garcia, where P_n emerges as a first arrival, to the end of the profile is only 0.625 km, which is the topographic relief from Table 3.3. This causes a delay on the order of 0.01 sec, which is smaller than the timing accuracy. Consequently no correction was

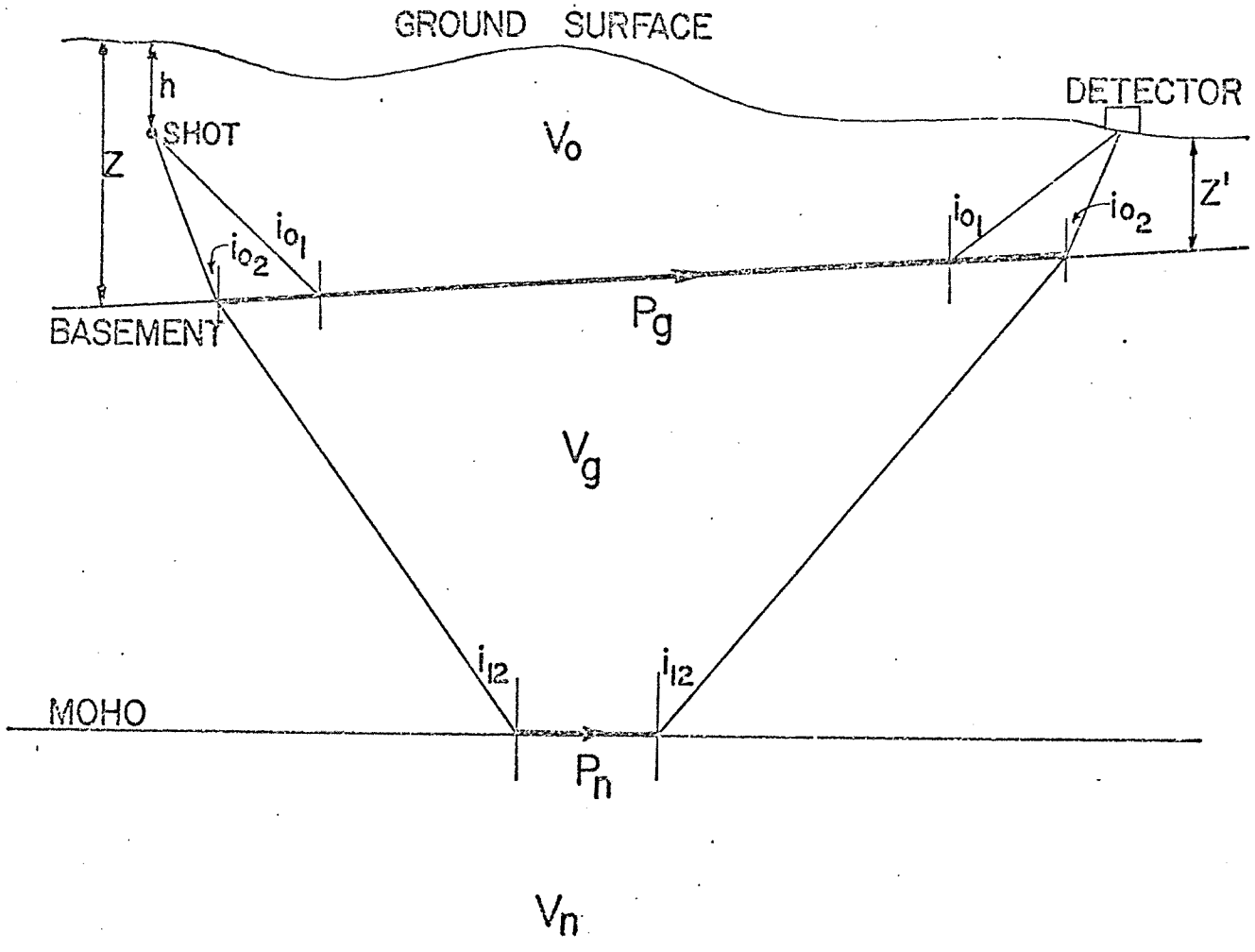

Figure 3.3. Schematic crustal model used in making the geologic corrections. Depth of shot, thickness of the overburden, and critical angles are indicated.

made for difference in basement elevation.

Method Employed

Corrections to the basement surface were made using the principle of delay times (Nettleton, 1940). Referring to Figure 3.3 the correction at the shot for P_g is

$$\frac{(Z-h)\cos i_{01}}{V_0}$$

and for P_n is

$$\frac{(Z-h)\cos i_{02}}{V_0}$$

The correction at the station for P_g is

$$\frac{Z'\cos i_{01}}{V_0}$$

and for P_n is

$$\frac{Z'\cos i_{02}}{V_0}$$

The angles are given by

$$i_{01} = \arcsin V_0/V_g$$
$$i_{02} = \arcsin V_0/V_n$$
$$i_{12} = \arcsin V_g/V_n$$

The parameters in the above equations were evaluated as follows. Depth of shot h was known (Table 3.1). The thicknesses Z and Z' of Post-Paleozoic

rocks beneath the shot and each detector were estimated from the logs of deep wells, and from depths to the Precambrian surface (Foster and Stipp, 1961).

First estimates of V_g and V_n, obtained from linear least squares fits of the raw travel times, were 6.29 and 8.12 km/sec respectively. The E.S.S.A.-C.G.S. (1968) report states that the El Paso time is questionable, consequently this time was excluded from the least squares fitting.

An estimate of V_0 based on sonic logs of deep wells close to the northern end of the profile was about $3\frac{1}{2}$ km/sec. A better estimate of the average V_0 was obtained knowing Z, h, V_g and T_i. The latter is the zero distance intercept of the P_g raw travel times (see Figure 3.4), resulting from the section of rocks above basement. This estimate was based on the following equation (Nettleton, 1940, p. 250):

$$2Z-h = T_i \cdot \frac{V_g V_0}{(V_g^2-V_0^2)^{\frac{1}{2}}}$$

whence,

$$V_0 = \left(\frac{V_g^2 \cdot (2Z-h)^2}{V_g^2 T_i^2 + (2Z-h)^2} \right)^{\frac{1}{2}}$$

The value of V_0 obtained in this way was 3.47 km/sec, and was used in making the corrections.

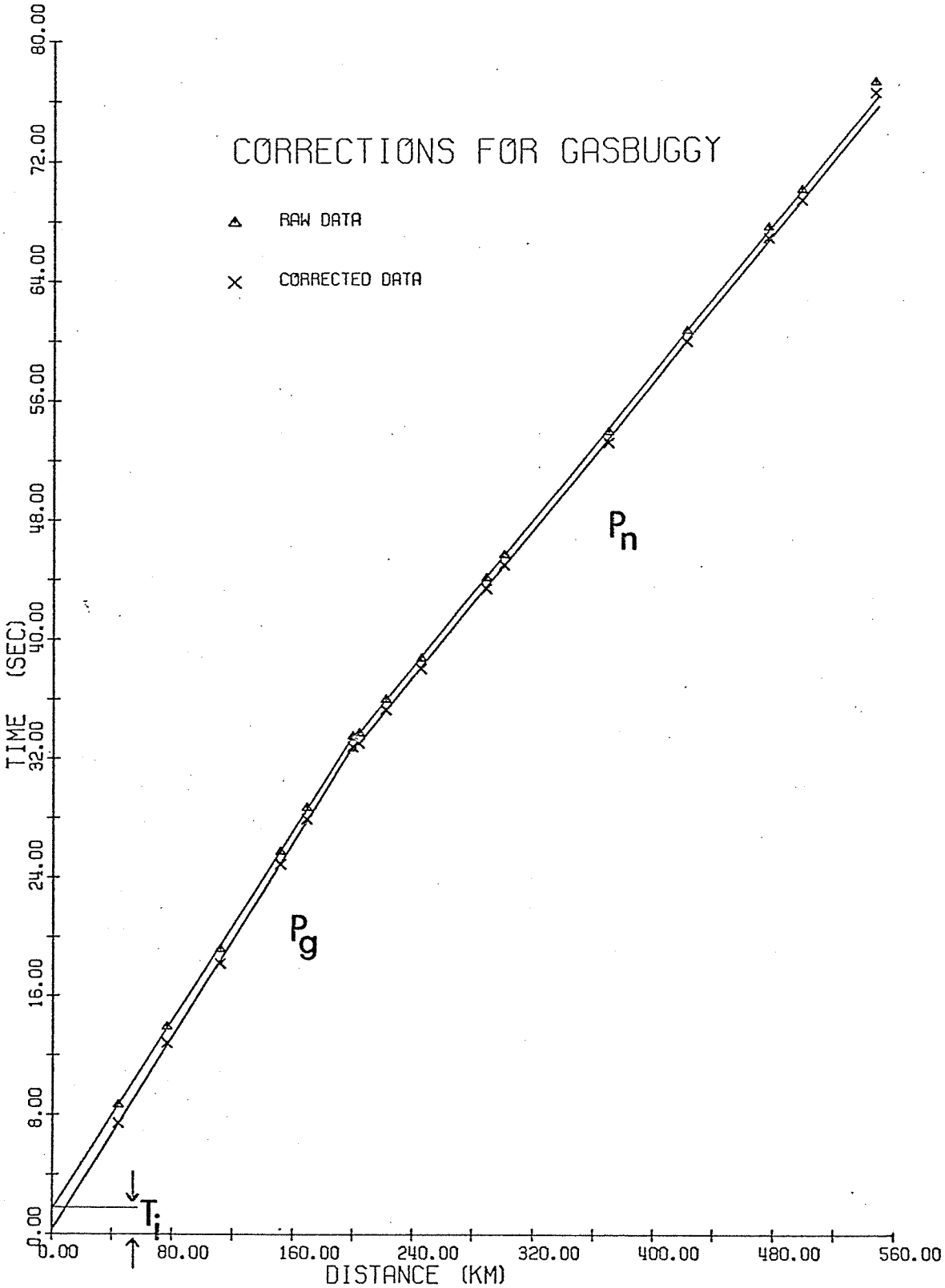

Figure 3.4. Linear least squares fits of raw and corrected P_g and P_n arrival times. Ti is the intercept time of the raw arrivals.

After making the geologic corrections, second estimates of V_g and V_n obtained from linear least squares fits of the corrected travel times were 6.15 and 8.12 km/sec respectively.

Table 3.4 summarizes the geologic corrections, listing station name, distance from shot, time of first arrival, thickness of rocks overlying the basement, shot correction, station correction, total correction, and finally the corrected arrival time. Ladron was given zero station correction due to its close proximity to basement. Figure 3.4 is a graph of first arrival travel times versus distance, showing linear least squares fits of the raw and corrected data. The P_g intercept time, T_i, was reduced from 1.62 sec to 0.25 sec after the geologic corrections were applied. This confirms the correctness of the value of V_0 employed. The computer program used in making the geologic corrections is given in Appendix I.

Record Section

A reduced time scale (T minus delta/6) was used for the record section shown in Figure 3.5. This reduced scale improves time resolution and emphasizes differences in velocity near 6 km/sec. The small circle at 204 km is the corrected ALQ arrival time, which was included in the

Table 3.4. Arrival Times and Geologic Corrections for the Gasbuggy Profile

Station	Delta (km)	Observed Arrival Time(sec)	Depth to Basement (km)	Shot Correction (sec)	Station Correction (sec)	Total Correction (sec)	Corrected Arrival Time (sec)
Lindrith	44.090	8.660	2.377	0.656	0.571	1.226	7.434
Cuba	76.340	13.900	1.829	0.656	0.439	1.095	12.805
San Luis	111.710	19.100	1.158	0.656	0.278	0.934	18.166
Puerco Dam	151.500	25.700	0.823	0.656	0.198	0.853	24.847
Mesa Blanca	169.060	28.630	0.427	0.656	0.103	0.758	27.872
South Garcia	200.190	33.470	0.0	0.708	0.0	0.708	32.762
Albuquerque	204.250	33.700	0.0	0.708	0.0	0.708	32.992
Mesa Aparejo	222.360	35.980	0.0	0.708	0.0	0.708	35.272
Ladron	246.530	38.730	0.0	0.708	0.0	0.708	38.022
Socorro	290.150	44.120	0.0	0.708	0.0	0.708	43.412
India	301.600	45.690	0.0	0.708	0.0	0.708	44.982
Bear Den	370.650	53.960	0.0	0.708	0.0	0.708	53.252
Hembrillo	423.510	60.660	0.0	0.708	0.0	0.708	59.952

Table 3.4 (continued)

Station	Delta (km)	Observed Arrival Time(sec)	Depth to Basement (km)	Shot Correction (sec)	Station Correction (sec)	Total Correction (sec)	Corrected Arrival Time (sec)
Las Cruces	477.560	67.600	0.0	0.708	0.0	0.708	66.892
Kilo	499.650	70.090	0.0	0.708	0.0	0.708	69.382
El Paso	547.920	77.200	0.0	0.708	0.0	0.708	76.492

Figure 3.5. Gasbuggy record section. First arrivals having velocities 6.15 and 8.12 km/sec are P_g and P_n. Late arrivals having velocities 6.5 and 5.8 km/sec were picked from this record section. The circle at 204 km is the ALQ arrival time.

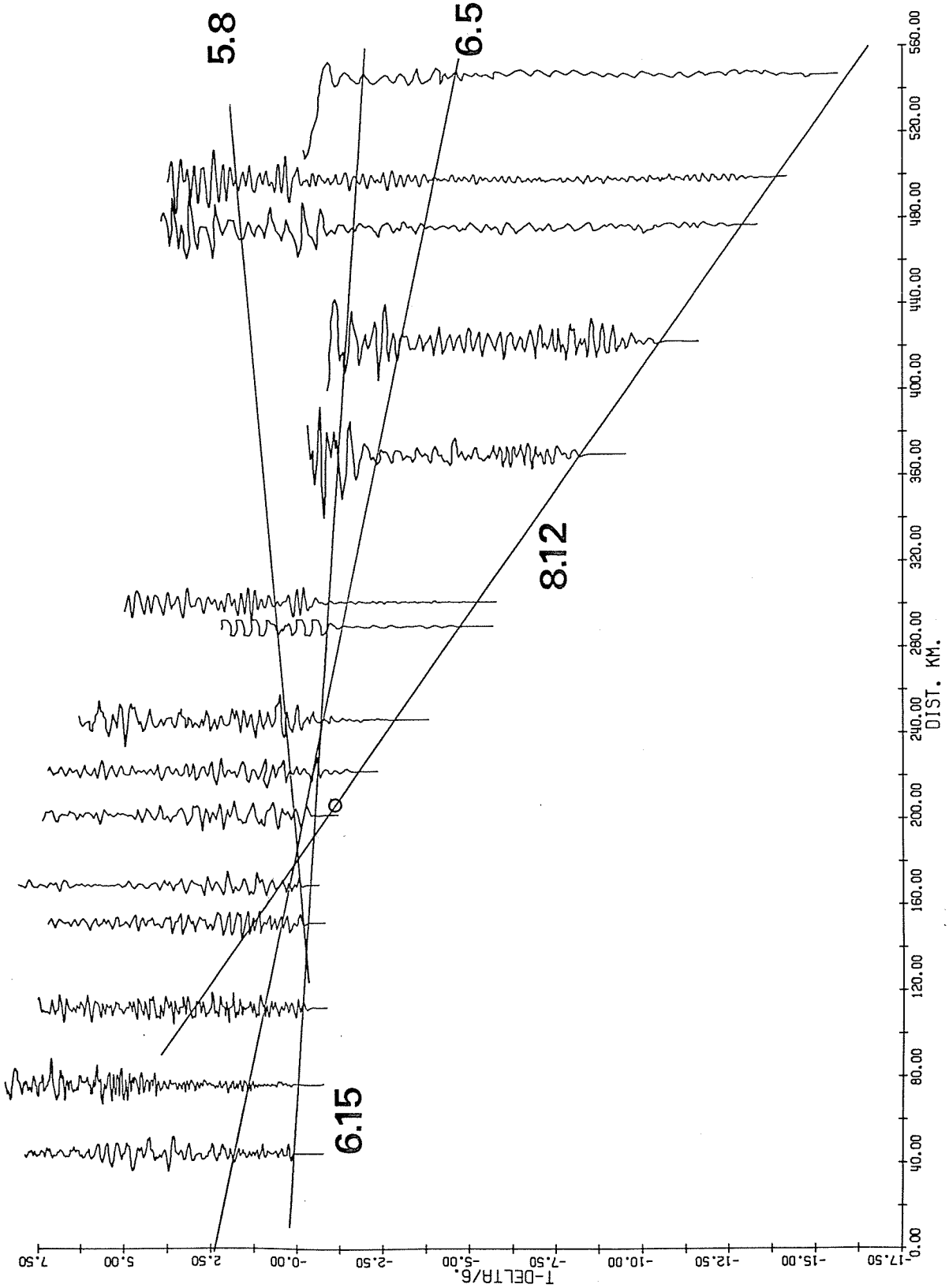
5.8
6.5
8.12
6.15
T-DELTA/6.
7.50
5.00
2.50
-0.00
-2.50
-5.00
-7.50
-10.00
-12.50
-15.00
-17.50
0.00
40.00
80.00
120.00
160.00
200.00
240.00
280.00
320.00
360.00
400.00
440.00
480.00
520.00
560.00
DIST. KM.

linear least squares fit.

Amplitudes of the seismograms were adjusted to enhance the late arrivals and assist in their correlation across the record section. The seismograms from stations Ladron and Bear Den are composites of high gain recordings for the first arrivals and low gain recordings for the later arrivals. The two linear least squares fits for the corrected P_g and P_n arrivals were superposed on the record section.

Beyond the P_g to P_n cross-over distance, the record section (Figure 3.5) reveals conspicuous late arrivals. The first of these never appears as a first arrival, is only moderately strong, and lines up with a slope of 1/6.5 sec/km. The second late arrival falls approximately on the extension of the P_g branch. The third set, which also never appears as a first arrival, lines up with a slope of 1/5.8 sec/km. Straight lines were visually fitted, in Figure 3.5, to the 2 arrivals having apparent velocities 6.5 and 5.8 km/sec.

Interpretation

Assumptions

Since the profile was single ended, determination of dip was not possible, and the crust was assumed to

consist of horizontal layers.

The velocity was assumed constant in each layer, with abrupt changes at the interface between two layers. This was justified by the various arrivals having linear trends. Hughes (1960) and Birch (1960) have demonstrated that velocity gradients are induced in rocks by increase in pressure and temperature. These more gentle gradients were not detected, since straight line segments fitted the arrival times well.

The velocity was assumed to be greater in each successive layer, because a decrease in velocity with depth would go undetected with refraction information.

The final assumption was that each layer yields a recognizable arrival on the record section. This need not be a first arrival, since the record section allows identification of late arrivals.

Velocities

The velocity of 6.15 km/sec for the P_g phase outside the Rio Grande rift is significantly higher than 5.8 km/sec determined from detailed microearthquake studies within the rift (Sanford et al., 1973). Also P_g interval velocities between SNM and ALQ, both located inside the rift, average about 5.8 km/sec. This is illustrated in Figure 3.6, in which each point corresponds

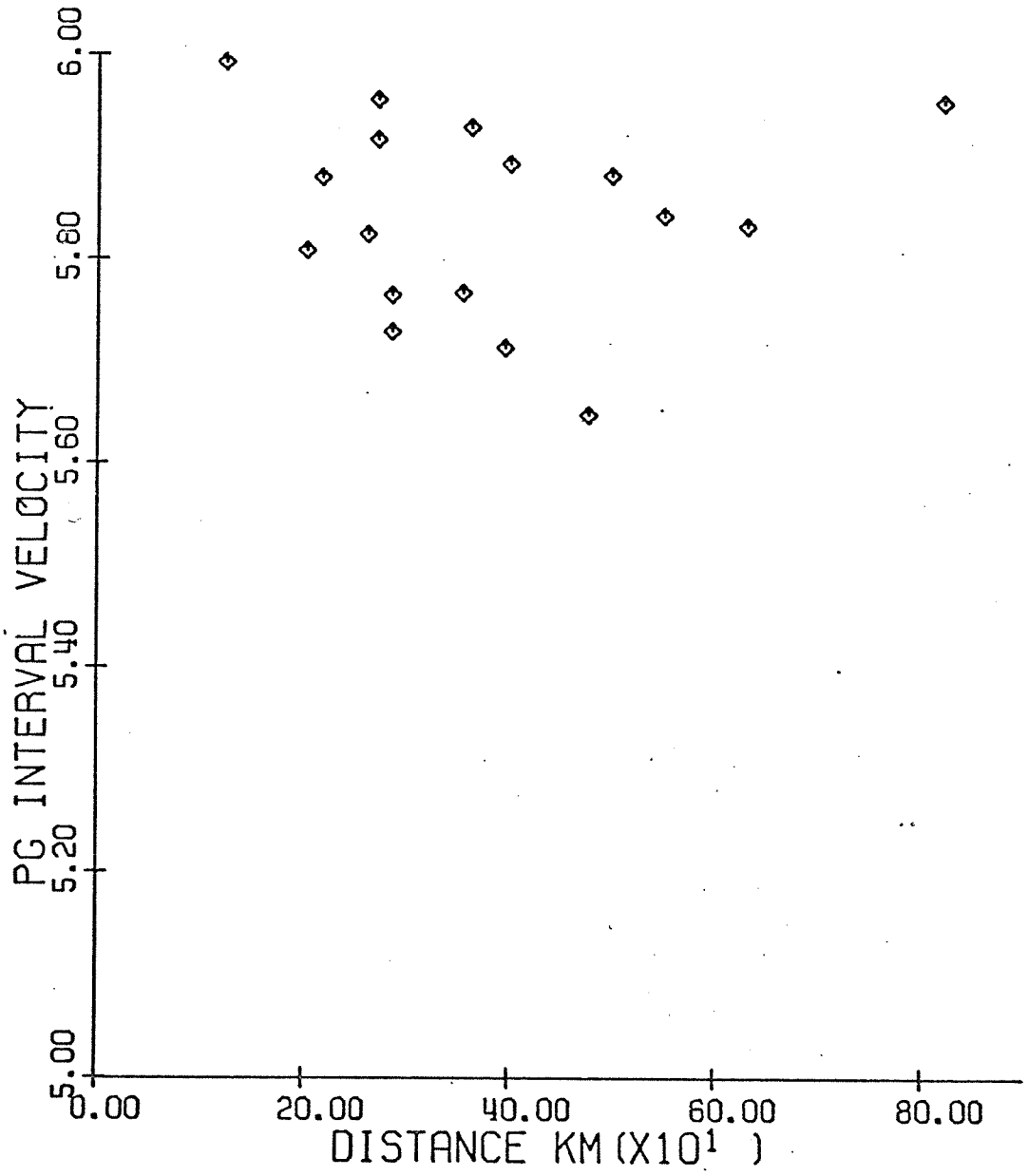

Figure 3.6. P_g interval velocities between SNM and ALQ. Each point corresponds to a single event

to a separate event. Origin times, coordinates, and arrival times at both stations, of these events, are listed in Table 3.5. They include explosions as well as earthquakes, and fall both north and south of the station pair. The distance from the events to the mid-point of the two stations is plotted as the abscissa in Figure 3.6, and apparently does not affect V_g, whose value remains near 5.8 km/sec.

Beyond the cross-over of P_g to P_n the profile lies entirely in the rift. The conspicuous late arrival in Figure 3.5 having velocity 5.8 km/sec should correspond to the P_g phase observed within the rift. No vertical velocity structure of any description can produce a wave having surface phase velocity less than that in the surface layer. This is illustrated in Figure 3.7, which shows parallel rays incident on the surface with an angle of emergence e, in a medium having velocity V_g; if energy traverses from A to B in unit time, then

$$\begin{aligned} AB &= V_g \\ \text{and} \quad CB &= AB/\cos(e) \\ &= V_g/\cos(e) \end{aligned}$$

where CB is the surface velocity. Clearly the surface velocity is always larger than V_g, since cos(e) is less than unity. Velocity inversions or decrease in velocity

Table 3.5. Data for P_g Interval Velocities Between ALQ and SNM

Date of Event	Origin Time Hr:Min:Sec	Latitude	Longitude	Arrival Time at ALQ Hr:Min:Sec	Arrival Time at SNM Hr:Min:Sec	Distance to ALQ (km)	Distance to SNM (km)	V_g (km/sec)
18 Feb.71	11:28:14.1	36.30	105.70	11:28:40.8	11:28:58.9	165.63	272.06	5.88
30 Nov.70	05:35:21.7	36.30	106.20	05:35:48.3	05:36:06.2	152.51	256.47	5.81
7 Aug.70	11:59:06.5	35.45	105.98	11:59:18.5	11:59:36.1	71.39	176.87	5.99
23 Jan.66	19:43:19.7	36.96	106.95	19:43:57.1	19:44:12.6	228.29	320.60	5.96
23 Jan.66	23:48:08.1	36.96	106.95	23:48:46.7	23:49:02.3	228.29	320.60	5.92
3 Oct.66	02:26:02.3	37.40	104.10	02:26:56.5	02:27:14.8	345.51	450.03	5.71
27 Nov.67	05:09:22.7	40.00	104.70	05:10:56.0	05:11:14.0	582.31	687.28	5.83
10 Sep.69	21:00:00.1	39.40	107.90	21:02:25.2	21:02:40.0	510.92	597.38	5.84
29 Sep.67	03:52:46.0	32.14	106.92	03:53:38.8	03:53:21.7	313.64	214.04	5.82
12 May 69	08:26:18.7	31.93	106.45	08:27:14.8	08:26:58.7	333.98	241.75	5.73
12 May 69	08:49:16.3	31.93	106.45	08:50:12.3	08:49:56.3	333.98	241.75	5.76
18 Nov.63	14:38:28.9	29.90	113.60	14:40:28.1	14:40:12.5	872.81	779.96	5.95
9 Mar.72	18:45:00.0	32.75	110.49	18:46:16.3	18:46:02.0	445.29	361.02	5.89

Table 3.5 (continued)

Date of Event	Origin Time Hr:Min:Sec	Latitude	Longitude	Arrival Time at ALQ Hr:Min:Sec	Arrival Time at SNM Hr:Min:Sec	Distance to ALQ (km)	Distance to SNM (km)	V_g (km/sec)
19 Aug.66	04:15:44.6	30.30	105.60	04:17:06.9	04:16:52.0	520.84	436.72	5.65
20 Oct.64	00:53:07.8	31.30	107.00	00:54:16.3	00:53:59.0	406.95	307.20	5.77
20 Aug.66	06:36:02.7	30.10	105.50	06:37:29.6	06:37:15.4	544.22	460.70	5.88
12 Jan.70	11:21:15.4	36.07	103.18	11:22:04.6	11:22:19.1	322.26	408.24	5.93
							Std Dev.	5.84 .096

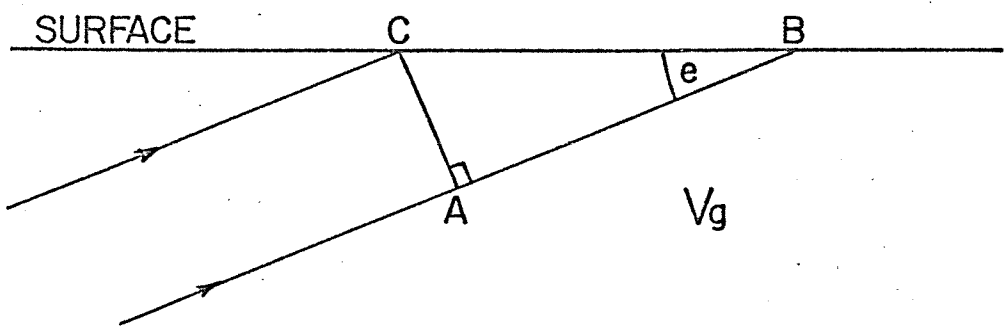

Figure 3.7. Plane parallel rays emerging with angle e at the free surface.

with depth will produce delayed arrivals, but the surface phase velocity will always be larger than V_g.

Thus the profile suggests that the velocity of the P_g phase changes from a value of 6.15 km/sec outside the rift to 5.8 km/sec inside. The point in Figure 3.5 where the extension of the arrival with velocity 5.8 km/sec intersects the 6.15 km/sec P_g branch, defines the approximate border of the rift structure. This point lies about 140 km from the shot, but could easily be shifted due to the oblique intersection of the profile with the rift, and the fact that the velocity change is probably gradational.

Since the evidence available indicated a variation of V_g only, V^* and V_n were assumed to be unaffected by the rift. The basic structure for the profile is shown in the cross-section in Figure 3.8.

Depths

Thicknesses Z_1 and Z_2 in Figure 3.8 were assumed to be the same inside and outside the rift, and were calculated from the intercept times of P^* and P_n. The observed intercept time of the line with velocity 6.5 km/sec in Figure 3.5, corresponding to P^*, is 2.44 sec. Referring to Figure 3.8, and following Nettleton (1940, p. 254), the intercept time was equated to the sum of the

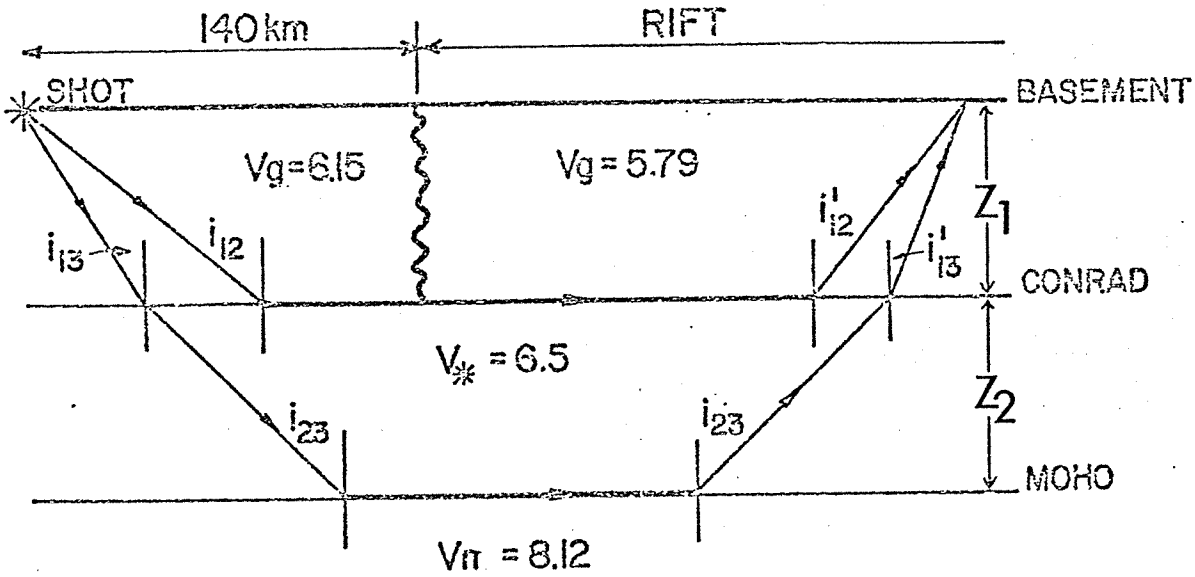

Figure 3.8. Cross section along profile showing velocities and critical angles.

delay times :

$$2.44 = Z_1\left(\frac{\cos i_{12}}{6.15} + \frac{\cos i'_{12}}{5.8}\right)$$

where $i_{12} = \arcsin \frac{6.15}{6.5}$

$i'_{12} = \arcsin \frac{5.8}{6.5}$

thus $\underline{Z_1 = 18.6 \text{ km}}$

Similarly the observed intercept time of the P_n branch in Figure 3.5 is 7.82 sec. Again referring to Figure 3.8, the intercept time is equated to the sum of the delay times :

$$7.82 = Z_1\left(\frac{\cos i_{13}}{6.15} + \frac{\cos i'_{13}}{5.8}\right) + 2Z_2 \frac{\cos i_{23}}{6.5}$$

where $i_{13} = \arcsin \frac{6.15}{8.12}$

$i'_{13} = \arcsin \frac{5.8}{8.12}$

$i_{23} = \arcsin \frac{6.5}{8.12}$

thus $\underline{Z_2 = 19.6 \text{ km}}$

Uncertainties involved in the intercept time of the P^* arrival could introduce errors of $\pm$ 1 km in Z_1 and Z_2.

Reversed P_n interval velocities discussed in a later section of this dissertation indicate that the Moho

surface dips about 2 degrees northward. The true V_n is 7.92 km/sec, and when this value is employed the depths become :

$$Z_1 = 18.6 \text{ km} \quad \text{(unchanged)}$$
$$Z_2 = 21.3 \text{ km}$$

The assumption of horizontal layers must still be applied to the Conrad surface, because no reversal information on the P^* velocity was available. These depths are measured from the basement surface, and apply at the cross-over distance, about 190 km from the shot.

If the depths are different inside the rift than outside, then the depths calculated above would fall between the two. Figure 3.9 is a simplified block diagram, depicting the rift as a pod of material having velocity 5.8 km/sec embedded in an upper crust having velocity 6.15 km/sec.

Theoretical Times

The values of Z_1 and Z_2 obtained from the observed apparent velocities were used in conjunction with the model in Figure 3.8, to generate theoretical travel times. Curves for P_g, P^*, P_n, and the two reflections P_*P and P_nP from the Conrad and Mohorovicic discontinuities, respectively, were deduced. The computer program used

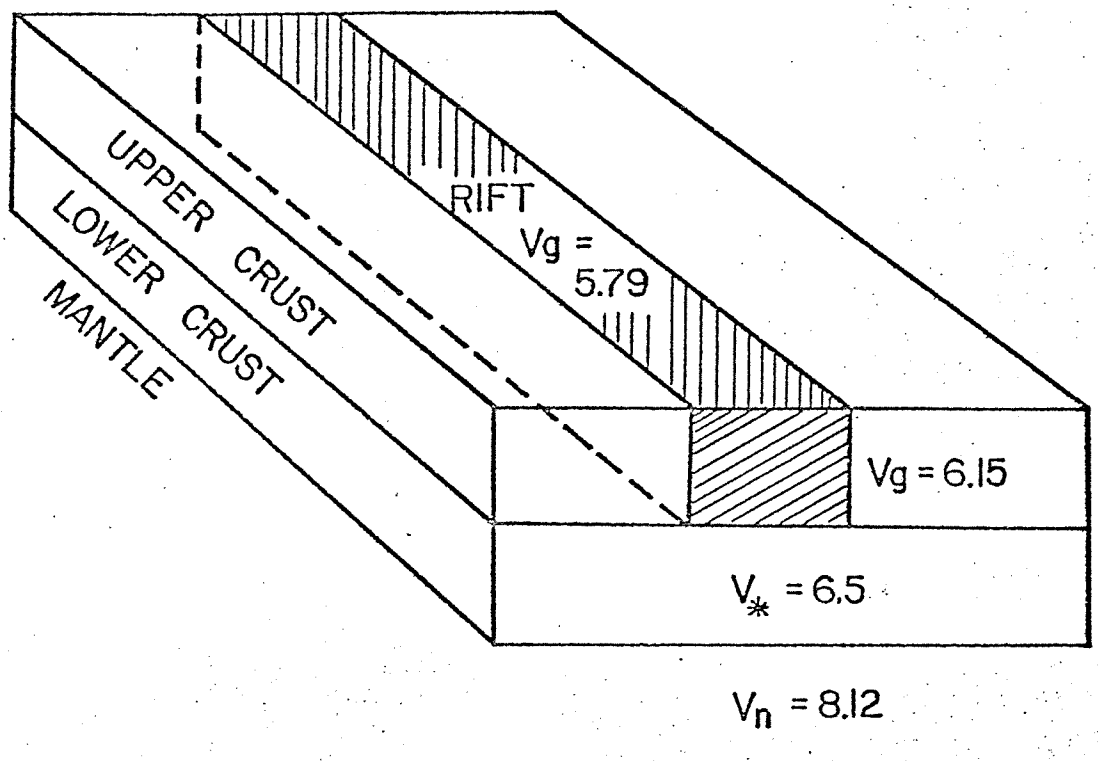

Figure 3.9. Simplified block diagram, showing the rift as a pod of material having velocity 5.8 km/sec embedded in an upper crust of velocity 6.15 km/sec. The vertical scale is exaggerated 3 times relative to the horizontal.

to obtain these travel times is given in Appendix II. Figure 3.10 shows the theoretical travel time curves, and Figure 3.11 is a superposition of these curves on the record section. The border of the rift, 140 km from the shot, was taken as a vertical discontinuity, and gave rise to the kinks on the curves at this distance. The theoretical travel time curves succeed in accounting for most of the conspicuous arrivals on the record section.

Additional Observed Arrival

The model in Figure 3.8 does not produce an arrival with velocity 6.15 km/sec after the profile enters the rift. However strong arrivals marked by X's on Figure 3.11 fall almost on the extension of the 6.15 km/sec P_g branch, from 350 km to the end of the profile. These arrivals can be explained by considering the third dimension which Figure 3.8 does not provide. In the map, Figure 3.12, the rift border is approximated by the 2 continuous straight lines which meet at the point A. The locations of the seismic stations are indicated by triangles. Circular wave-fronts are drawn from the shot point at 10 sec intervals. The continuation of these circles inside the rift are dashed. As far south as the point A, at the latitude of South Garcia, the wave-fronts suffer slight horizontal refraction in traversing from the 6.15 km/sec to the 5.8 km/sec crustal

Figure 3.10. Theoretical travel time curves derived from the observed apparent velocities and the calculated depths. M is reflection off Moho, and C is reflection off Conrad.

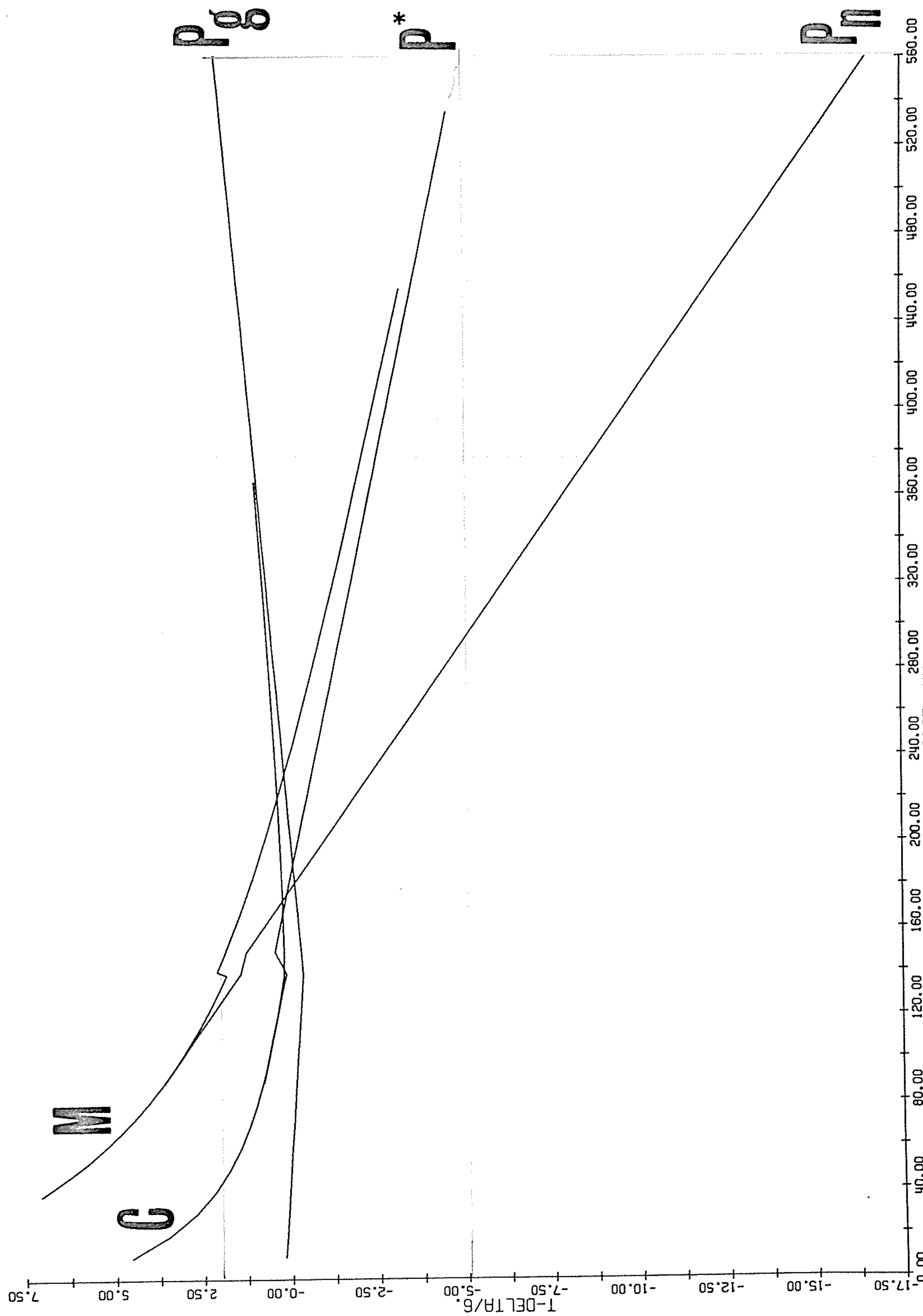

Pg
P*
Pn
M
C
DIST. KM.
0.00
40.00
80.00
120.00
160.00
200.00
240.00
280.00
320.00
360.00
400.00
440.00
480.00
520.00
560.00
T-DELTA/6.
-17.50
-15.00
-12.50
-10.00
-7.50
-5.00
-2.50
-0.00
2.50
5.00
7.50

Figure 3.11. Superposition of theoretical travel time curves upon the record section. x's are strong arrivals that are not completely explained by the model.

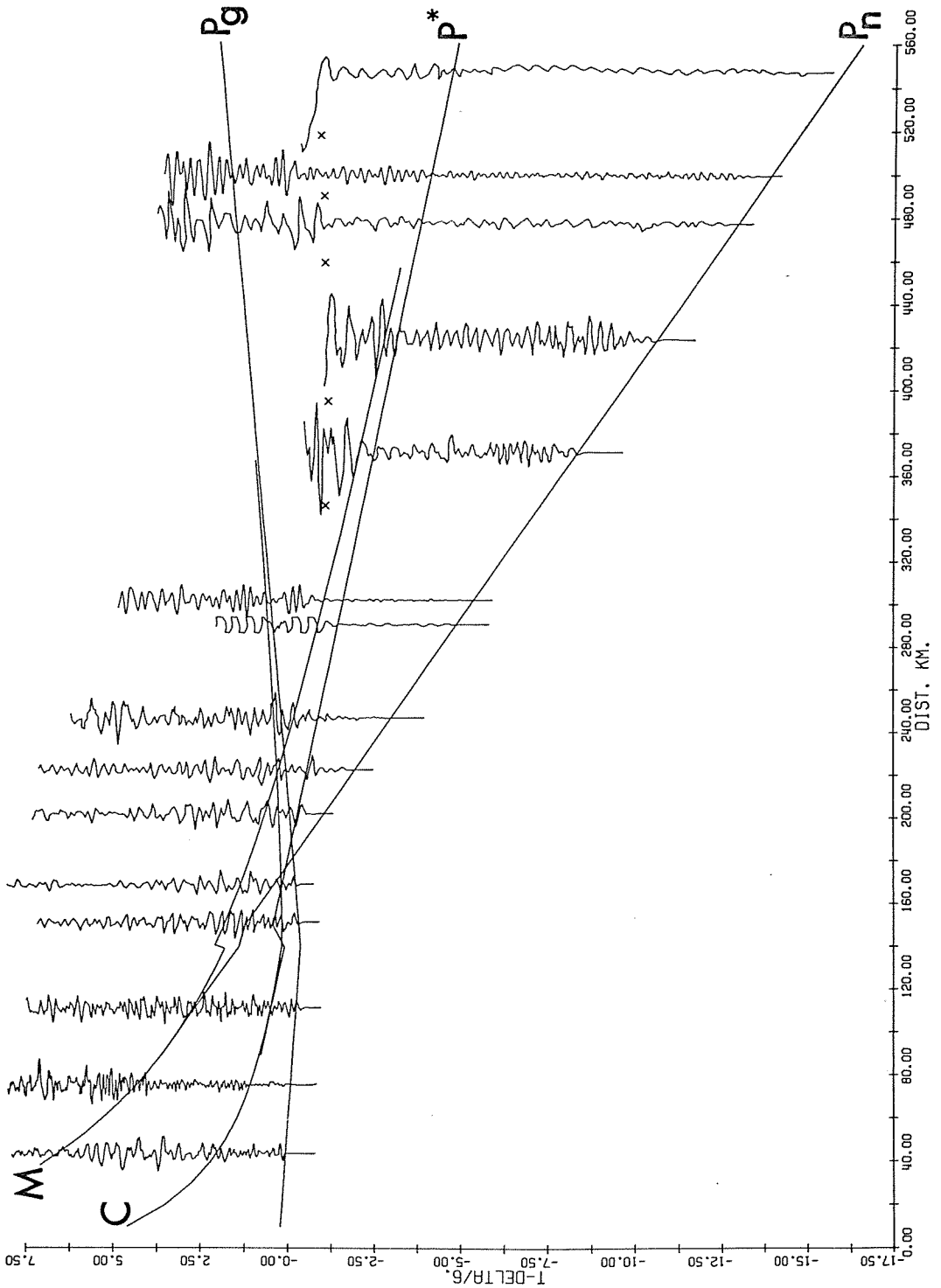
Pg
P*
Pn
M
C
T-DELTA/6.
DIST. KM.
7.50
5.00
2.50
0.00
-2.50
-5.00
-7.50
-10.00
-12.50
-15.00
-17.50
0.00
40.00
80.00
120.00
160.00
200.00
240.00
280.00
320.00
360.00
400.00
440.00
480.00
520.00
560.00

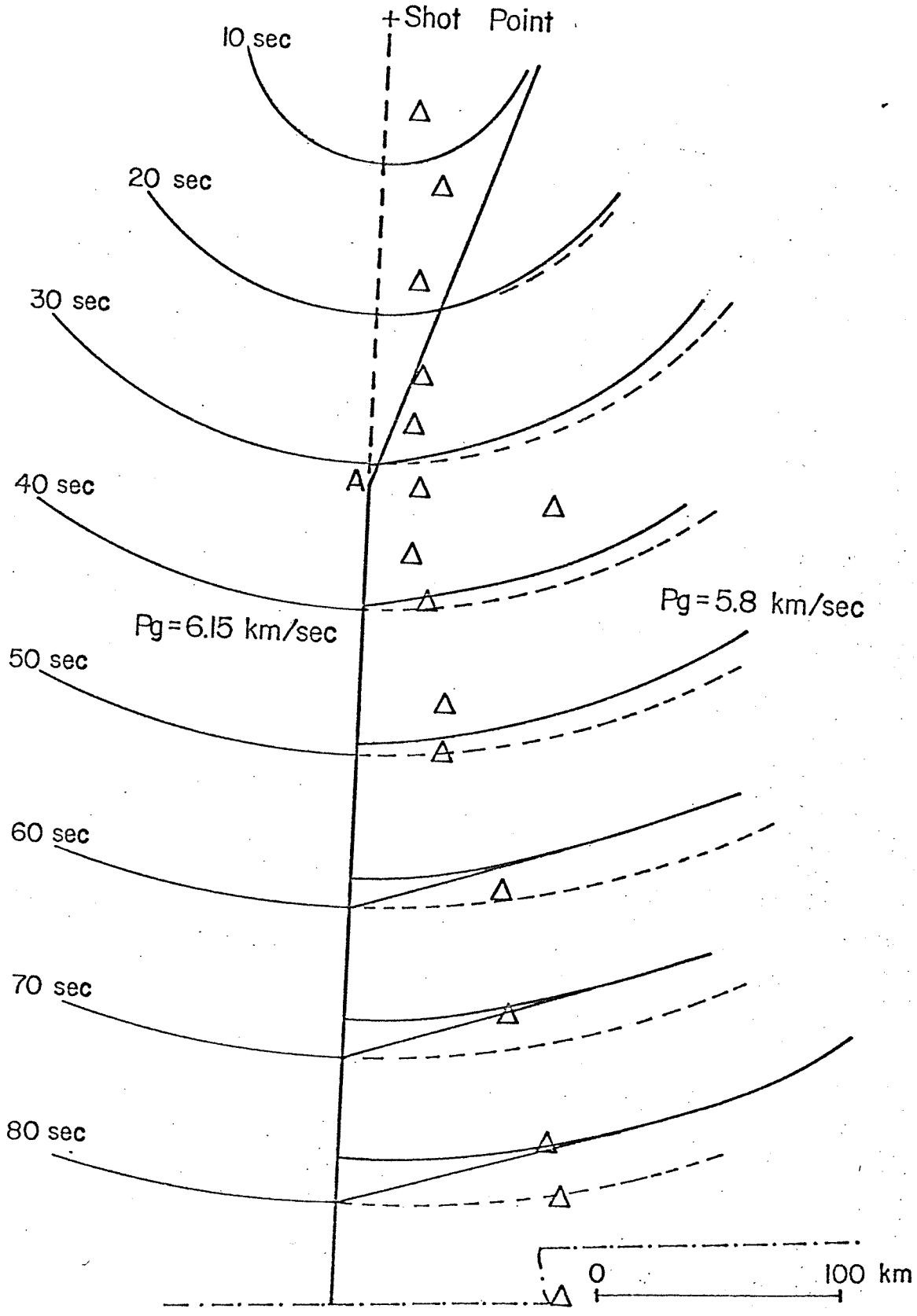

Figure 3.12. Plan view of wave-fronts from Gasbuggy at 10 sec intervals. The rift border is approximated by the two solid straight lines which meet at A. Triangles are the seismic stations.

material. At point A the border changes course and becomes radial to the shot point. Southward from this point the wave-fronts become detached at the interface, and a conical type wave is generated which extends from the faster wave-front and is tangent to the slower wave-front. The conical wave travels with the higher velocity, 6.15 km/sec, and could account for the arrivals marked X. The observed non-linear delay of the X's can be explained by the fact that the last 5 stations get progressively farther from the rift border. Whereas the existence of a wave having velocity 6.15 km/sec inside the rift can be explained, the observed amplitudes of this arrival are much larger than what would be expected from a conical wave.

Earthquake Character

The 3-dimensional crustal structure obtained in this interpretation, and illustrated in Figure 3.9, succeeds in explaining the difference in character between earthquakes occurring inside and outside the rift. To demonstrate this, travel time curves were constructed for P_g, P^*, and P_n arrivals, recorded inside the rift, from 10 km deep earthquakes. The focal depth of 10 km is a common value for microearthquakes in the rift (Sanford et al., 1973).

Travel time curves in Figure 3.13 are for earthquakes with locations that require seismic energy to travel 100 km before entering the rift. Examples of such events are the earthquakes of 19 May 1968 and 8 June 1969 (Toppozada and Sanford, 1972) whose locations appear in Figure 3.14. The travel time curves indicate that the P_g to P_n cross-over distance is 160 km, and that P^* is almost never a first arrival. Seismograms of these events recorded at ALQ appear in Figure 3.15. These seismograms show a strong first arrival appropriate for the direct P_g.

Travel time curves in Figure 3.16 are for earthquakes located in the rift. Locations of two events occurring close to the rift border appear in Figure 3.14. These are the earthquakes of 28 April 1971 and 4 June 1971 (Toppozada and Sanford, 1972). The travel time curves indicate that P^* is a first arrival between 110 km and 155 km from the source. Seismograms of these events recorded at ALQ appear in Figure 3.17. These seismograms show that the strong P_g arrival is preceded by a weak arrival that could well be a head wave from the Conrad discontinuity.

The four earthquakes mentioned above lie within a narrow range of distances from ALQ. The closest event, that of 28 April 1971, lies 125 km from ALQ and the

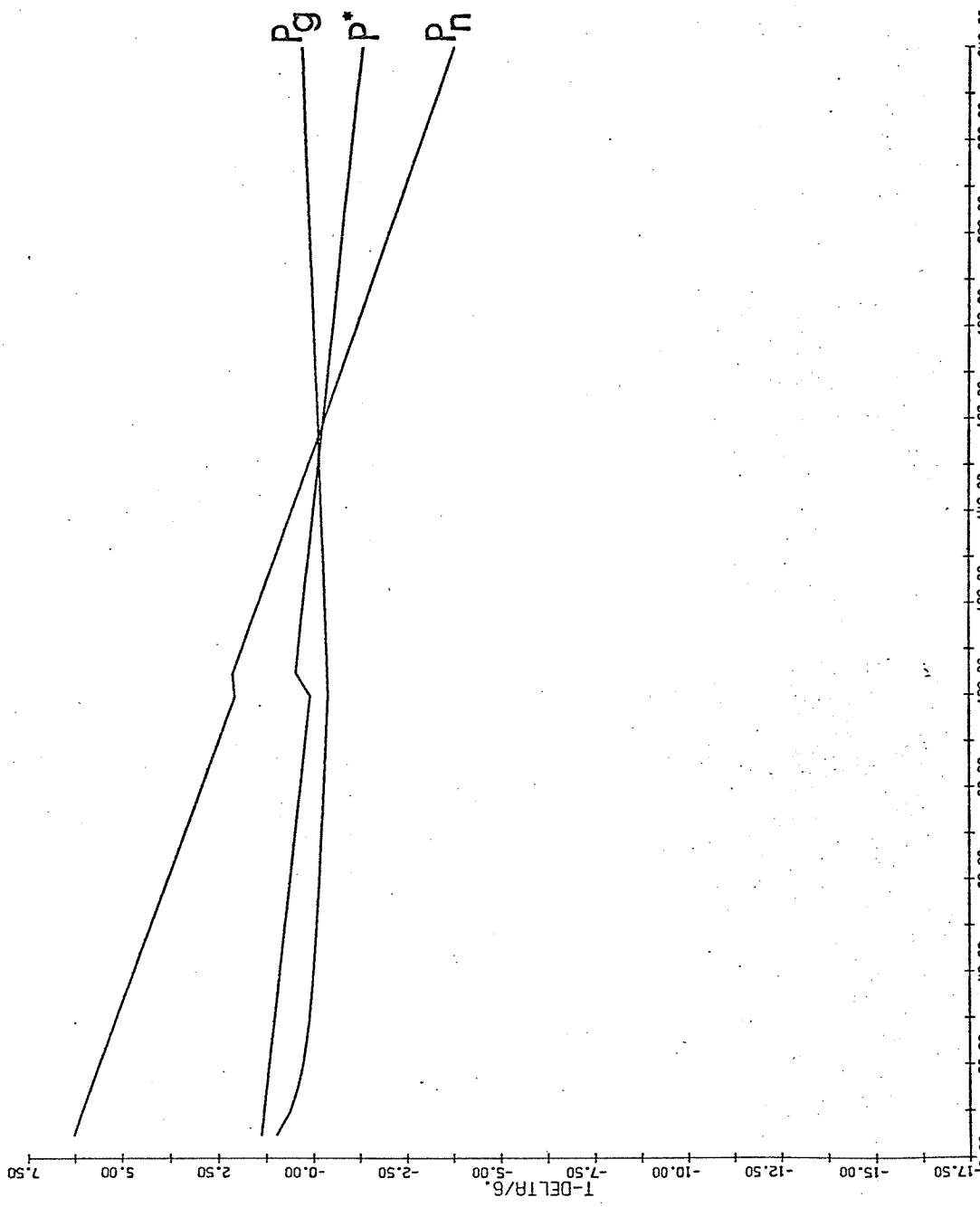

Figure 3.13. Travel time curves for 10 km deep earthquakes, located 100 km outside the rift and recorded inside the rift.

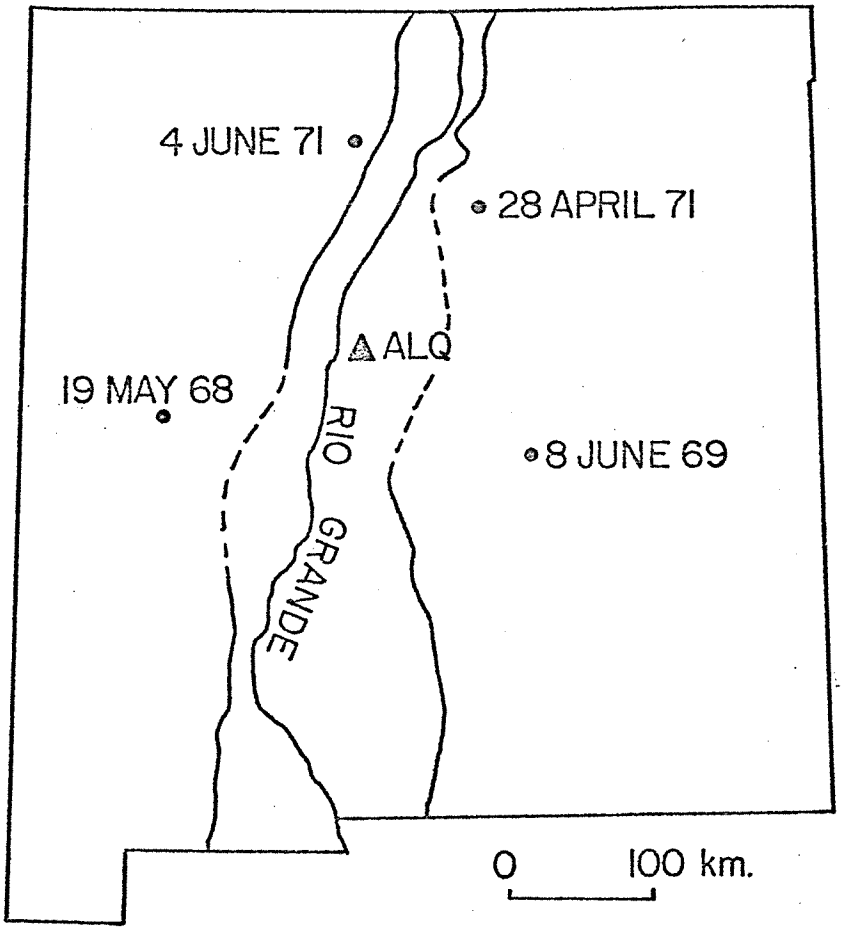

Figure 3.14. Locations of earthquakes referred to in explaining different earthquake character. Border of rift is indicated.

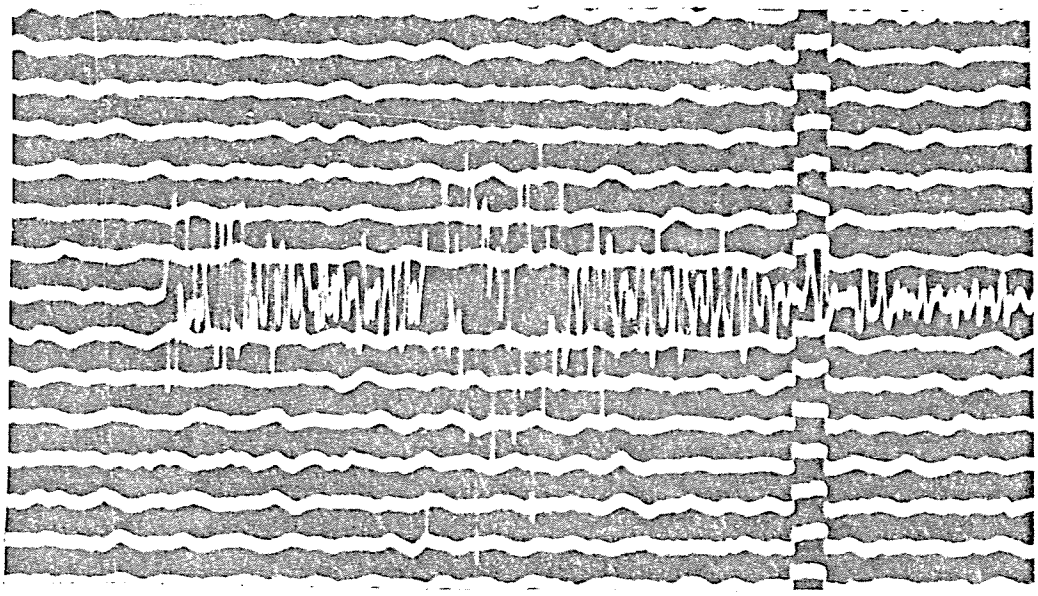

(a)

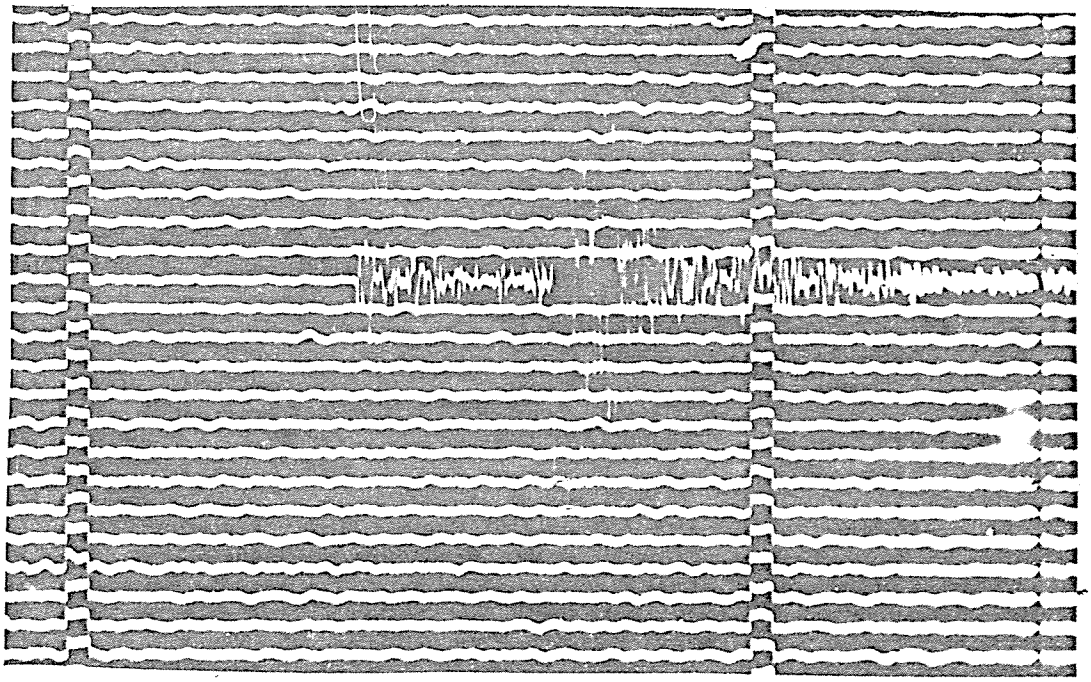

(b)

Figure 3.15. ALQ seismograms of (a) the earthquake of 19 May 1968, delta = 147 km, (b) the earthquake of 8 June 1969, delta = 139 km. Both have strong P_g direct arrivals.

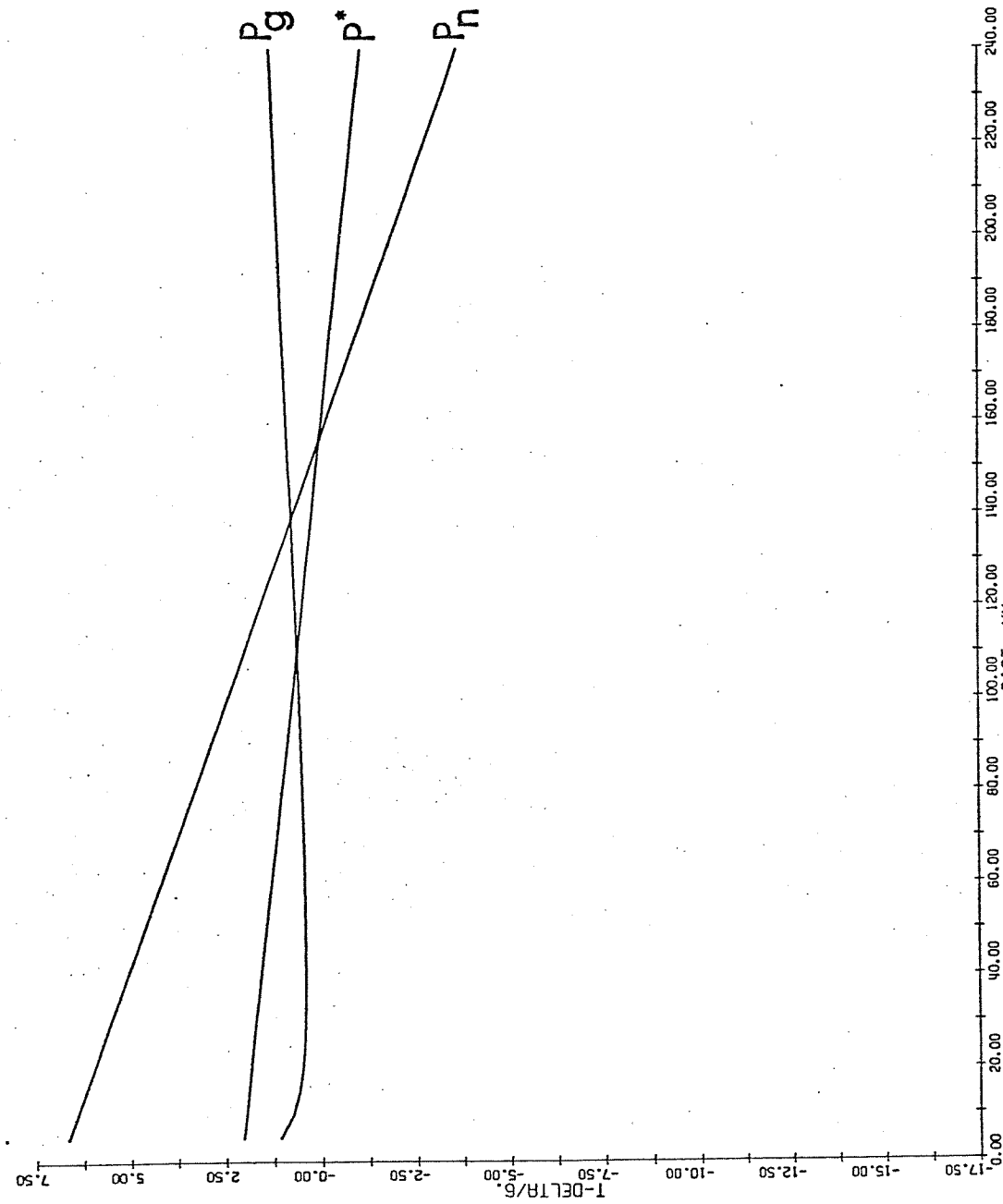

Figure 3.16. Travel time curves for 10 km deep earthquakes located and recorded inside the rift.

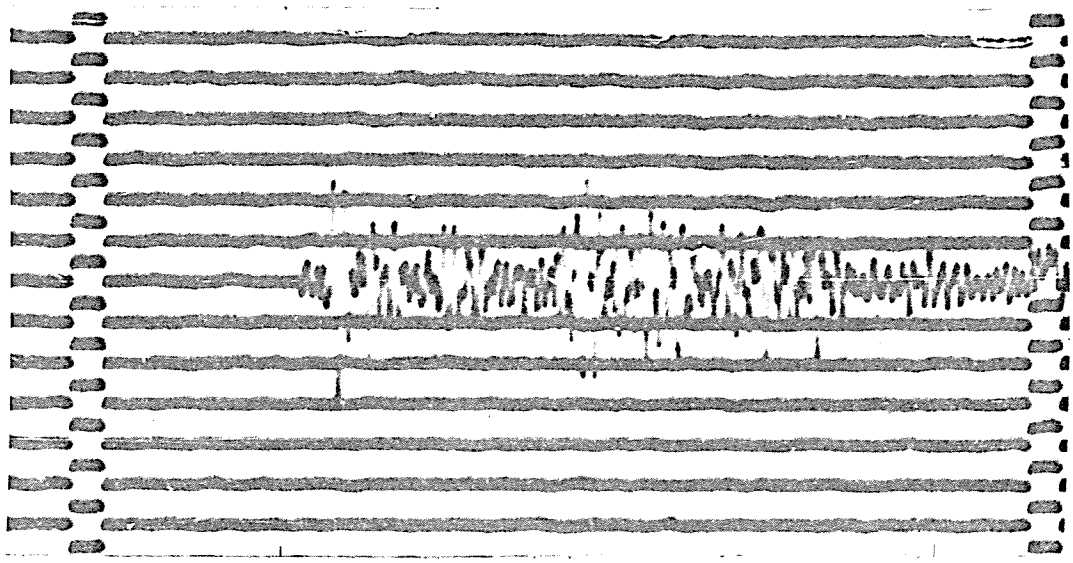

(a)

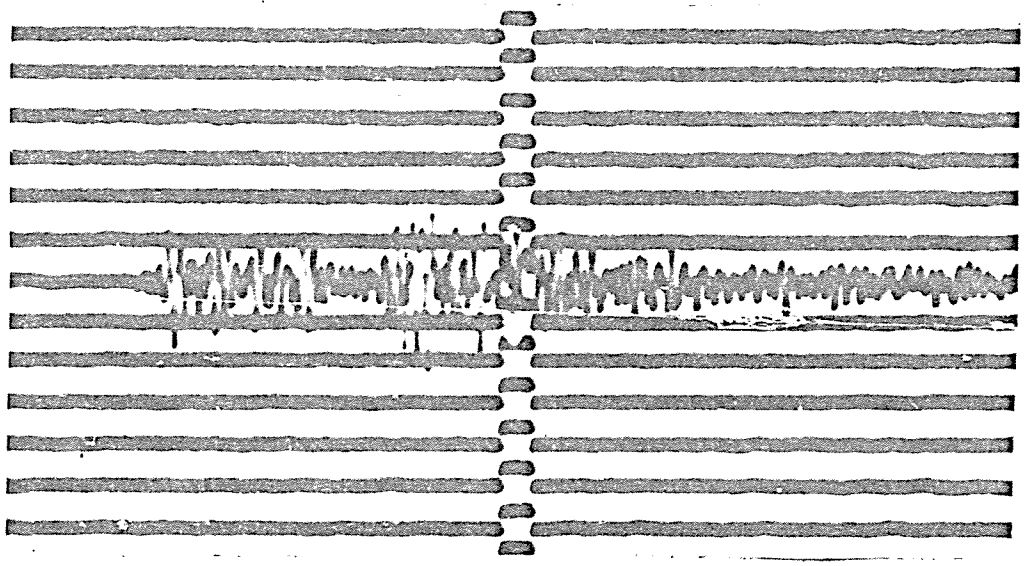

(b)

Figure 3.17. ALQ seismograms of (a) the earthquake of 28 April 1971, delta = 125 km, (b) the earthquake of 4 June 1971, delta = 143 km. Both have a weak head wave first arrival followed by P_g.

farthest event, that of 19 May 1969, lies 147 km from ALQ. Thus the difference in character is probably controlled by the difference in crustal structure from the source to the station, rather than by the distance. The velocity contrast between P^* and P_g inside the rift (6.5-5.8, km/sec), is greater than that between the same two phases outside the rift (6.5-6.15, km/sec). Consequently P^* has a better chance of appearing as a first arrival for travel paths inside the rift.

Comparison with Other Areas

Surrounding Areas

The crustal structure deduced here is similar to that previously obtained for northeastern Arizona by Roller (1965) (Number 9 in Table 2.2). Velocity of the P_g phase is apparently constant at 6.1 $\pm$0.1 km/sec in Oklahoma, Colorado, southern Utah, eastern Arizona (see Figure 2.1 and Table 2.2), and in New Mexico. Lateral variation such as that associated with the Rio Grande rift covers limited areas.

The apparent velocity of the P^* phase on the Gasbuggy profile (6.5 km/sec) is 0.2 to 0.3 km/sec less than that in surrounding areas as indicated in Table 2.2. P^* on this profile was unreversed, and so the smaller velocity

may be the result of down-dip shooting. It may also be an actual drop in V^*, possibly associated with the rift structure. Apparent P_n velocity is 8.12 km/sec along the Gasbuggy profile. The reversed P_n velocity from Las Cruces (LCN) to ALQ is known from Mexican earthquakes to be 7.72 km/sec. Thus the true P_n velocity is about 7.9 km/sec, and lies between 8.23 km/sec determined in eastern New Mexico, and 7.8 km/sec in eastern Arizona and southeastern Utah (see Figure 2.1 and Table 2.2).

Regarding the lateral variation in P_g velocity from 6.15 to 5.8 km/sec, it is noteworthy that a similar variation was observed for a refraction profile in eastern Colorado by Jackson, Stewart and Pakiser (1963). They conclude :

> "The velocities 5.8 and 6.1 km/sec, for layers 4 and 5, correspond to P_g in conventional terminology. It is not known whether the transition from 5.8 to 6.1 km/sec represents penetration to a deeper layer or a lateral change in the velocity of compressional waves in the crust."

Jackson et al., (1963), observed the phase having 5.8 km/sec velocity first, followed at greater distance by the phase having 6.1 km/sec velocity. For Gasbuggy the higher velocity was observed first followed at greater distance by the lower velocity. As demonstrated earlier in this section, this sequence cannot be explained by vertical variation in velocity.

Comparable Rifts

The Rhinegraben is a continental rift structure having dimensions comparable to the Rio Grande rift (Illies, 1970). Figure 3.18 is a crustal cross section across the Rhinegraben. P wave velocity in the upper crust is 5.9 to 6.0 km/sec. P wave velocity in the lower crust is 6.7 to 6.9 km/sec. The low velocity layers in the Rhinegraben region are identified from reflection data at small distances (Mueller and Landisman, 1971 ; Landisman et al., 1971). The paucity of data for Gasbuggy in this range, only three seismograms in the first 150 km, made it difficult to detect any correlatable reflections. Consequently low velocity layers, if present, may have been missed on the Gasbuggy profile. The rift "cushion" (Illies, 1970; St. Mueller, 1970; Ansorge et al., 1970) with P velocity 7.6 to 7.7 km/sec extending beneath the crust in the Rhinegraben area, is not observed on the Gasbuggy profile.

The crust near the Rhinegraben is similar to that in Utah and Nevada (see Figure 2.1). The total thickness is about 30 km, with a thick upper crust and a thin lower crust, and a low P_n velocity of 7.5 to 7.7 km/sec. In northwestern New Mexico the crust is thicker, is almost evenly divided into upper and lower layers, and the P_n velocity is about 7.9 km/sec.

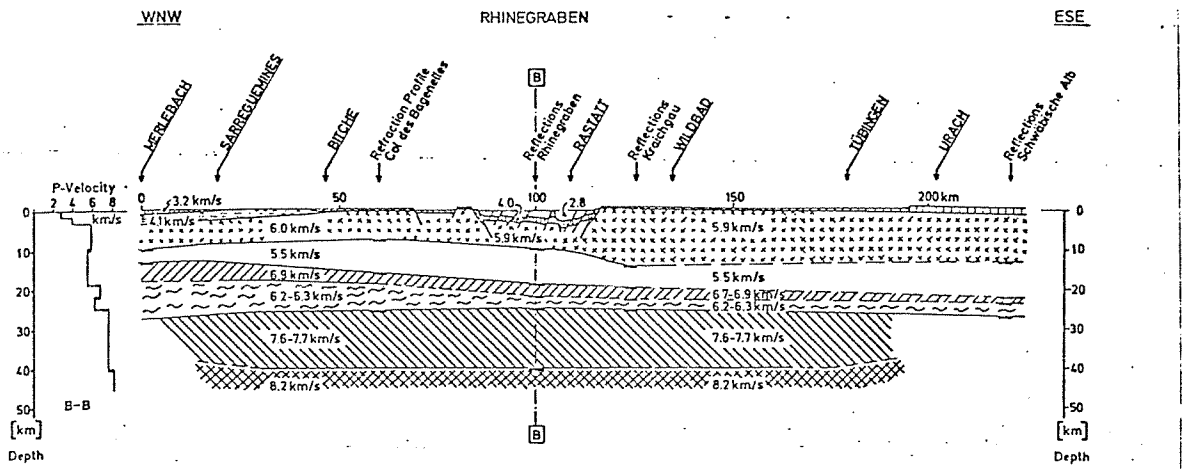

Figure 3.18. Crustal cross section through the Rhinegraben after Ansorge et al., 1970.

Summary and Conclusions

Analysis of a seismic profile extending from near Farmington, New Mexico, to El Paso, Texas, with the added knowledge of the reversed V_n, yields the crustal model shown in Figure 3.19. This model applies at the cross-over distance, about 50 km west of ALQ. This interpretation differs significantly from previous work by Warren and Jackson (1968), whose model appears in Table 3.2, and by Reagor, Gordon and Jordan (1968), mentioned earlier in this section.

The lower P_g velocity inside the rift could be due to the abundant faulting and fracturing associated with this structure (Sanford et al., 1972) which would hinder the propagation of elastic energy. Any effect the rift structure may have on the velocity of P^* cannot be deduced from this profile, because P^* is observed only inside the rift. The rift has little effect on the P_n velocity, which at 7.9 km/sec falls between the values reported for eastern New Mexico and eastern Arizona.

Recommendation

If the crustal thickness is different outside the rift than inside, the thickness derived in this interpretation would fall between the two values. If this

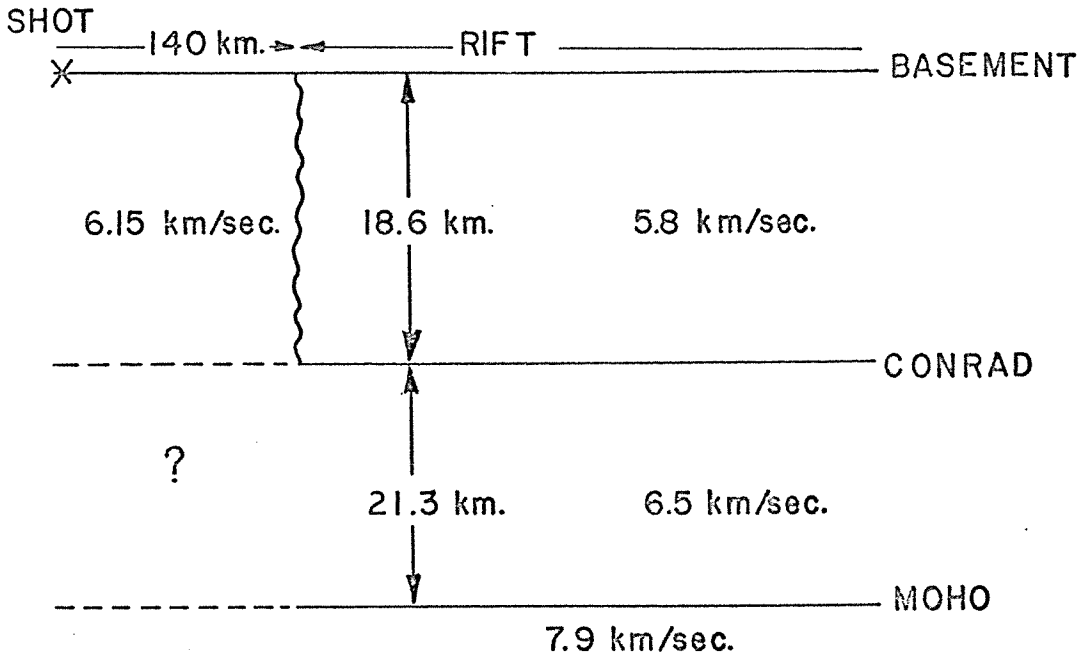

Figure 3.19. Crustal model along the profile showing values of reversed V_n and unreversed V^*, and the depths to the Conrad and the Moho at the cross-over distance.

difference exists, it cannot be detected on the Gasbuggy profile. A change in thickness of the upper crust would offset the P^* arrival, and a change in total crustal thickness would offset the P_n arrival. Since both the P^* and P_n arrivals are observed only inside the rift, possible changes in thickness at the rift border could not be detected. In order to determine whether there is a change in crustal thickness associated with the rift, a profile should be recorded such that the P_g to P_n cross-over occurs prior to when the profile enters the rift. This would make it possible to observe any offset of the P_n branch on entering the rift. Such a profile could commence at the Morenci open pit copper mine in eastern Arizona, where the daily detonation of tons of explosives may be used as a source of seismic waves. The profile should extend northeastward and enter the rift near Magdalena, about 230 km from the shot point. This distance is about 50 km beyond the expected P_g to P_n cross-over. Thus P_n would be identified as a first arrival, and its velocity could be determined, before entering the rift. Any offset of the P_n branch, or change in V_n, after entering the rift could then be detected.

4. REGIONAL P_n VELOCITIES

Introduction

The velocity of the P_n phase was determined by calculating interval velocities (Herrin and Taggart, 1962). Figure 4.1 illustrates how interval velocities are measured. The epicenter is at A, and the seismograph stations are at B and C. The interval velocity is obtained by dividing the distance between the stations along the radial from the source (AC-AB) by the difference in arrival times at the two stations. The wavefronts are assumed to be circular and concentric about the epicenter. Three factors that can influence the values of velocity determined in this way are discussed separately below.

Epicentral Distance. If the P_n phase is a true head wave, the value of V_n should not be a function of epicentral distance. On the other hand, a strong downward increase in V_n below the Moho would cause the ray path for P_n to dip downward, and the apparent value of V_n measured would depend on the distance. The Gasbuggy south profile showed no detectable change in V_n for epicentral distances from 200 to 500 km. In addition, P_n interval velocities between ALQ and SNM do not depend on

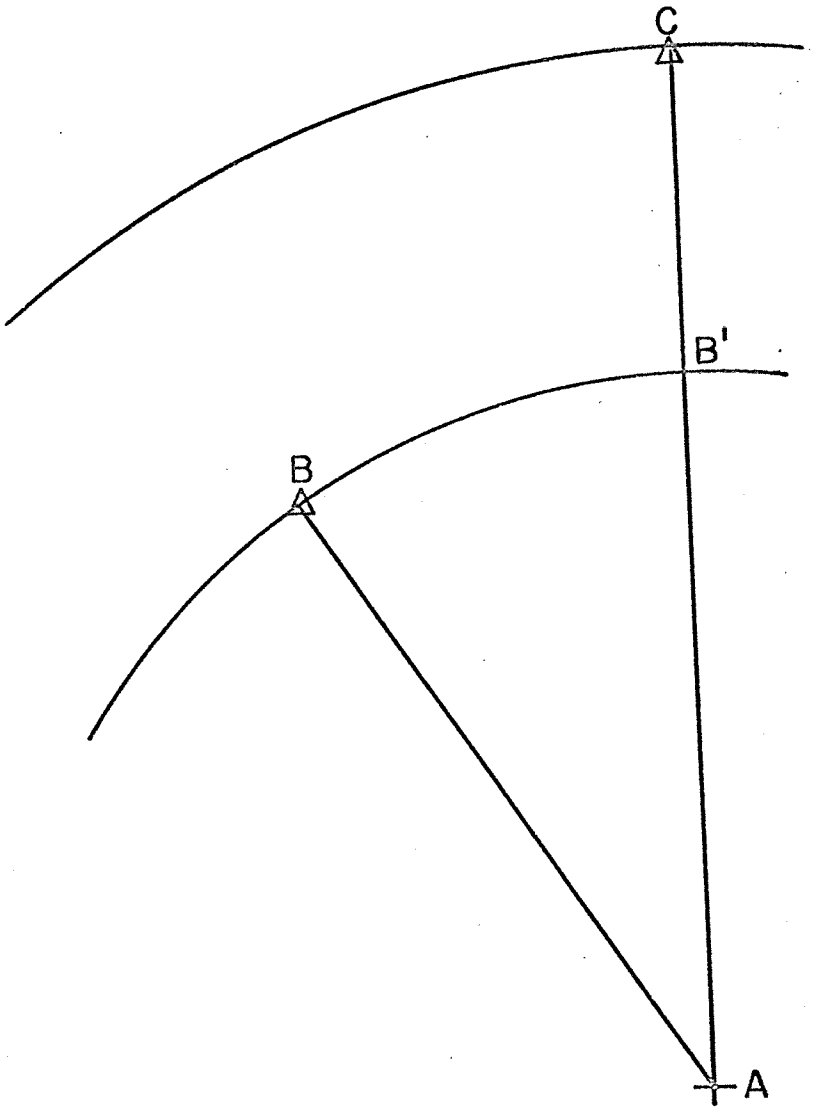

Figure 4.1. Geometry for measuring interval velocities. 'A' is the epicenter. Two circular wavefronts are drawn through the stations B and C.

the distance of the source. In Figure 4.2 the squares are values of P_n velocity, from sources to the south, measured from SNM to ALQ. The abscissa is the distance from the source to the mid-point of the two stations; it ranges from less than 300 km to more than 800 km and apparently does not affect V_n. Thus, inside the Rio Grande rift, V_n is independent of epicentral distance, and P_n is a true head wave.

Dip of Moho. The apparent velocity of a conical wave generated at a dipping interface, is greater when measured up-dip than when measured down-dip (Dix. 1952). Values of reversed P_n velocities between ALQ and SNM, plotted in Figure 4.2, illustrate this effect. Apparent P_n velocities measured from ALQ to SNM, plotted as circles, are greater than those measured from SNM to ALQ, plotted as squares in Figure 4.2. This indicates that the Moho dips northward, or that the crustal thickness at ALQ is greater than that at SNM. For values of dip less than 10^o, the true P_n velocity is the average of the two apparent velocities measured in opposite directions. Unreversed P_n velocities are apparent values, and reversed coverage is necessary to determine the true V_n.

Epicentral Error. The method of interval velocities does not require knowledge of an origin time, therefore earthquake sources can be used. However,

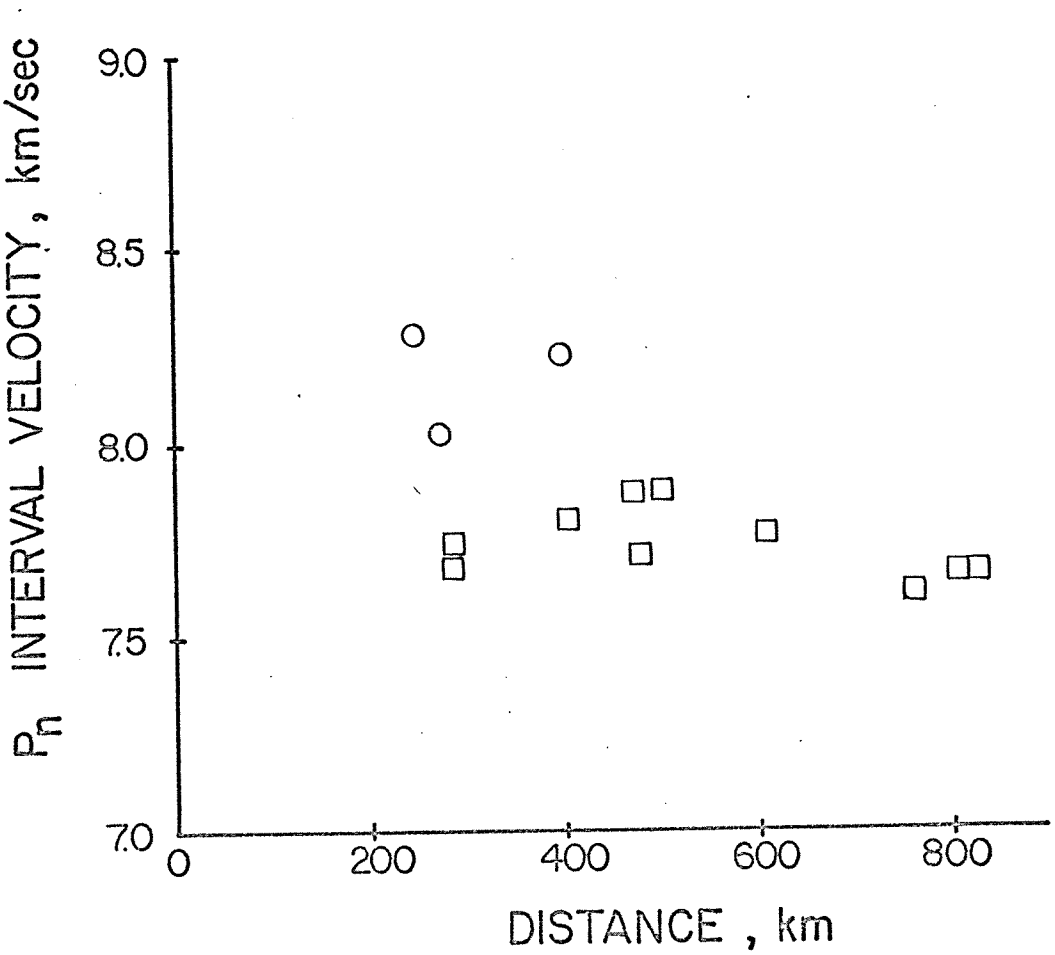

Figure 4.2. P_n interval velocities between ALQ and SNM. Circles are velocities for the interval ALQ to SNM. Squares are velocities for the interval SNM to ALQ. The abscissa is distance from the source to the mid-point of the two stations.

error in epicentral location can affect the velocity measurements. The magnitude of this error was determined using a real combination of source and station pair. The source was the El Paso earthquake of 12 May 1969, and the station pair was SNM and ALQ. Figure 4.3 shows the locations of the stations, and the computed epicenter E surrounded by a circle of error. If the true epicenter was at A, the distances to both stations would increase, and there would be minimum error in the difference. If the epicenter was at B, the distance to SNM would increase more than the distance to ALQ, and there would be maximum error in the difference. Thus error in the distance between stations is a function of azimuth of the epicentral error. In Figure 4.4, relative percent error in distance for the El Paso earthquake is contoured as a function of azimuth. The contours are straight lines converging towards the mid-point between the two station ALQ and SNM. The areas producing a relative error of 2% or greater cover about 20% of the circle with a radius of 15 km. Thus for an epicentral error of 15 km at El Paso, the error in distance between SNM and ALQ is 2% or less at the 80% level of confidence. The distance between SNM and ALQ is the shortest interval used in the study. Most intervals are on the order of 250 km, so that the effect of a 15 km epicentral error on the P_n velocities to be reported should be about 1%.

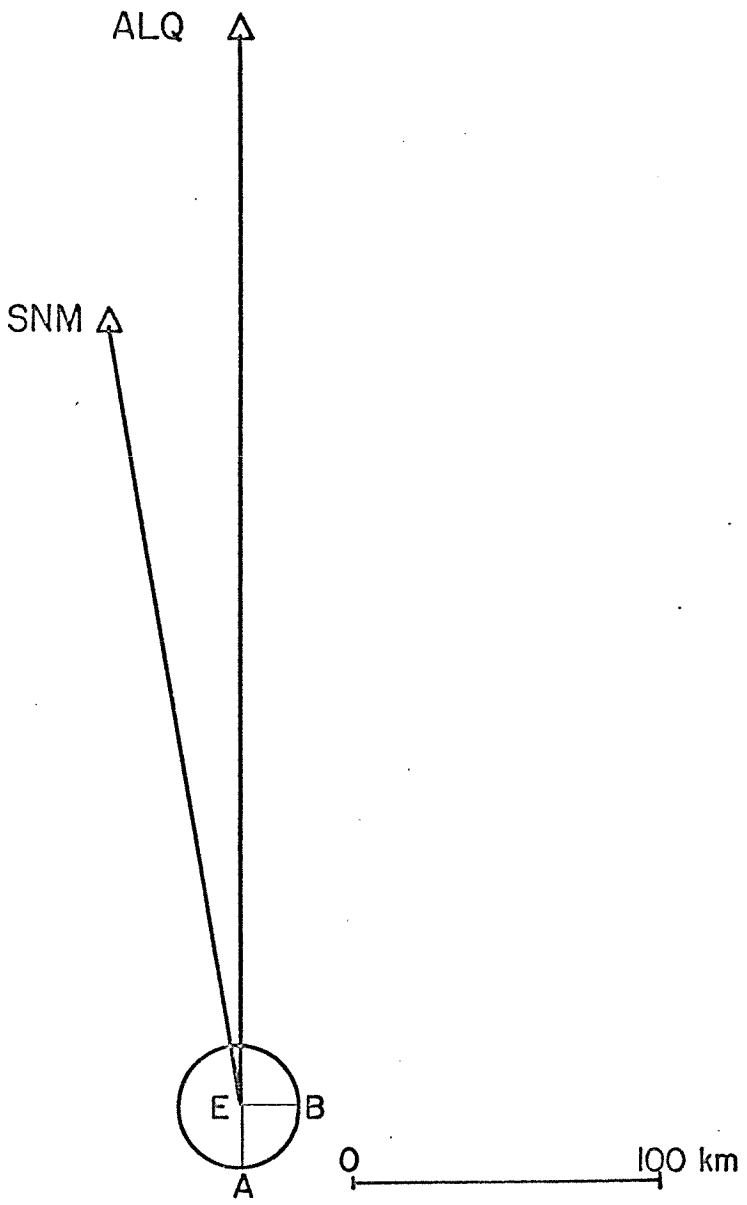

Figure 4.3. Location of the El Paso earthquake of 12 May 1969 relative to SNM and ALQ. The epicenter, E, is surrounded by a circle indicating the possible error in location.

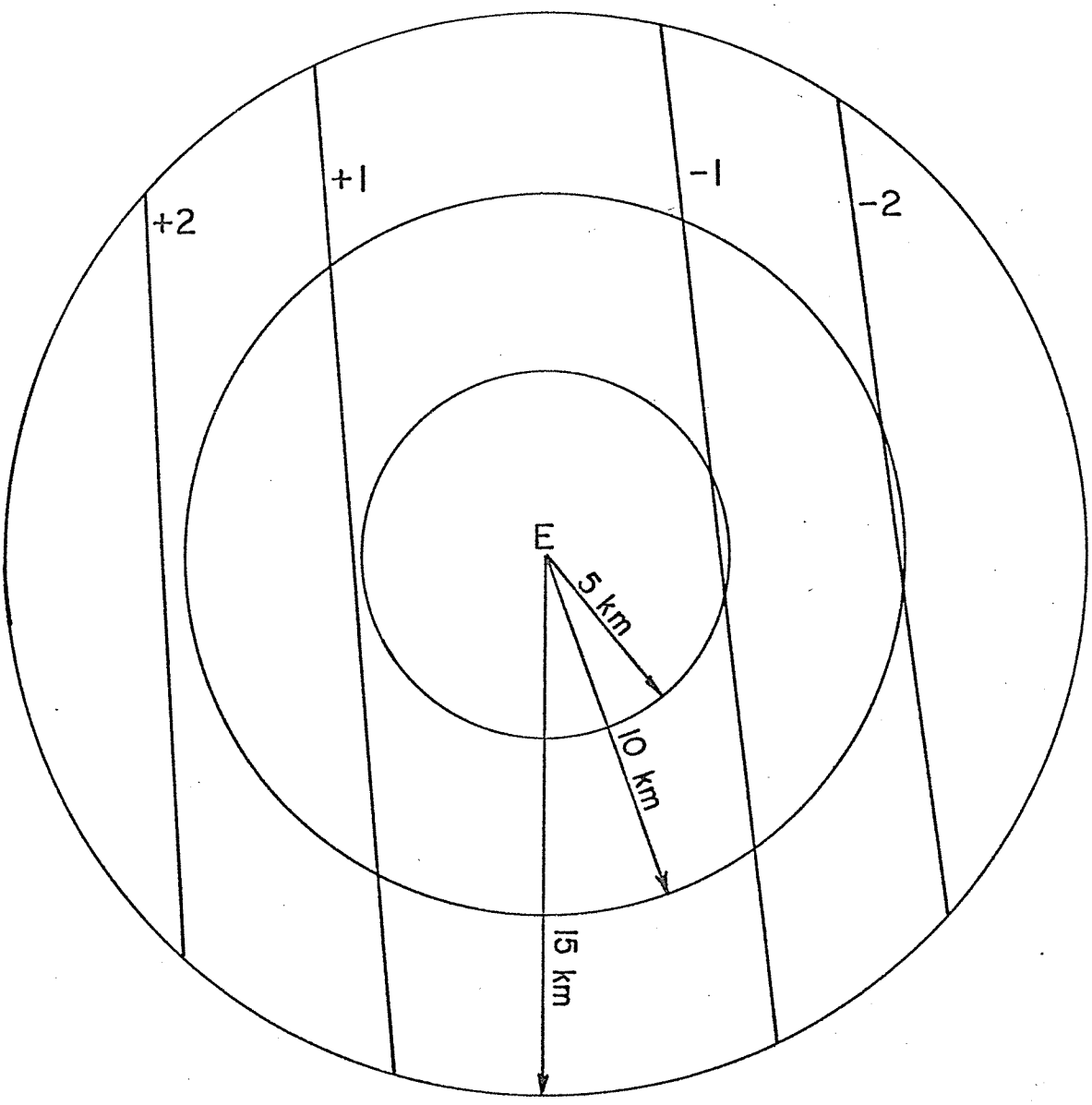

Figure 4.4. Error in distance between SNM and ALQ, resulting from an epicentral error for the El Paso earthquake located at E. Concentric circles about E are circles of epicentral error. The straight lines are contours of the error in distance between the two stations, and are labelled in percent relative error.

A program for computing the error in distance, resulting from a given epicentral error, is given in Appendix III.

Data Used

Gasbuggy

The Gasbuggy explosion was used to obtain unreversed velocities along the 5 profiles shown in Figure 3.1. Least squares fits were made of the P_n arrival times on each profile. Information on all profiles, except the southern one, was obtained from Warren and Jackson (1968). The values of velocity obtained are indicated on the profiles in Figure 4.5, with arrows pointing in the direction of coverage.

Earthquakes and Other Explosions

A search was made for earthquakes and explosions which approximately lined up with a pair of seismograph stations. Table 4.1 lists the seismograph stations employed in this study. Two primary sources of data were consulted during the search :

(1) Earthquake publications of the New Mexico State Bureau of Mines and Mineral Resources (Sanford, 1965; Sanford and Cash, 1969; Toppozada and Sanford, 1972).

Table 4.1. Seismograph Stations Used for Determining Interval Velocity.

Station	Type*	Location	Lat. N.	Long.W.	Elevation meters	Nominal Magnification at 1 Hz
ALQ	1	Albuquerque, N.M.	34°56.5'	106°27.5'	1853	200k
DRC	2	Durango, Co.	37°27.9'	107°47.0'	2220	400k
DUG	1	Dugway, Ut.	40°11.7'	112°48.8'	1477	200k
FOT	2	Ft.Stockton, Tex.	30°54.0'	102°42.0'	880	400k
GOL	1	Golden, Co.	39°42.0'	105°22.3'	2359	200k
JCT	1	Junction, Tex.	30°28.8'	99°48.1'	591	200k
KNU	2	Kanab, Ut.	37°01.4'	112°49.6'	1740	400k
LCN	2	Las Cruces, N.M.	32°24.1'	106°36.0'	1580	400k
LUB	1	Lubbock, Tex.	33°35.0'	101°52.0'	200	25k
SNM	3	Socorro, N.M.	34°04.2'	106°56.6'	1511	130k
TFO	4	Tonto Forest, Ariz.	34°17.2'	111°16.0'	1609	1000k
TJC	3	Trinidad, Co.	37°13.0'	104°41.1'	2103	100k
TUC	1	Tucson, Ariz.	32°18.6'	110°46.8'	985	200k
UBO	4	Uinta Basin, Ut.	40°19.3'	109°34.1'	1596	1000k
WMO	4	Wichita Mtns, Ok.	34°43.1'	98°35.3'	505	1000k

* 1 World Wide Standard Seismograph Station
2 Long Range Seismic Measurement Station
3 College Operated Station
4 Array Type Seismological Observatory

(2) The earthquake data file issued on magnetic tape by the National Geophysical Data Center, of the National Oceanic and Atmospheric Administration (recently under the direction of the United States Geological Survey).

Table 4.2 lists the events used, their magnitudes, locations, and the stations selected for interval velocity measurements. Seismograms were obtained for each event at each station listed. For a particular event, only those stations underlined in Table 4.2 gave usable data. Seismograms at the remaining stations did not have a P_n phase that could be accurately timed. The number of usable seismograms was about 45% of the seismograms requested.

Results

Figure 4.5 is a map showing the seismograph stations, and the location of those events which yielded usable interval velocity data. Also shown on this map are the intervals across which the velocity was determined, the value of the velocity, and the direction in which it was measured. The combinations of events and stations which produced usable values of velocity are listed in Table 4.3. This table gives, for each combination of event and station pair, the arrival times,

Figure 4.5. Seismograph stations (triangles) and epicenters providing interval velocity data. Epicenters are indicated by circles giving the date of the event. Solid circles are explosions, and empty circles are earthquakes. The values of interval velocity are given at the mid-points of the intervals, with an arrow showing the direction of measurement.

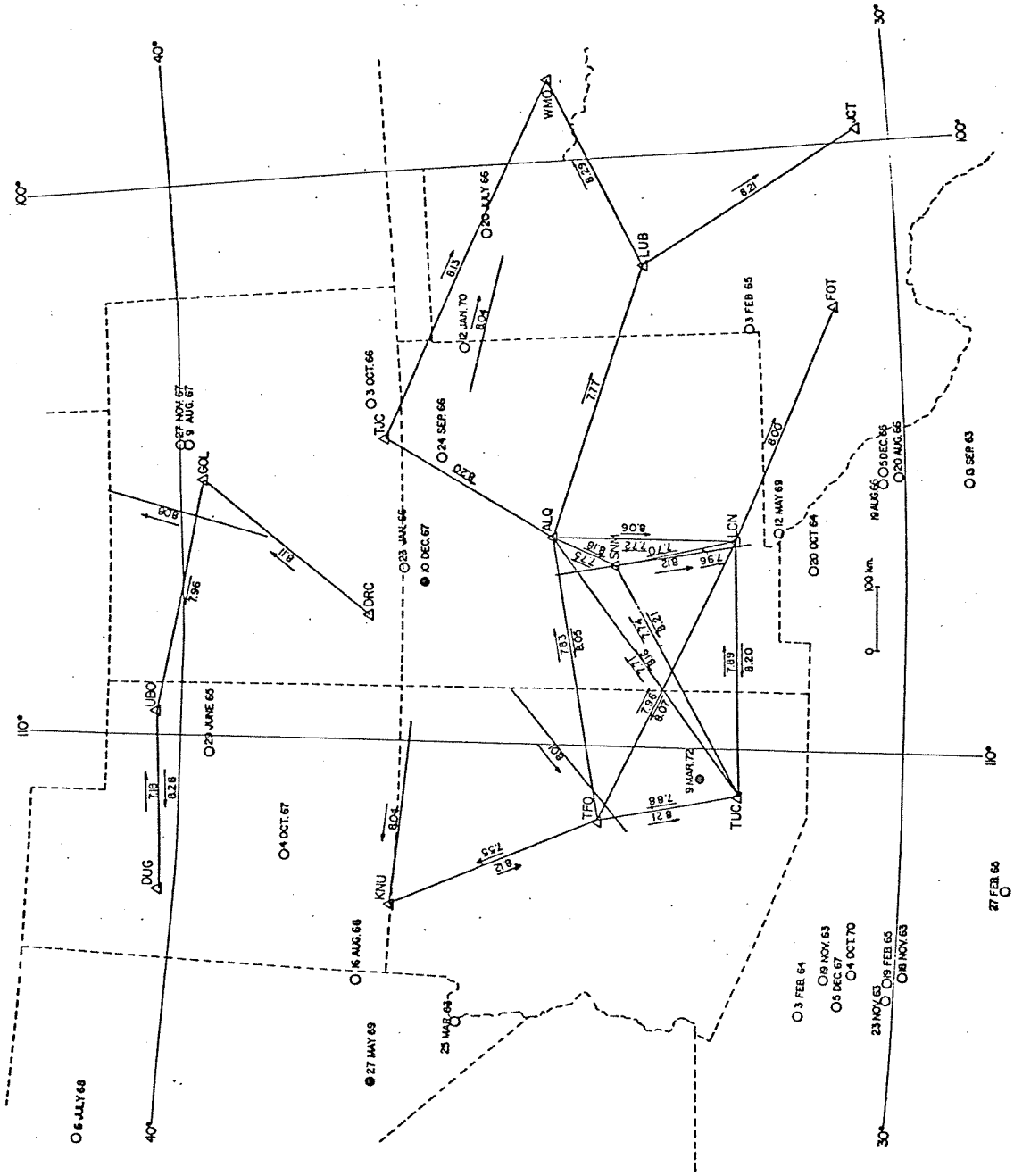
40°
100°
110°
30°
WMC
ICT
LUB
FOT
TJC
DRC
GGL
UBO
DUG
KNU
ALQ
LCN
SNM
TFO
TUC
20 JULY 66
3 OCT. 66
24 SEP. 66
12 JAN. 70
3 FEB 65
27 NOV. 67
9 AUG. 67
23 JAN. 66
10 DEC. 67
12 MAY 69
20 OCT. 64
19 AUG. 66
20 AUG. 66
5 SEP 63
29 JUNE 65
4 OCT. 67
9 MAR. 72
16 AUG. 66
27 MAY 69
25 MAR. 68
6 JULY 68
3 FEB. 64
9 NOV. 63
5 DEC. 67
4 OCT. 70
23 NOV. 63
9 FEB. 65
8 NOV. 63
27 FEB. 65
100 km.

Table 4.2. Events and Stations Selected for Calculating Interval Velocity.

Date	Origin Time	m_b	Lat.°N	Long.°W	Stations*
25 Mar. 63	09:28:43.0	4.6	36.00	114.80	ALQ, TUC, GOL, TFO, LCN, DRC
6 June 63	08:05:36.3	3.8	36.50	104.30	ALQ, GOL, LUB, DUG, DRC, LCN, TFO, SNM
19 Aug. 63	00:08:23.4	2.9(M_L)	32.45	107.13	ALQ, SNM
13 Sep. 63	10:51:56.6	4.7	29.10	105.60	ALQ, TUC, LUB, TFO, LCN, SNM
18 Nov. 63	14:38:28.9	6.5	29.90	113.60	ALQ, SNM, TUC
19 Nov. 63	01:11:43.2	4.9	31.00	113.70	ALQ, TUC, LCN, SNM
23 Nov. 63	07:50:46.3	5.1	30.10	114.00	ALQ, TUC, LCN, SNM
2 Feb. 64	08:22:44.1	3.9	35.10	99.70	ALQ, GOL, LUB, LCN
3 Feb. 64	13:51:07.4	4.2	31.30	114.30	ALQ, TUC, LCN
28 Mar. 64	10:08:45.0	5.1	42.90	101.60	ALQ, GOL, DRC, UBO
21 Aug. 64	19:41:37.5	4.7	30.60	113.80	LCN, FOT
22 Aug. 64	05:26:05.0	4.4	31.40	113.40	LCN, FOT
23 Sep. 64	18:09:38.0	4.4	35.90	114.80	LCN, FOT
20 Oct. 64	00:53:07.8	3.4(M_L)	31.30	107.00	ALQ, LCN, SNM Note: This is a new location and has not been published
5 Nov. 64	15:00:00.1		37.17	116.07	LCN, FOT

Table 4.2. (continued)

Date	Origin Time	m_b	Lat.°N	Long.°W	Stations *
3 Feb. 65	19:59:32.0	4.0(M_L)	32.10	103.00	LUB, WMO
11 Feb. 65	21:52:17.0	4.6	31.60	113.90	LCN, FOT
19 Feb. 65	14:50:23.0	4.4	30.10	113.70	LCN, FOT
27 Feb. 65	07:46:29.1	5.3	28.50	112.10	ALQ, TUC, TFO, LCN, SNM
13 Apr. 65	09:35:46.0	4.2	30.30	105.10	ALQ, LCN, SNM
29 June 65	07:46:28.2	4.3	39.60	110.30	GOL, KNU, TFO
30 Aug. 65	05:17:38.0	3.5	32.10	102.30	ALQ, LUB, JCT, WMO
23 Jan. 66	01:56:38.8	5.5	36.96	106.95	ALQ, TUC, LUB, JCT, UBO, WMO, TFO, KNU, TJC, SNM
31 Mar. 66	00:56:39.3	4.3	29.90	111.80	TUC, TFO
20 July 66	09:04:58.6	3.9	35.70	101.20	ALQ, TUC, GOL, LUB, JCT, WMO
14 Aug. 66	15:25:52.5	3.4	32.00	102.60	ALQ, LUB, WMO
16 Aug. 66	18:02:36.6	5.6	37.40	114.20	ALQ, TUC, TFO
19 Aug. 66	04:15:44.6	4.1	30.30	105.60	ALQ, TUC, LUB, JCT, WMO, SNM
20 Aug. 66	06:36:02.7	4.3	30.10	105.50	ALQ, SNM
21 Aug. 66	02:57:25.2	4.1	30.00	105.60	ALQ, SNM
17 Sep. 66	09:25:21.0	3.3(M_L)	32.25	109.75	ALQ, SNM
24 Sep. 66	07:33:46.4	3.8	36.45	105.05	ALQ, TUC, SNM

Table 4.2. (continued)

Date	Origin Time	m_b	Lat.°N	Long.°W	Stations *
3 Oct. 66	02:26:02.3	4.5	37.40	104.10	ALQ, TUC, GOL, LUB, DUG, JCT, TFO, UBO, SNM
5 Dec. 66	10:10:37.8	4.2	30.40	105.40	ALQ, SNM
9 Aug. 67	13:25:06.2	5.3	39.90	104.70	ALQ, LUB, DUG, TFO, WMO, UBO, LCN, KNU, SNM, TJC
4 Oct. 67	10:20:14.0	5.2	38.50	112.10	TUC, TFO
27 Nov. 67	05:09:22.7	5.2	40.00	104.70	ALQ, LUB, DUG, WMO, UBO, LCN, SNM, TJC
5 Dec. 67	11:09:37.4	5.0	30.80	114.10	ALQ, TUC, TFO, LCN, KNU, SNM
10 Dec. 67	18:30:00.1	5.1	36.68	107.21	ALQ, TUC, GOL, LUB, DUG, WMO, TFO, KNU, LCN, SNM, TJC
16 Jan. 68	09:17:52.3	3.9	39.3	112.1	TUC, TFO
9 Mar. 68	21:54:23.3	3.2(M_L)	32.60	106.10	LUB, ALQ, WMO, SNM
6 July 68	14:02:42.0	5.1	40.98	117.38	DUG, UBO
12 May 69	08:26:18.7	3.8(M_L)	31.93	106.45	ALQ, LUB, WMO, SNM,
12 May 69	08:49:16.3	4.3	31.93	106.45	ALQ, SNM
27 May 69	14:15:00.0	5.0	37.07	115.99	ALQ, TUC, DUG, TFO, UBO
10 Sep. 69	21:00:00.1	5.3	39.41	107.95	ALQ, LUB, TJC, SNM

Table 4.2. (continued)

Date	Origin Time	m_b	Lat.°N	Long.°W	Stations *
19 Oct. 69	11:51:34.4	3.8	30.77	105.72	ALQ, SNM
25 Dec. 69	12:49:10.1	4.4	33.36	110.65	ALQ, GOL, JCT, SNM, TJC
12 Jan. 70	11:21:15.4	3.5	36.07	103.18	ALQ, LUB, JCT, TUC, SNM
23 May 70	22:55:22.4	4.6	38.07	112.40	TUC, TFO
21 Sep. 70	07:04:36.9	4.4	43.18	110.76	GOL, UBO
4 Oct. 70	17:39:45.5	5.0	30.63	113.65	ALB, TUC, TFO
9 Mar. 72	18:45:00.0	4.5	37.75	110.49	ALB, LUB, JCT, TJC, SNM
20 Apr. 72	13:28:16.3	3.7	35.31	111.64	ALQ, TJC,
2 June 72	03:15:48.2	4.6	38.64	112.17	ALQ, SNM, TJC

*Only those stations underlined gave usable data.

Table 4.3. Data for Intervals and Events which Produced Good Values of P_n Velocity.

Interval	Date	T1 Hr:Min:Sec	T2 Hr:Min:Sec	D1* (km)	D2* (km)	V_n (km/sec)
ALQ to SNM	23 Jan.66	01:57:14.6	01:57:26.1	228.29	320.60	8.03
	3 Oct.66	02:26:52.3	02:27:05.0	345.51	450.03	8.23
	10 Dec.67	19:30:33.8	19:30:44.2	204.28	290.37	8.28
				Mean Velocity		8.18
SNM to ALQ	13 Sep.63	10:53:11.4	10:53:22.5	565.41	652.50	7.84
	18 Nov.63	14:40:09.7	14:40:21.8	779.90	872.81	7.67
	19 Nov.63	01:13:21.3	01:13:32.5	719.65	804.95	7.62
	19 Aug.66	04:16:44.4	04:16:55.3	436.72	520.84	7.72
	20 Aug.66	06:37:05.0	06:37:15.6	460.70	544.22	7.88
	5 Dec.66	10:11:35.6	10:11:45.9	432.07	513.18	7.87
	5 Dec.67	11:11:16.4	11:11:27.5	763.78	848.92	7.67

Table 4.3 (continued)

Interval	Date	T1 Hr:Min:Sec	T2 Hr:Min:Sec	D1* (km)	D2* (km)	V_n (km/sec)
	12 May 69	08:26:55.7	08:27:07.7	241.75	333.98	7.69
	12 May 69	08:49:53.2	08:50:05.1	241.75	333.98	7.75
	9 Mar.72	18:45:53.1	18:46:03.9	361.02	445.29	7.80
				Mean Velocity		7.75
ALQ to LCN	10 Dec.67	19:30:33.8	19:31:07.6	204.23	477.48	8.06
LCN to ALQ	13 Sep.63	10:52:47.1	10:53:22.5	274.17	378.32	7.75
	20 Oct.64	00:53:29.2	00:54:05.5	127.96	406.95	7.69
				Mean Velocity		7.72

Table 4.3 (continued)

Interval	Date	T1 Hr:Min:Sec	T2 Hr:Min:Sec	D1* (km)	D2* (km)	V_n (km/sec)
TJC to ALQ	9 Aug.67	13:25:53.2	13:26:26.2	297.81	571.65	8.31
	27 Nov.67	05:10:09.5	05:10:42.7	308.91	582.31	8.24
				Mean Velocity		8.27
ALQ to LUB	23 Jan.66	01:57:14.6	01:58:02.2	228.29	594.86	7.70
	10 Dec.67	19:30:33.8	19:31:23.6	206.28	596.14	7.83
				Mean Velocity		7.77
ALQ to TFO	23 Jan.66	01:57:14.6	01:57:47.1	228.29	492.16	8.12
	3 Oct.66	02:26:52.3	02:27:40.8	345.51	734,47	8.02
	9 Aug.67	13:26:26.2	13:27:00.8	571.65	854.40	8.17

Table 4.3 (continued)

Interval	Date	T1 Hr:Min:Sec	T2 Hr:Min:Sec	D1* (km)	D2* (km)	V_n (km/sec)
	10 Dec.67	19:30:33.8	19:31:05.7	206.28	457.27	7.87
				Mean Velocity		8.05
TFO to ALQ	25 Mar.63	09:29:36.0	09:30:26.0	374.65	765.47	7.82
	27 Feb.65	07:47:52.7	07:48:24.8	644.05	891.10	7.70
	5 Dec.67	11:10:39.3	11:11:27.5	467.33	848.92	7.87
	27 May 69	14:16:13.9	14:16:58.9	528.88	890.60	8.04
	4 Oct.70	17:40:47.2	17:41:34.2	461.03	824.86	7.74
				Mean Velocity		7.83
ALQ to TUC	24 Sep.66	07:34:19.6	07:35:19.8	217.48	705.56	8.09
	23 Jan.66	01:57:14.6	01:58:03.0	228.29	623.78	8.17

Table 4.3 (continued)

Interval	Date	T1 Hr:Min:Sec	T2 Hr:Min:Sec	D1* (km)	D2* (km)	Vn (km/sec)
	10 Dec.67	19:30:33.8	19:31:20.2	206.28	587.38	8.21
				Mean Velocity		8.16
TUC to ALQ	25 Mar.63	09:29:57.8	09:30:26.0	551.83	765.47	7.58
	19 Nov.63	01:12:28.8	01:13:32.5	312.48	804.95	7.73
	23 Nov.63	07:51:40.2	07:52:43.8	392.40	887.82	7.79
	5 Dec.67	11:10:23.4	11:11:27.5	356.66	848.92	7.68
	4 Oct.70	17:40:30.5	17:41:34.2	329.71	824.86	7.77
				Mean Velocity		7.71
SNM to LCN	10 Dec.67	19:30:44.2	19:31:07.6	290.32	477.48	7.96

Table 4.3 (continued)

Interval	Date	T1 Hr:Min:Sec	T2 Hr:Min:Sec	D1* (km)	D2* (km)	V_n (km/sec)
LCN to SNM	13 Sep.63	10:52:47.1	10:53:11.4	378.32	565.41	7.70
SNM to TUC	23 Jan.66	01:57:26.1	01:58:03.0	320.60	623.78	8.22
	10 Dec.67	19:30:44.2	19:31:20.2	292.69	587.38	8.19
				Mean Velocity		8.21
TUC to SNM	19 Nov.63	01:12:28.8	01:13:21.3	312.48	719.65	7.76
	23 Nov.63	07:51:40.2	07:52:32.2	392.40	797.65	7.79
	5 Dec.67	11:10:23.4	11:11:16.4	356.66	763.78	7.68
				Mean Velocity		7.74

Table 4.3 (continued)

Interval	Date	T1 Hr:Min:Sec	T2 Hr:Min:Sec	D1* (km)	D2* (km)	V_n (km/sec)
LCN to TFO	13 Sep.63	10:52:47.1	10:53:37.5	378.32	784.92	8.07
TFO to LCN	25 Mar.63	09:29:36.0	09:30:36.2	374.65	853.64	7.96
LCN to TUC	13 Sep.63	10:52:47.1	10:53:15.4	378.32	610.42	8.20
TUC to LCN	25 Mar.63	09:29:57.8	09:30:36.2	551.83	853.64	7.86
	19 Nov.63	01:12:28.2	01:13:15.5	312.48	690.37	7.99
	23 Nov.63	07:51:40.2	07:52:25.5	392.40	749.09	7.87
	3 Feb.64	13:51:56.2	13:52:44.6	351.36	738.43	7.96

Table 4.3 (continued)

Interval	Date	T1 Hr:Min:Sec	T2 Hr:Min:Sec	D1* (km)	D2* (km)	Vn (km/sec)
	5 Dec.67	11:10:23.4	11:11:11.9	356.66	733.07	7.76
				Mean Velocity		7.89
LCN to FOT	19 Feb.65	14:52:00.0	14:52:42.0	722.34	1058.28	8.00
TJC to WMO	9 Aug.67	13:25:53.2	13:26:53.7	297.81	789.16	8.12
	27 Nov.67	05:10:10.5	05:11:10.0	308.91	797.01	8.14
				Mean Velocity		8.13
DRC to GOL	25 Mar.63	09:30:10.4	09:30:44.6	647.02	924.43	8.11

Table 4.3 (continued)

Interval	Date	T1 Hr:Min:Sec	T2 Hr:Min:Sec	D1* (km)	D2* (km)	V_n (km/sec)
TFO to TUC	25 Mar.63	09:29:36.0	09:29:57.8	374.65	551.83	8.13
	23 Jan.66	01:57:47.1	01:58:03.0	492.16	623.78	8.28
	16 Aug.66	18:03:35.0	18:04:00.5	436.73	645.02	8.17
	4 Oct.67	10:21:20.5	10:21:47.6	475.38	696.77	8.17
	27 May 69	14:16:13.9	14:16:36.1	528.88	711.83	8.28
				Mean Velocity		8.21
TUC to TFO	13 Sep.63	10:53:15.4	10:53:37.5	610.42	784.92	7.90
	4 Oct.70	17:40:30.5	17:40:47.2	329.71	461.03	7.86
				Mean Velocity		7.88

Table 4.3 (continued)

Interval	Date	T1 Hr:Min:Sec	T2 Hr:Min:Sec	D1* (km)	D2* (km)	V_n (km/sec)
LUB to JCT	23 Jan.66	01:58:02.2	01:58:48.0	594.86	975.94	8.32
	20 Jul.66	09:05:32.9	09:06:16.5	242.60	593.27	8.04
	12 Jan.70	11:21:59.0	11:22:46.6	300.92	694.91	8.28
				Mean Velocity		8.21
LUB to WMO	23 Jan.66	01:58:02.2	01:58:26.3	594.86	794.46	8.28
	14 Aug.66	15:26:20.8	15:26:57.1	188.56	479.65	8.08
	19 Aug.66	04:16:54.4	04:17:31.7	506.92	820.07	8.40
	10 Dec.67	19:31:23.3	19:31:48.7	596.14	808.81	8.37
				Mean Velocity		8.29
KNU to TFO	29 Jun.65	07:47:23.1	07:47:52.0	361.44	597.79	8.12

Table 4.3 (continued)

Interval	Date	T1 Hr:Min:Sec	T2 Hr:Min:Sec	D1* (km)	D2* (km)	V_n (km/sec)
TFO to KNU	5 Dec.67	11:10:39.3	11:11:10.1	467.33	699.80	7.55
GOL to UBO	3 Oct.66	02:26:45.6	02:27:22.8	278.31	574.50	7.96
DUG to UBO	6 Jul.68	14:03:34.5	14:04:11.8	396.27	664.27	7.19
	27 May 69	14:16:02.5	14:16:33.4	443.35	664.58	7.16
				Mean Velocity		7.18

Table 4.3 (continued)

Interval	Date	T1 Hr:Min:Sec	T2 Hr:Min:Sec	D1* (km)	D2* (km)	Vn (km/sec)
UBO to DUG	9 Aug.67	13:26:06.7	13:26:39.9	417.59	692.55	8.28
	27 Nov.67	05:10:23.4	05:10:56.7	416.19	691.62	8.27
				Mean Velocity		8.28

* Distances calculated using the geodetic formulas of Ball (1972).

epicentral distances, and the velocity derived. Where there was more than one velocity measured over the same interval, the mean value is also given, and is used in Figure 4.5.

All values of velocity from Figures 2.1, 2.5, and 4.5 are combined in Figure 4.6. Three additional control points are used, one in western Arizona, (Diment et al., 1961), one in southwestern Wyoming (Willden, 1965), and one in northern Utah (Braile et al., 1973). The value of velocity is placed at the mid-point of the spread or interval over which it was measured. Reversed or true velocities are indicated by solid circles and are underlined. Apparent velocities are indicated by open circles and are capped by an arrow showing the direction of measurement.

The contours of equal V_n in Figure 4.6 indicate a velocity greater than 8.3 km/sec in the Great Plains of eastern Oklahoma and northeastern Texas. To the northwest this value diminishes to less than 7.7 km/sec in the eastern Basin and Range Province of central Utah. In the Colorado Plateau of southwestern Utah and northern Arizona, a salient having velocity greater than 8.0 km/sec protrudes to the west. This high velocity is flanked to the south by an east-west zone of lower velocity, which bends southward in western New Mexico. The

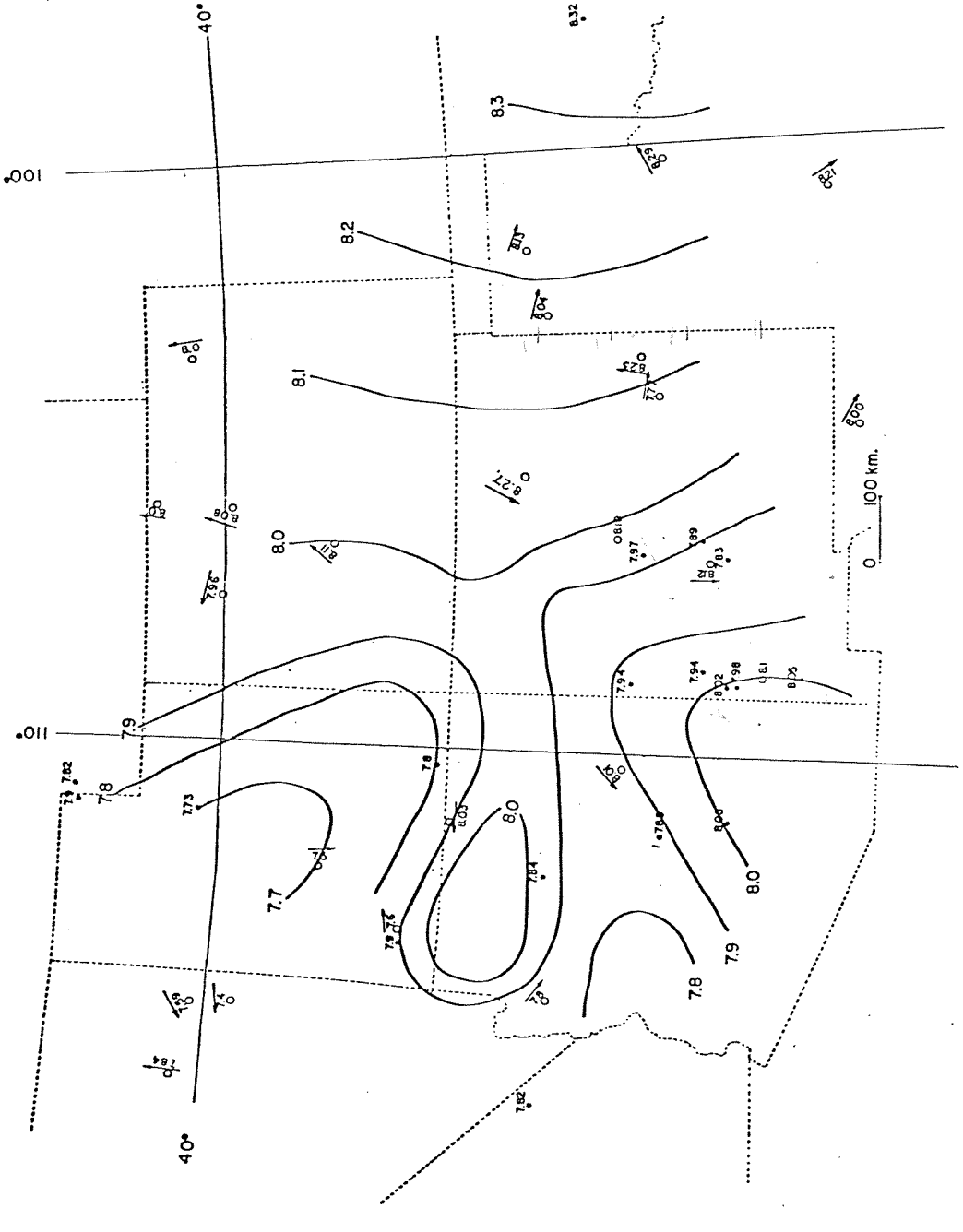

Figure 4.6. Contours of P_n velocity in New Mexico and vicinity. Solid control points indicate true or reversed values, empty control points indicate apparent or unreversed values of velocity.

same low velocity zone surrounds a high velocity area in southeastern Arizona. In New Mexico this low velocity zone coincides with the southern part of the Rio Grande rift.

Figure 4.6 generally resembles Herrin's map of P_n velocities (Figure 2.6). Herrin's dashed velocity high on the southern part of the Arizona-New Mexico border has been confirmed in Figure 4.6, but has been shifted to the north and west. The east-west low velocity zone across central Arizona is less pronounced in Figure 4.6 than on Herrin's map. The velocity high in the Colorado Plateau has been shifted southward in Figure 4.6 relative to the same high in Figure 2.6. Finally the velocity low in central Utah has been increased in magnitude, and has been rotated in a clockwise direction compared to the same feature on Figure 2.6.

Herrin's map may lack the data published in 1965, for sections 9, 10 and 11, in Tables 2.1 and 2.2. It certainly lacks the data published from 1966 onwards, for sections 12, 13, 14 and 15 in Tables 2.1 and 2.2. Additional control in Figure 4.6 not used in Figure 2.6, are the reversed values of interval velocity obtained in this study, in New Mexico, Arizona, and Utah, as well as the point in northern Utah (Braile et al., 1973).

5. REGIONAL CRUSTAL THICKNESS

The apparent dip of the Moho surface can be deduced from reversed values of P_n velocity, as indicated in the previous section. This technique was employed to study the configuration of the Moho, and with the help of information from previous work, a map was made of the variation in crustal thickness.

Procedure

The dip of the Moho was estimated from the values of reversed P_n velocity using the relation (Dix, 1952),

$$\theta = (\arcsin(V_1/V_{2d}) - \arcsin(V_1/V_{2u}))/2$$

where V_1 is the average crustal velocity

V_{2d} is the down-dip velocity in the upper mantle

V_{2u} is the up-dip velocity in the upper mantle

An average velocity for the entire crust was used because the value of velocity in the lower crust and the dip of the Conrad discontinuity are not always known. V_1 was assigned a value of 6.2 km/sec, which was the average crustal velocity deduced by Warren (1969) from reflection and refraction studies in central Arizona.

The 11 station pairs in Table 4.3 which have reversed coverage are listed in Table 5.1. Table 5.1 gives the apparent dip angle across each interval, the tangent of this angle, the length of the interval, and finally the change in crustal thickness across the interval. The second column in Table 5.1 gives the number of measurements which have been averaged to obtain each velocity. This number is a measure of the reliability of the velocities listed. For example 10 measurements were averaged to obtain a velocity of 7.75 from SNM to ALQ, and only a single measurement of 8.07 was available from LCN to TFO. Therefore the former velocity is more reliable than the latter.

Results

The reversed intervals listed in Table 5.1 cover the two intervals TFO-KNU and UBO-DUG, as well as the 8 closed loops shown in Figure 5.1. Differences in crustal thickness in going around the closed loops are given in Table 5.2, with a positive sign indicating an increase in thickness and a negative sign indicating a decrease. The closure of the last 5 loops in Table 5.2 is good whereas the first 3 loops have misclosures of -3.9, -5.3, and -4.5 km. The first 3 loops all end in the two intervals (TUC-TFO and TFO-ALQ), which suggests that the

Table 5.1. Dips and Depths Deduced from Reversed Velocities.

Interval	Number of Measure-ments	V (km/sec)	θ (degrees)	Tan(θ)	Delta (km)	Z(km)
ALQ-SNM	3	8.18				
SNM-ALQ	10	7.75	1.923	0.0336	106	3.6
ALQ-LCN	1	8.06				
LCN-ALQ	2	7.72	1.572	0.0274	281	7.7
ALQ-TFO	4	8.05				
TFO-ALQ	5	7.83	0.993	0.0173	442	7.6
ALQ-TUC	3	8.16				
TUC-ALQ	5	7.71	2.041	0.0356	493	17.5
SNM-LCN	1	7.96				
LCN-SNM	1	7.70	1.235	0.0216	189	4.1
SNM-TUC	2	8.21				
TUC-SNM	3	7.74	2.094	0.0366	403	14.7
LCN-TFO	1	8.07				
TFO-LCN	1	7.96	0.480	0.0084	482	4.0

Table 5.1 (continued)

Interval	Number of Measure-ments	V (km/sec)	θ (degrees)	Tan(θ)	Delta (km)	Z(km)
LCN-TUC	1	8.20				
TUC-LCN	5	7.89	1.337	0.0233	394	9.2
TFO-TUC	5	8.21				
TUC-TFO	2	7.88	1.423	0.0248	219	5.4
TFO-KNU	1	7.55				
KNU-TFO	1	8.12	2.713	0.0474	339	16.1
UBO-DUG	2	8.28				
DUG-UBO	2	7.18	5.613	0.0983	273	26.8

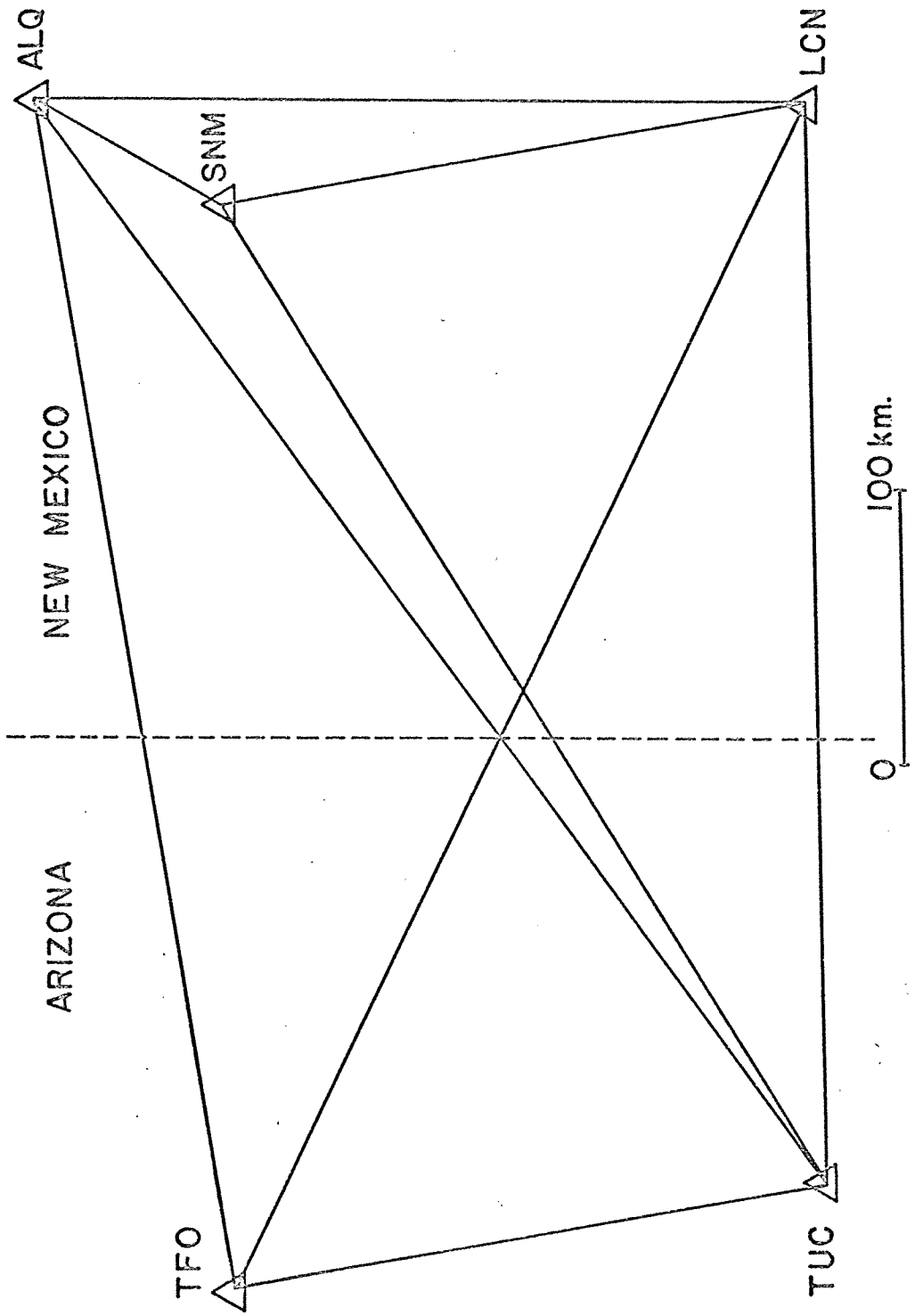

Figure 5.1. Intervals having reversed values of velocity, and constituting closed loops.

Table 5.2. Differences in Crustal Thickness around the Closed Loops.

Loop	Interval	Z(km)
ALQ-LCN-TUC-TFO	ALQ	
	to	-7.7
	LCN	
	to	-9.2
	TUC	
	to	+5.4
	TFO	
	to	+7.6
	ALQ	____
	Misclosure	-3.9 km
ALQ-SNM-TUC-TFO	ALQ	
	to	-3.6
	SNM	
	to	-14.7
	TUC	
	to	+5.4
	TFO	
	to	+7.6
	ALQ	____
	Misclosure	-5.3 km

Table 5.2 (continued)

Loop	Interval	Z(km)	
ALQ-TUC-TFO	ALQ		
	to	-17.5	
	TUC		
	to	+5.4	
	TFO		
	to	+7.6	
	ALQ	____	
	Misclosure	-4.5	km
ALQ-LCN-TUC	ALQ		
	to	-7.7	
	LCN		
	to	-9.2	
	TUC		
	to	+17.5	
	ALQ	____	
	Misclosure	+0.6	km

Table 5.2 (continued)

Loop	Interval	Z(km)
SNM-LCN-TUC	SNM	
	to	-4.1
	LCN	
	to	-9.2
	TUC	
	to	+14.7
	SNM	———
	Misclosure	+1.4 km
SNM-TUC-ALQ	SNM	
	to	-14.7
	TUC	
	to	+17.5
	ALQ	
	to	-3.6
	SNM	———
	Misclosure	-0.8 km

Table 5.2 (continued)

Loop	Interval	Z(km)	
SNM-ALQ-LCN	SNM		
	to	+3.6	
	ALQ		
	to	-7.7	
	LCN		
	to	+4.1	
	SNM	———	
	Misclosure	0.0	km
LCN-TUC-TFO	LCN		
	to	-9.2	
	TUC		
	to	+5.4	
	TFO		
	to	+4.0	
	LCN	———	
	Misclosure	+0.2	km

error is in these two intervals. The increase in thickness from TUC to ALQ is 13 km; 5.4 km from TUC to TFO, and 7.6 km from TFO to ALQ. The misclosure in the 3 loops averages -4.5 km, and would be reduced substantially if the change in thickness from TUC to TFO to ALQ were increased from +13 km to +17.5 km. When the 4.5 km increase in crustal thickness is distributed between the 2 intervals TUC-TFO and TFO-ALQ, in proportion to their lengths, the former interval gets 1.5 km and the latter 3.0 km. The first 3 loops adjusted in this way have good closure as seen in Table 5.3. The only other loop influenced by this adjustment is the last one in Table 5.2, because it contains the interval TUC-TFO. The adjustment causes the misclosure for this loop to increase from +0.2 to +1.7 km, which is tolerable considering the great improvement in the first 3 loops.

The observed misclosures could be caused by abrupt changes in crustal thickness near the stations. If changes occur within the critical distance (about 50 km) of the stations, they would not fully influence the reversed values of P_n velocity. An example of such changes near TFO, deduced from a detailed seismic survey, is shown in Figure 5.2.

Two values of crustal thickness are known (numbers 8 and 13 in Figure 2.1 and Table 2.1) for converting

Table 5.3. Adjusted Differences in Crustal Thickness for the First Three Loops of Table 5.2.

Loop	Interval	Z(km)
ALQ-LCN-TUC-TFO-ALQ	ALQ	
	to	-7.7
	LCN	
	to	-9.2
	TUC	
	to	+6.9
	TFO	
	to	+10.6
	ALQ	
	Misclosure	+0.6 km
ALQ-SNM-TUC-TFO-ALQ	ALQ	
	to	-3.6
	SNM	
	to	-14.7
	TUC	
	to	+6.9
	TFO	
	to	+10.6
	ALQ	
	Misclosure	-0.8 km

Table 5.3 (continued)

Loop	Interval	Z(km)
ALQ-TUC-TFO-ALQ	ALQ	
	to	-17.5
	TUC	
	to	+6.9
	TFO	
	to	+10.6
	ALQ	
	Misclosure	0.0 km

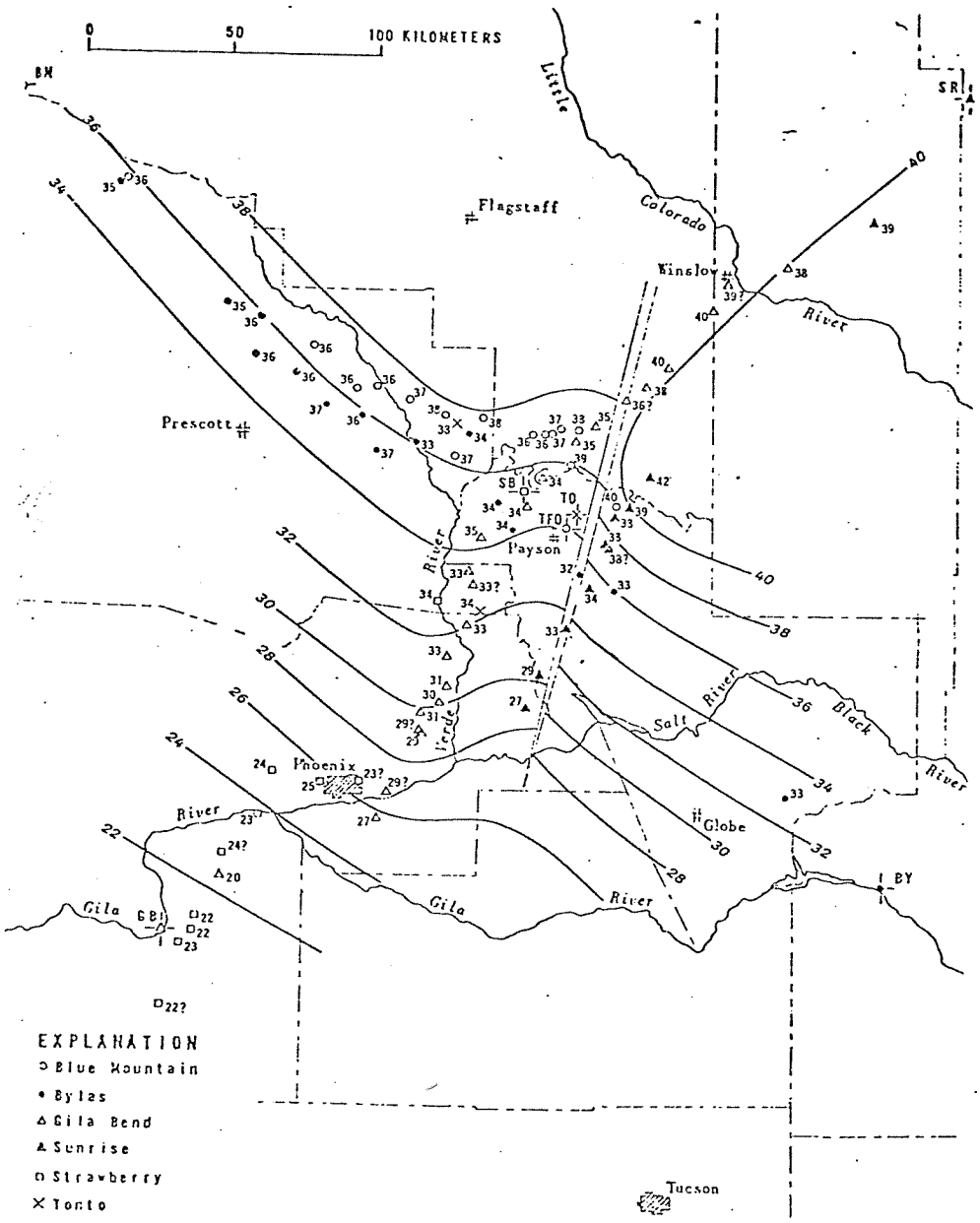

Figure 5.2. Configuration of the Moho surface relative to sea level in the vicinity of TFO, after Warren (1969).

the differences in crustal thickness around the loops in Figure 5.1 into values of crustal thickness. These two values are at ALQ and TFO, and have a maximum difference, according to Table 2.1, of 5 km. However, the difference between ALQ and TFO, according to Table 5.3, is 10.6 km. As mentioned in the section on previous work, the crustal section at ALQ (number 8) is the only one in Figure 2.1 that is not derived from a refraction profile. It results from a study at a single station, and possibly is the least accurate section in Figure 2.1. On the other hand, the section at TFO (number 13) results from a detailed seismic survey involving tens of field stations. Consequently the crustal thickness reported for TFO is the one used in the present study.

The closed loops listed in Tables 5.2 and 5.3 were adjusted with respect to TFO. The thicknesses at the stations were rounded to the nearest kilometer, and used as control points in the map of crustal thickness, Figure 5.3. The largest discrepancy between the thicknesses used in Figure 5.3 and Tables 5.1 and 5.3 is 2 km between LCN and TFO, which are the two stations having the largest distance separation in Figure 5.1. Depth differences across the two intervals TFO-KNU and UBO-DUG, from Table 5.1, were also used in Figure 5.3.

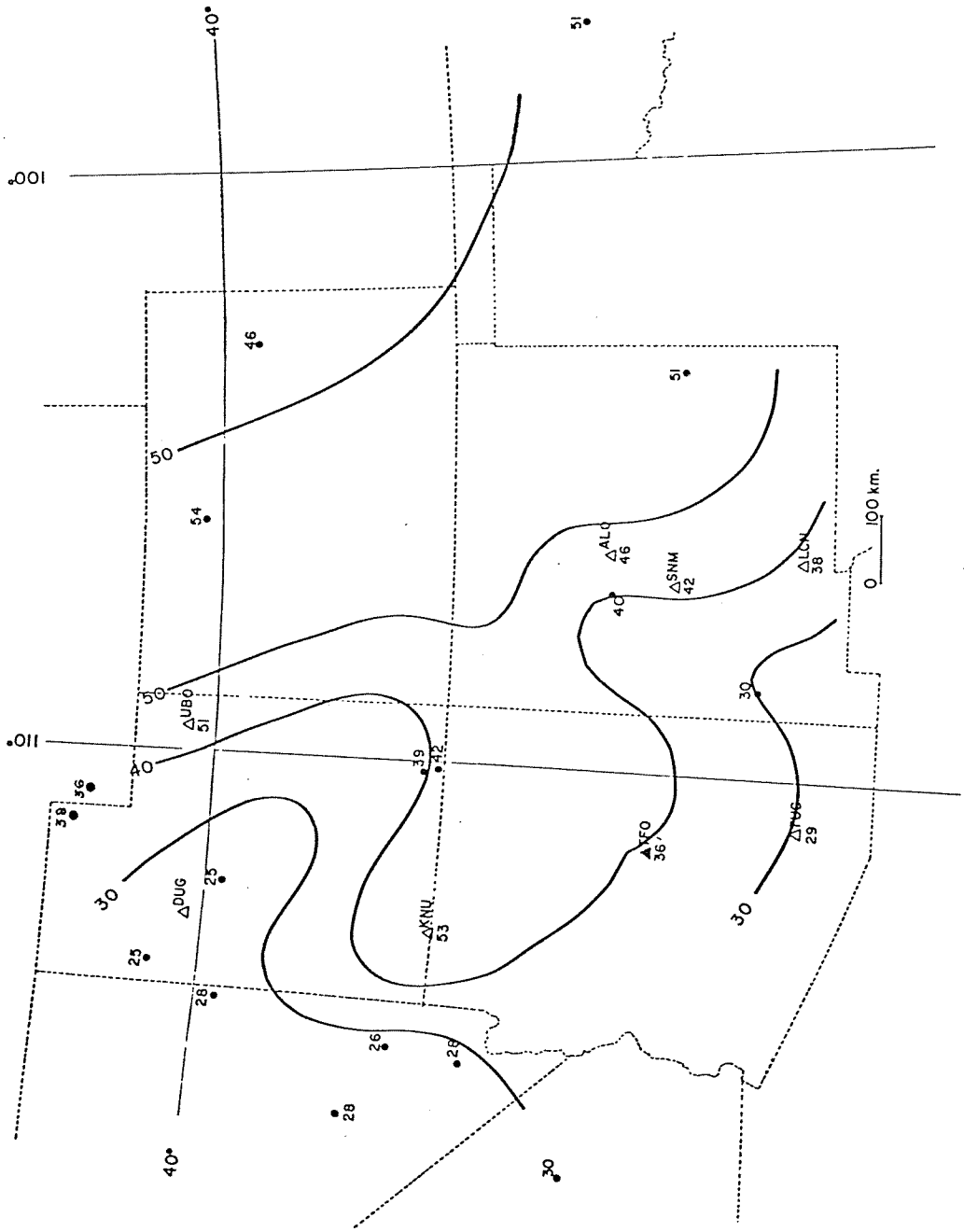

Figure 5.3. Contours of crustal thickness in New Mexico and vicinity. Control points are shown.

Contour Map

All the sections listed in Table 2.1, except that for ALQ, are used as control points in Figure 5.3. In addition control points in southeastern Nevada (Diment et al., 1961), southwestern Wyoming (Willden, 1965), northern Utah (Braile et al., 1973), and the thickness derived earlier from the Gasbuggy south profile, are also used. The value at each control point, in Figure 5.3, is the thickness between the basement and the Moho, and is placed at the approximate location of the cross-over distance.

The contours in Figure 5.3 indicate a crustal thickness greater than 50 km below the Rocky Mountains in Colorado and northern New Mexico. This thickness persists into the Great Plains of northeastern New Mexico, northern Texas and southern Oklahoma. A salient having a thickness greater than 40 km projects from the southern Rocky Mountains westward into the Colorado Plateau of southern Utah and northern Arizona. This region is flanked to the north by an area having thickness less than 30 km in central Utah, and to the south by a thin crust in southeastern Arizona and southwestern New Mexico.

Figure 5.3 bears little resemblance to the map

of Stuart et al. (1965) shown in Figure 2.2. The only feature that is common to both maps is the thick crust in Colorado and northeastern New Mexico. The alternation in Figure 5.3 of a thin crust in central Utah, a thick crust in northern Arizona, and a thin crust in southeastern Arizona and southwestern New Mexico, has no parallel in Figure 2.2. The crustal thicknesses shown indicate that the Colorado Plateau Province (Figure 1.1) is underlain by a thick crust, and that the Basin and Range Province is underlain by a thin crust.

The reason Figure 5.3 differs from the map by Stuart et al., is that it is based on the following additional control points not used in the earlier study :

(1) Sections 11, 12, 13 and 14 in Tables 2.1 and 2.2

(2) Control points in southwestern Wyoming (Willden, 1965), and northern Utah (Braile et al., 1973).

(3) The thicknesses at ALQ, SNM, LCN, TUC and TFO, which result from the 8 loops shown in Figure 5.1, and which are internally consistent.

(4) Approximate thicknesses at KNU and UBO from reversed P_n information.

(5) The depth derived earlier in this study from Gasbuggy.

6. SUMMARY

Interpretation of the seismic profile extending southward from the Gasbuggy nuclear test of 10 December 1967. yielded the following crustal structure at a point located 50 km west of ALQ. The crust between the basement and the Moho is 39.9 km thick. It consists of an upper layer 18.6 km thick having P_g velocity 6.15 km/sec, and a lower layer 21.3 km thick having apparent P^* velocity 6.5 km/sec. The uppermost mantle has an apparent P_n velocity 8.12 km/sec. Supplementary information from earthquakes and explosions indicates that the velocity in the upper crust drops to 5.8 km/sec in the Rio Grande rift, and that the true velocity in the uppermost mantle is 7.9 km/sec.

A study of interval velocities has shown that there is no detectable increase in V_n with distance, which confirms than P_n is a true head wave, at least in New Mexico. Values of P_n interval velocity measured in this study were added to values previously measured, and the variation in P_n velocity was mapped. The V_n contour map derived resembles, in a general sense, that presented by Herrin (1966, 1969). The value of P_n velocity decreases westward, from more than 8.3 km/sec in Oklahoma and northern Texas to 8.0 km/sec in central Colorado

and central New Mexico. In Utah and Arizona V_n varies in a north-south sense as well as in an east-west sense. The southern Colorado Plateau has a high P_n velocity, greater than 8.0 km/sec, and is surrounded by lower velocities in the Basin and Range Province. An exceptional region in the Basin and Range Province is the area surrounding the seismic station TUC which has a P_n velocity greater than 8.0 km/sec. In western New Mexico a strip about 100 km wide from Grants to Las Cruces has a P_n velocity lower than 7.9. This strip covers the southern portion of the Rio Grande rift.

Differences in crustal thickness were estimated from the values of reversed P_n velocity. Closure, around loops of stations, of these differences was satisfactory. Four additional control points were added to the map of crustal thickness in this way. Moreover, approximate estimates of crustal thickness, from reversed P_n velocities, were made at the 2 seismic stations KNU and UBO, which did not form part of closed loops. Contours of crustal thickness indicate that the crust is more than 50 km thick in Oklahoma and northern Texas. This coincides with the area of highest P_n velocity. Coincidence of thick crust with high upper mantle velocity has been noted by various investigators, for example Pakiser (1963). The same pattern occurs in northern Arizona

and in Utah. The southern Colorado Plateau Province has a crustal thickness greater than 40 km and a high P_n velocity. The Basin and Range Province in central Utah has a crustal thickness less than 30 km and a low P_n velocity.

Elsewhere the association of thick crust with high P_n velocity is not so clear. In Colorado, crustal thickness in excess of 50 km does not coincide with high P_n velocity. In southwestern New Mexico the crustal thickness of 35 km to the west of SNM is only partly matched by a low P_n velocity. In southeastern Arizona the high P_n velocity near TUC is associated with relatively thin crust.

In the state of New Mexico, maximum variation in both crustal thickness and P_n velocity occurs from the northeast to the southwest. P_n velocity, greater than 8.1 in the northeast portion of the state, drops to less than 7.9 southwest of LCN. Crustal thickness, greater than 50 km in the northeastern portion of the state, diminishes to less than 30 km in the southwestern corner.

The Datil-Mogollon volcanic field of western New Mexico extends from the latitude of Socorro to the Mexican border (Figure 1.3). This area has both a thin crust and a low P_n velocity, which confirms that it is an extension of the Basin and Range Province into New

Mexico. These results are in harmony with the observations, mentioned in the introductory section, of high heat flow and numerous hot springs in this area.

At the level of resolution available in this study, no strong anomaly could be related to the Rio Grande rift. The largest observed anomaly was a drop of about 5% in the upper crustal seismic velocity, from 6.15 km/sec to 5.8 km/sec. The drop in P_n velocity centered on the western flank of the southern portion of the rift was less, about $2\frac{1}{2}$%. Detection of a thin crust, or a mantle bulge, underlying the rift (Lipman, 1969), was beyond the resolution of this study.

APPENDIXES

APPENDIX I

Geologic Corrections for Gasbuggy

A computer program is presented which (1) makes linear least squares fits of the observed P_g arrival times, (2) makes geologic corrections to all the observed arrival times, by placing the shot and all stations on Paleozoic basement rocks, (3) makes linear least squares fits of the corrected P_g arrival times, (4) makes linear least squares fits of observed P_n arrival times, (5) makes linear least squares fits of the corrected P_n arrivals, and finally, (6) plots all the observed and corrected arrivals and the 4 least squares lines, as in Figure 3.4.

Comment cards in the program indicate when each operation is performed.

```
C  CORRECTIONS FOR GASBUGGY
      DIMENSION          DELTA(33),T(33),Z(33),SHOTCR(33),STNCR(33),TCR(3
     $3),TRED(33),TOTCR(33),X(99),TT(99),A(33,2),D1(33),D2(33),D3(66),
     $COEF(2),R(33),IER(33),CCOEF(2),TTT(99),CCCOEF( 2),TTCR(33),TTTT(99
     $),AA(33,2),STN(3,33),DSAVE(2),XX(111),TN(33),COEFN(2),TNN(111)
      INTEGER STN
      J=5
      JJ=J+11
       READ 11,((STN(L,K) ,L=1,3),DELTA(K),T(K),Z(K),K=1,JJ)
      DO 100 K=1,J
      A(K,1)=1.
      A(K,2)=DELTA(K)
  100 CONTINUE
C  TO GET LEAST SQUARES FIT FOR PG RAW   DATA
      CALL SOLVIT (A,T,R,COEF,D1,D2,D3,J,2,33,IER)
      PRINT 14
      PRINT 88,COEF(1),COEF(2)
      PRINT  16
      PRINT 77,(A(K,2),T(K),R(K),K=1,J)
      V1=1./COEF(2)
C B IS DEPTH TO PALEOZOIC & H IS DEPTH OF SHOT
       B=4.023
       H=1.292
      V0 = SQRT ((2*B-H)**2*(V1**2)/((V1**2)*(COEF(1)**2)+(2*B-H)**2))
      PRINT 22,V0,V1
      THETA=ARSIN(V0/V1)
      DO 222 K=1,J
      SHOTCR(K)=  (COS(THETA)/V0)*(B-H)
```

```
      STNCR(K)=Z(K)*COS(THETA)/VO
   44 TOTCR(K)=SHOTCR(K)+STNCR(K)
      TCR(K)=T(K)-TOTCR(K)
  222 CONTINUE
      ALPHA = ARSIN (VO/8. )
      JJJ=J+1
      DO 333 K=JJJ,JJ
      SHOTCR(K)=  (COS(ALPHA)/VO)*(B-H)
      STNCR(K)=Z(K)*COS(ALPHA)/VO
      TOTCR(K)=SHOTCR(K)+STNCR(K)
       TCR(K)=T(K)-TOTCR(K)
  333 CONTINUE
C  TO GET LEAST SQUARES FIT FOR PG CORR. DATA
      CALL SOLVIT (A,TCR,R,CCOEF,D1,D2,D3,J,2,33,IER)
      PRINT  18
      PRINT 88, CCOEF(1),CCOEF(2)
      PRINT  16
      PRINT 77,(A(K,2),TCR(K),R(K),K=1,J)
      V1CORR=1./ CCOEF(2)
      PRINT  13,  V1CORR
      PRINT  65
      PRINT 66
      DO 555 K=1,JJ
       PRINT  55 ,  (STN(L,K),L=1,3),DELTA(K),T(K),Z(K),SHOTCR(K),STNCR(
     $K),TOTCR(K),TCR(K)
      KK=K-J
      IF (K.GT.J)  GO TO 33
```

```
      GO TO 555
   33 TTCR(KK)=TCR(K)
      TN(KK)=T(K)
      AA (KK,1)=1.
      AA(KK,2)=DELTA(K)
  555 CONTINUE
C  TO GET LEAST SQUARES FIT FOR PN RAW DATA
      CALL SOLVIT  ( AA,TN,R,COEFN,D1,D2,D3,10,2,33,IER)
      PRINT 20
      PRINT  88,  COEFN(1),COEFN(2)
      PRINT  16
      PRINT  77,  (AA(KK,2),TN(KK),R(KK),KK=1,11)
      V2=1./COEFN(2)
      PRINT  26,V2
C  TO GET LEAST SQUARES FIT FOR PN CORR. DATA
       CALL SOLVIT ( AA     ,TTCR   ,R,CCCOEF,D1,D2,D3,10,2,33,IER)
      PRINT  24
      PRINT 88, CCCOEF(1), CCCOEF(2)
      PRINT 16
      PRINT 77,(AA(KK,2),TTCR(KK),R(KK),KK=1,11)
      V2COR=1./CCCOEF(2)
      PRINT  28,V2COR
      NN=55
      DO 444 I=20,NN
      XX(I)=10.*I
      TTTT(I)=CCCOEF(1)+CCCOEF(2)*XX(I)
      TNN(I)=COEFN(1)+COEFN(2)*XX(I)
  444 CONTINUE
      N=21
      DO 111 I=1,N
```

```
      X(I)=10.*(I-1)
      TT(I)=COEF(1)+COEF(2)*X(I)
      TTT(I)=CCOEF(1)+CCOEF(2)*X(I)
  111 CONTINUE
      CALL PLOT  (1.0,0.5,-3)
      DELTA(JJ+1)=0.
      DELTA(JJ+2)=80.
      T(JJ+1)=0.
      T(JJ+2)=8.
      CALL AXIS (0.0,0.0,'DISTANCE (KM)',-13,07.0,0.0,DELTA(JJ+1),DELTA(
     $JJ+2),20.)
      CALL AXIS (0.0,0.0,'TIME  (SEC)',11,10.,90.0,T(JJ+1),T(JJ+2),20.)
      CALL SYMBOL  (1.5,9.0,0.200,'CORRECTIONS FOR GASBUGGY',0.,24)
      CALL SYMBOL  (1.5,8.5,0.100,2   ,0.,-1)
      CALL SYMBOL  (-0.,-0.,0.100, '   RAW DATA',0.,11)
      CALL SYMBOL (1.5,8.0,0.100,4  ,0.,-1)
      CALL SYMBOL  (-0.,-0.,0.100,'   CORRECTED DATA',0.,17)
C PLOT  ALL  RAW  DATA  POINTS
      CALL LINE (DELTA,T,JJ  ,1,-1,2)
      TT(N+1)=0.
      TT(N+2)=8.
      X(N+1)=0.
      X(N+2)=80.
C PLOT  LEAST SQUARES FIT  OF  RAW  PG  DATA
      CALL LINE (X,TT,N,1,0,U)
      TTT(N+1)=0.
      TTT(N+2)=8.
C PLOT  LEAST SQUARES FIT  OF  CORR.PG  DATA
      CALL LINE (X,TTT,N,1,0,U)
       DSAVE(1)=DELTA(J+1)
```

```
      DSAVE(2)=DELTA(J+2)
      DELTA(J+1)=0.
      DELTA(J+2)=80.
      TCR(J+1)=0.
      TCR(J+2)=8.
C PLOT   CORR.  PG  POINTS
      CALL LINE (DELTA,TCR,J  ,1,-1,4)
      DELTA(J+1)=DSAVE(1)
      DELTA(J+2)=DSAVE(2)
      DELTA(JJ+1)=0.
      DELTA(JJ+2)=80.
      TTCR(JJ-4)=0.
      TTCR(JJ-3)=8.
C PLOT   CORR.  PN  POINTS
      CALL LINE  (DELTA(6),TTCR   ,11,1,-1,4)
      XX(NN+1)=0.
      XX(NN+2)=80.
      TTTT(NN+1)=0.
      TTTT(NN+2)=8.
C PLOT  LEAST SQUARES FIT  OF  CORR.PN  DATA
      CALL LINE (XX(20),TTTT(20),36,1,0,U)
C  PLOT LEAST SQUARES FIT TO RAW PN DATA
      TNN (NN+1)=0.
      TNN(NN+2)=8.
```

```
      CALL LINE (XX(20),TNN(20),36,1,0,2)
      CALL PLOT (20.0,-1.5,-3)
      CALL PLOT (0.0,0.0,999)
      STOP
   14 FORMAT ( '1',45X,'TABLE 2A.    RAW PG DATA'///)
   16 FORMAT   (' ',37X,'DIST.(KM)',12X,'TIME(SEC)',12X,'RESIDUAL(SEC)')
   18 FORMAT  ('2',40X,'TABLE 2B.    CORRECTED PG DATA')
   20 FORMAT  ('1',40X,'TABLE 3A. RAW PN DATA')
   26 FORMAT  ('0',40X,'FIRST ESTIMATE OF V2=',F6.2)
   24 FORMAT  ('2',35X,'TABLE 4B. CORRECTED PN DATA')
   28 FORMAT  (//,' ',40X,'CORRECT PN VELOCITY=',F6.4)
   11 FORMAT(3A4,F6.2,F5.2,F5.3)
   13 FORMAT  (/// ,' ',30X,' CORRECT PG VELOCITY = ',F6.4)
   22 FORMAT  ( /// ,' ',30X,'V0=',F6.4,10X,'FIRST ESTIMATE OF V1=',F6.4
     $)
   55 FORMAT('0',25X,3A4,3X,8(F7.3,2X))
   65 FORMAT ('1',45X,'TABLE 4.    GEOLOGIC CORRECTIONS'///)
   66 FORMAT  (' ',25X,'STATION',8X,'DELTA(KM)',4X,'T',8X,'Z(KM)',2X,'SH
     $OTCR',5X,'STNCR',3X,'TOTCR',4X,'TCR',//)
   77 FORMAT (('0',37X,F6.2,14X,F6.2,14X,F10.6))
   76 FORMAT (('0',2(5X,F6.2)))
   88 FORMAT  (( ///,' ',30X,'INTERCEPT=',F10.6,'  SEC',20X,' SLOPE=',F1
     $0.6,' SEC/CM'))
   99 FORMAT((!0',5X,2(F7.3,5X)))
      END
```

APPENDIX II

Arrival Times Calculated from a Given Model

A computer subroutine is presented to calculate and plot the arrival times for P_g, P^*, P_n, P_cP, and P_nP for the crustal model shown in Figure 3.8. The symbols denoting the various arrivals are identified in comment cards in the program.

```
      SUBROUTINE MODEL
      N=56
     DIMENSION TDIR(229),TRFL(329),TRFR(229),IX(229),TTRFR(229),X(229),
     1TTRFL(229),TPXS(229),XX(229),IY(229),D(900),T(11),S(11)
      REAL IX,IY
      RAD=3.14159265358/180.
       VVV=8.1175
        VO=3.47
      V=6.1497
       VP=5.8
        VV=6.3988
        Z=20.722
          ZZ=16.2342
       PRINT 22, Z ,ZZ
      CALL PLOT(1.0,0.5,-3)
      CALL AXIS(0.,0.,'T-DELTA/6.',10,10.,90.,-17.5,2.5,20.)
      CALL AXIS(0.0,0.0,'DIST. KM.',-9,14.,0.,0.,40.,20.)
       CALL PLOT (0.0,7.0,-3)
       A12P=ARSIN(V/VV)
       A23=ARSIN(VV/VVV)
       A13P=ARSIN(V/VVV)
       A13=ARSIN(VP/VVV)
       A12=ARSIN (VP/VV)
      DO 11 K=1,14
      IX(K)=10*K
            TDIR(K)=IX(K)/V+0.249889
       IY(K)=IX(K)
         TRFL(K)=SQRT(IY(K)**2+4*Z**2)/V
C   TRFR IS HEAD WAVE OFF MOHO
         TRFR(K)=IX(K)/VVV+2*ZZ*COS(A23)/VV+2*                    Z*COS(A13P)/V
C   TTRFR IS HEAD WAVE OFF CONRAD
                TTRFR(K)=IX(K)/VV+2*                  Z*COS(A12P)/V
         TTRFR(K)=TTRFR(K)-IX(K)/6.
```

```
      TDIR(K)=TDIR(K)-IX(K)/6.
      TRFR(K)=TRFR(K)-IX(K)/6.
      TRFL(K)=TRFL(K)-IY(K)/6.
   11 CONTINUE
       DO 88 L=15,N
       IX(L)=10*L
      TRFR(L)=IX(L)/VVV+2*ZZ*COS(A23)/VV+Z*COS(A13)/VP    + Z*COS(A13P)/V
            TTRFR(L)=IX(L)/VV+Z*COS(A12)/VP    + Z*COS(A12P)/V
       TDIR(L)=140./V+0.249889+(IX(L)-140.)/VP
      TTRFR(L)=TTRFR(L)-IX(L)/6.
      TDIR(L)=TDIR(L)-IX(L)/6.
      TRFR(L)=TRFR(L)-IX(L)/6.
   88 CONTINUE
         MM=73
C  TTRFL  IS REFLECTION OFF MOHO
      DO 55 J=26 ,MM
      M=J-25
      A=J*RAD
       B=ARSIN(SIN(A)*VP    /V       )
       IF(J.GT.61 ) GO TO 2
       GO TO 44
2     X(M)=Z*TAN(A)+2.*ZZ*VV/V*SIN(A)/SQRT(1.-(VV/V*SIN(A))**2)+Z*TAN(B)
      TTRFL(M)=    Z/(V*COS(A))+2.*ZZ/(VV*SQRT(1.-(VV/V*SIN(A))**2))+Z/(V
     1P*COS(B))
       GO TO 4
   44 TTRFL(M)=2.*Z/(V*COS(A))+2.*ZZ/(VV*SQRT(1.-(VV/V*SIN(A))**2))
      X(M)=2.*(Z*SIN(A)/COS(A)+ZZ*VV/V*SIN(A)/SQRT(1.-(VV/V*SIN(A))**2))
4      PRINT 77, TTRFL(M),X(M),J
      TTRFL(M)=TTRFL(M)-X(M)/6.
   55 CONTINUE
```

```
C  TRFL IS REFLECTION OFF CONRAD
      DO 111 I=74,85
      II=I-73
      ARG=(90-I)*RAD
      P=ARSIN(SIN(ARG)*VP/V)
      IF(I.LT.82) GO TO 10
      GO TO 20
   10    Y=Z/TAN(ARG)
      R=SQRT(Y**2+Z**2)
       ZP=(140-Y)*TAN(ARG)
      R1=SQRT(ZP**2+(140-Y)**2)
      XP=(Z-ZP)/TAN(P)
      RP=SQRT(XP**2+(Z-ZP)**2)
      TRFL(14+II)=(R+R1)/V+RP/VP
      IY(14+II)=140+XP
      TRFL(14+II)=TRFL(14+II)-IY(14+II)/6.
      GO TO 111
   20    Z2=140*TAN(ARG)
      RR=SQRT(Z2**2+140**2)
      RRP=(Z-Z2)/SIN(P)
      X1=SQRT(RRP**2-(Z-Z2)**2)
      RRPP=Z/SIN(P)
      X2=SQRT(RRPP**2-Z**2)
      TRFL(14+II)=RR/V+(RRP+RRPP)/VP
      IY(14+II)=140+X1+X2
      TRFL(14+II)=TRFL(14+II)-IY(14+II)/6.
  111 CONTINUE
```

```
      X(MM-24 )=0.
      X(MM-23 )=40.
       TTRFL(MM-24 )=0.
       TTRFL(MM-23 )=2.5
      CALL LINE(X,TTRFL,MM-25 ,1,0,4)
      IX(N+1)=0.
      IX(N+2)=40.
      TDIR(N+1)=0.
      TDIR(N+2)=2.5
      TRFR(N+1)=0.
      TRFR(N+2)=2.5
      TRFL(27 )=0.
      TRFL(28 )=2.5
       IY(27)=0.
       IY(28)=40.
      TTRFR(N+1)=0.
      TTRFR(N+2)=2.5
      CALL LINE (IX,TDIR,N,1,0,U)
       CALL LINE (IX(03),TRFR(03),N-2,1,0,3)
      CALL LINE (IY   ,TRFL   ,26 ,1,0,1)
      CALL LINE (IX(08),TTRFR(08),N-7 ,1,0,5)
   22 FORMAT  ('2',20X,'Z1=',F10.3,20X,'Z2 =',F20.3)
   33 FORMAT (('0',2(20X,F10.4)))
   66 FORMAT ('1',3(20X,F10.4))
   77 FORMAT(' ',2(30X,F10.4),10X,I4)
   99 FORMAT (3F5.1)
       RETURN
      END
```

APPENDIX III

Error in Velocity Resulting from a Given Epicentral Error

A computer program is presented which gives the percent relative error in the distance between SNM and ALQ, along the radial from the El Paso earthquake of 12 May 1969, resulting from an epicentral error of 15 km. The azimuth of the 15 km epicentral error is varied from zero to 360° in 10° increments, and the error in distance between the two stations is calculated as a function of this azimuth. The variables in the computer program are defined as follows :

U azimuth of the epicentral error, measured from due east.

Y projection of the epicentral error on the east-west direction.

X projection of the epicentral error on the north-south direction.

DLON Longitude of the epicenter in minutes of arc, adjusted for epicentral error (Richter, 1958; Appendix XII).

DLAT Latitude of the epicenter in minutes of arc, adjusted for epicentral error (Richter, 1958; Appendix XII).

ELAT DLAT in degrees

ELON DLON in degrees

ALAT and ALON coordinates of SNM

BLAT and BLON coordinates of ALQ

The next 22 statements are calculations of distances from the epicenter to both stations, according to the geodetic formulas of Ball (1972).

DLDS the distance between SNM and ALQ measured along the radial from the epicenter, for a given epicentral error.

ERR the error in distance = DLDS minus the distance for zero epicentral error.

PERR percent error in distance.

```
C       EL PASO  12 MAY 1969
          RAD=3.141593/180.
        PRINT 8
      8 FORMAT('4',5X,'DIST1',10X,'DIST2',11X,'DLDS',13X,'U',13X,'ERR',11X
       $,'PERR')
        DO 7 K=1,36
        U=10.*K
        U=U*RAD
        Y=15.*SIN(U)
        X=15.*COS(U)
        IF(U.GT.90.)GO TO 2
        GO TO 15
      2 X=-X
        Y=Y
        IF(U.GT.180.)GO TO 3
        GO TO 15
      3 X=X
        Y=-Y
        IF(U.GT.270.)GO TO 4
        GO TO 15
      4 X=-X
        Y=Y
     15 CONTINUE
        DLON=6384-(X)/1.5783
        DLAT=1908+(Y)/1.8480
        ELAT=DLAT/60.
        ELON=DLON/60.
        ELAT=ELAT*RAD
        ELON=ELON*RAD
        ALAT=34.07*RAD
        ALON=106.9433*RAD
        BLAT=34.9416*RAD
        BLON=106.4583*RAD
```

```
      A=6378.2064
      ESQ=.006768657997291
      ANA=A/(SQRT(1.-ESQ*(SIN(ALAT)**2)))
      ANB=A/(SQRT(1.-ESQ*(SIN(BLAT)**2)))
      ANE=A/(SQRT(1.-ESQ*(SIN(ELAT)**2)))
      XA1=ANA*COS(ALAT)*COS(ALON)
      XA2=ANA*COS(ALAT)*SIN(ALON)
      XA3=(ANA*(1.-ESQ))*SIN(ALAT)
      XB1=ANB*COS(BLAT)*COS(BLON)
      XB2=ANB*COS(BLAT)*SIN(BLON)
      XB3=(ANB*(1.-ESQ))*SIN(BLAT)
      XE1=ANE*COS(ELAT)*COS(ELON)
      XE2=ANE*COS(ELAT)*SIN(ELON)
      XE3=(ANE*(1.-ESQ))*SIN(ELAT)
      XA1E=XA1-XE1
      XA2E=XA2-XE2
      XA3E=XA3-XE3
      XB1E=XB1-XE1
      XB2E=XB2-XE2
      XB3E=XB3-XE3
      DIST1=SQRT((XA1E)**2+(XA2E)**2+(XA3E)**2)
      DIST2=SQRT((XB1E)**2+(XB2E)**2+(XB3E)**2)
      DLDS=ABS(DIST1-DIST2)
          ERR=DLDS-91.6648
              PERR=100.*ERR/91.6648
      U=U/RAD
      WRITE(6,1)DIST1,DIST2,DLDS,U,ERR,PERR
    1 FORMAT(//6F15.5)
    7 CONTINUE
      STOP
      END
```

REFERENCES CITED

American Association of Petroleum Geologists (1967). Geological Highway Map, Southern Rocky Mountain Region.

Ansorge, J., D. Emter, K. Fuchs, J. P. Lauer, St. Mueller, and E. Peterschmitt (1970). Structure of the crust and upper mantle in the rift system around the Rhinegraben, in International Upper Mantle Project, Scientific Report No. 27: Graben Problems, J. H. Illies and St. Mueller, Editors, 190-197.

Ball, W. E., Jr. (1972). Three-dimensional forward and inverse computations, Proc. Am. Soc. Civil Eng., Surveying and Mapping Div. 98:SU2, 167-183.

Berg, J. W., Jr., K. L. Cook, H. D. Narans, Jr., and W. M. Dolan (1960). Seismic investigation of crustal structure in the eastern part of the Basin and Range Province, Bull. Seism. Soc. Am. 50, 511-535.

Birch, F. (1960). The velocity of compressional waves in rocks to 10 kilobars, 1, J. Geophys. Res. 65, 1083-1102.

Braile, L. W., R. B. Smith, G. R. Keller, R. M. Welch, and R. P. Meyer (1973). Crustal structure across the Wasatch Front from detailed seismic refraction studies (preprint).

Chapin, C. E. (1971). The Rio Grande rift, Part I: Modifications and additions, New Mex. Geol. Soc. 21st Field Conf. Guidebook, 191-201.

Dane, C. H. and G. O. Bachman (1965). Geologic Map of New Mexico, U. S. Geol. Survey.

Decker, E. R. and S. B. Smithson (1973). Geophysical studies in the southern Rio Grande rift, (abstract), Trans. Am. Geophys. Union 54, 463.

Diment, W. H., S. W. Stewart, and J. C. Roller (1961). Crustal structure from the Nevada test site to Kingman, Arizona, from seismic and gravity observations, J. Geophys. Res. 66, 201-214.

Dix, C. H. (1952). Seismic Prospecting for Oil, Harper and Brothers, New York, 414 p.

Edwards, C. L., M. A. Reiter, and C. Weidman (1973). Geothermal studies in New Mexico and southern Colorado, (abstract), Trans. Am. Geophys. Union 54, 463.

Fenneman, N. M. (1946). Physical Divisions of The United States, U. S. Geol. Survey, Map.

Foster, R. W. and T. F. Stipp (1961). Preliminary Geologic and Relief Map of the Precambrian of New Mexico, New Mexico Institute of Mining and Technology, State Bureau of Mines and Mineral Resources, Socorro, New Mexico, Circular 57, 37 p.

Hartman, H. and M. Reiter (1972). First report on a preliminary geothermal study of the Rio Grande rift, (abstract), Trans. Am. Geophys. Union 53, 516.

Herrin, E. T. (1966). Travel time anomalies and structure of the upper mantle, (abstract), Trans. Am. Geophys. Union 47, 44.

Herrin, E. (1969). Regional variations of P wave velocity in the upper mantle beneath North America, Am. Geophys. Union Mon. 13, 242-246.

Herrin, E. T. and J. Taggart (1962). Regional variations in P_n velocity and their effect on the location of epicenters, Bull. Seism. Soc. Am. 52, 1037-1046.

Hill, D. P. (1971). Velocity gradients and anelasticity from crustal body wave amplitudes, J. Geophys. Res. 76, 3309-3325.

Hughes, D. S. (1960). Properties of rocks under high pressure and temperature, Methods and Techniques in Geophysics 1, S. K. Runcorn, Editor, Interscience, 308-324.

Illies, J. H. (1970). Graben tectonics as related to crust-mantle interaction, in International Upper Mantle Project, Scientific Report No. 27: Graben Problems, J. H. Illies and St. Mueller, Editors, 4-26.

Jackson, W. H., S. W. Stewart, and L. C. Pakiser (1963). Crustal structure in eastern Colorado from seismic refraction measurements, J. Geophys. Res. 68, 5767-5776.

Jackson, W. H. and L. C. Pakiser (1965). Seismic study of crustal structure in the Southern Rocky Mountains, U.S.G.S. Prof. Paper 525D, D85-D92.

James, D. E. and J. S. Steinhart (1966). Structure beneath continents: A critical review of explosion studies 1960-1965, Am. Geophys. Union Mon. 10, 293-333.

Keller, G. R., R. B. Smith, and L. W. Braile (1973). Crustal structure studies of the eastern margin of the Great Basin, (abstract), Geol. Soc. Am. Abstracts with Programs 5:7, 689.

Kelley, V. C. (1952). Tectonics of the Rio Grande depression of central New Mexico, New Mex. Geol. Soc. 3rd Field Conf. Guidebook, 93-105.

Landisman, M., S. Mueller, and B. J. Mitchell (1971). Review of evidence for velocity inversions in the continental crust, Am. Geophys. Union Mon. 14, 11-34.

Lee, W. H. K. and R. D. Borcherdt (1968). P_n spectral variations of the Gasbuggy explosion at intermediate distance ranges, U.S.G.S. Open File Report, Tech. Letter NCER-9, 18 p.

Lipman, P. W. (1969). Alkalik and tholeiitic basaltic volcanism related to the Rio Grande depression, southern Colorado and northern New Mexico, Geol. Soc. Am. Bull. 80, 1343-1354.

Mueller, S. and M. Landisman (1971). An example of the unified method of interpretation for crustal seismic data, Geophys. J. 23, 365-371.

Nettleton, L. L. (1940). Geophysical Prospecting for Oil, McGraw-Hill, 444p.

New Mexico Geological Society (1961). Geologic Highway Map of New Mexico.

Pakiser, L. C. (1963). Structure of the crust and upper mantle in the Western United States, J. Geophys. Res.68, 5747-5756.

Pakiser, L. C. and D. P. Hill (1963). Crustal structure in Nevada and southern Idaho from nuclear explosions, J. Geophys. Res. 68, 5757-5766.

Pakiser, L. C. and I. Zeitz (1965). Transcontinental crustal and upper mantle structure, Rev. Geophys. 3, 505-520.

Phinney, R. A. (1964). Structure of the earth's crust from spectral behaviour of long-period body waves, J. Geophys. Res. 69, 2997-3017.

Reagor, B. G., D. W. Gordon, and J. N. Jordan (1968). Seismic Analysis of a Nuclear Explosion: Gasbuggy, U.S.C.G.S. Seismology Division, Washington, D.C., 73 p.

Reiter, M., C. L. Edwards, and C. Weidman (1973). Heat flow studies in New Mexico and neighboring areas of the southwestern United States, (abstract), Geol. Soc. Am. Abstracts with Programs 5:7, 779.

Richter, C. F. (1958). Elementary Seismology, W. H. Freeman and Co., 768 p.

Roller, J. C. and J. H. Healy (1963). Seismic refraction measurements between Santa Monica Bay and Lake Mead, J. Geophys. Res. 68, 5837-5850.

Roller, J. C. (1965). Crustal structure in the eastern Colorado Plateaus Province from seismic refraction measurements, Bull. Seism. Soc. Am. 55, 107-119.

Ryall, A. (1962). The Hebgen Lake, Montana, earthquake of August 18, 1959: P waves, Bull Seism. Soc. Am. 52, 235-271.

Ryall, A. and D. J. Stuart (1963). Travel times and amplitudes from nuclear explosions, Nevada Test Site to Ordway, Colorado, J. Geophys. Res. 68, 5821-5836.

Sanford, A. R. (1965). An Instrumental Study of New Mexico Earthquakes, New Mexico Institute of Mining and Technology, State Bureau of Mines and Mineral Resources, Circ. 78, 12 p.

Sanford, A. R. and D. J. Cash (1969). An Instrumental Study of New Mexico Earthquakes, July 1, 1964, through December 31, 1967, New Mexico Institute of Mining and Technology, State Bureau of Mines and Mineral Resources, Circ. 102, 7 p.

Sanford, A. R., A. J. Budding, J. P. Hoffman, O. Alptekin, C. A. Rush, and T. R. Toppozada (1972). Seismicity of the Rio Grande rift in New Mexico, New Mexico Institute of Mining and Technology, State Bureau of Mines and Mineral Resources, Circ. 120, 19 p.

Sanford, A. R., O. Alptekin, and T. R. Toppozada (1973). Use of reflection phases on microearthquake seismograms to map an unusual discontinuity beneath the Rio Grande rift, Bull. Seism. Soc. Am. 63.

Smithson, S. B. and E. R. Decker (1972). Heat flow and gravity studies across the Rio Grande rift in southern New Mexico and western Texas, Trans. Am. Geophys. Union 53, 516.

St. Mueller (1970). Geophysical aspects of graben formation in continental rift systems, in International Upper Mantle Project, Scientific Report No. 27: Graben Problems, J. H. Illies and St. Mueller, Editors, 27-36.

Steinhart, J. S. and R. P. Meyer (1961). Explosion studies of continental structure, Carnegie Inst. Wash. Publ. 622, 409 p.

Stewart, S. W. and L. C. Pakiser (1962). Crustal structure in eastern New Mexico interpreted from the Gnome explosion, Bull. Seism. Soc. Am. 52, 1017-1030.

Stuart, D. J., J. C. Roller, W. H. Jackson, and G. B. Mangan (1964). Seismic propagation paths, regional travel times, and crustal structure in the western United States, Geophysics 29, 178-187.

Summers, W. K. (1965). A preliminary report on New Mexico's geothermal energy resources, New Mexico Institute of Mining and Technology, State Bureau of Mines and Mineral Resources, Circ. 80, 41 p.

Tatel, H. E. and M. A. Tuve (1955). Seismic exploration of a continental crust, Geol. Soc. Am. Spec. Paper 62, 35-50.

Toppozada, T. R. and A. R. Sanford (1972). Instrumental study of New Mexico earthquakes, January 1968 through June 1971, New Mexico Institute of Mining and Technology, State Bureau of Mines and Mineral Resources, Circ. 126, 6 p.

Tryggvason, E. and B. R. Qualls (1967). Seismic refraction measurements of crustal structure in Oklahoma, J. Geophys. Res. 72, 3738-3740.

United States Department of Commerce, Environmental Science Services Administration, Coast and Geodetic Survey (1968). A Seismic Profile Southward from the Gasbuggy Explosion: Field Report.

Warren, D. H. (1969). A seismic refraction survey of crustal structure in central Arizona, Geol. Soc. Am. Bull. 80, 257-282.

Warren, D. H. and W. H. Jackson (1968). Surface seismic measurements of the project Gasbuggy explosion at intermediate distance ranges, U.S.G.S. Open File Report, 45 p.

Willden, R. (1965). Seismic refraction measurements of crustal structure between American Falls Reservoir, Idaho, and Flaming Gorge Reservoir, Utah, U.S.G.S. Prof. Paper 525C, C44-C50.